

NASA TM X-2794

NASA TECHNICAL
MEMORANDUM



NASA TM X-2794

CASE FILE
COPY

CONFIDENTIAL	CLASSIFIED
BY Henry A. [redacted] Security Classification Officer, NASA LaRC	
SUBJECT TO GENERAL DECLASSIFICATION SCHEDULE OF EXECUTIVE ORDER 11652 AUTOMATICALLY DOWNGRADED AT TWO YEAR INTERVALS AND DECLASSIFIED ON DEC 31 1979	

DOWNGRADED TO UNCLASSIFIED
BY AUTHORITY OF NASA CLASSIFICATION
CHANGE NOTICES NO. 240 DATED 30 SEP 76
ITEM NO. 44

EFFECTS OF WING HEIGHT ON LOW-SPEED
AERODYNAMIC CHARACTERISTICS OF
A MODEL HAVING A 42° SWEEP WING,
A SUPERCRITICAL AIRFOIL,
DOUBLE-SLOTTED FLAPS, AND A LOW TAIL



by Paul G. Fournier and William C. Sleeman, Jr.

*Langley Research Center
Hampton, Va. 23665*

1. Report No. NASA TM X-2794	2. Government Accession No.	3. Recipient's Catalog No.	
4. Title and Subtitle EFFECTS OF WING HEIGHT ON LOW-SPEED AERODYNAMIC CHARACTERISTICS OF A MODEL HAVING A 42° SWEEP WING, A SUPERCRITICAL AIRFOIL, DOUBLE-SLOTTED FLAPS, AND A LOW TAIL (U)		5. Report Date September 1973	
		6. Performing Organization Code	
7. Author(s) Paul G. Fournier and William C. Sleeman, Jr.		8. Performing Organization Report No. L-8832	
		10. Work Unit No. 760-64-60-04	
9. Performing Organization Name and Address NASA Langley Research Center Hampton, Va. 23665		11. Contract or Grant No.	
		13. Type of Report and Period Covered Technical Memorandum	
12. Sponsoring Agency Name and Address National Aeronautics and Space Administration Washington, D.C. 20546		14. Sponsoring Agency Code	
15. Supplementary Notes			
16. Abstract <p>A low-speed investigation was conducted in the Langley V/STOL tunnel to determine the static longitudinal and lateral stability characteristics of a general research model with the wing in a high position and a low position on the fuselage. The model had a wing with a quarter-chord sweep of 42°, an aspect ratio of 6.78, a supercritical airfoil, and a high-lift system which consisted of a leading-edge slat and a double-slotted flap. Various slat and flap deflections represented clean, take-off, and landing configurations. A 45° swept horizontal tail located slightly below the fuselage center line was investigated with both the low- and high-wing configurations.</p> <p style="text-align: center;">CLASSIFICATION CHANGE</p> <p style="text-align: center;">To UNCLASSIFIED</p> <p>By authority of <u>NASA HDQ. T.D. 77-163</u></p> <p>Changed by <u>L. Shirley</u> Date <u>6-15-76</u></p> <p>Classified Document Master Control Station, NASA Scientific a</p>			
17. Key Words (Suggested by Author(s)) High-lift flap system Supercritical wing Low-speed aerodynamic characteristi Swept wing Wing height			
19. Security Classif. (of this report) CONFIDENTIAL	20. Security Classif. (of this page) Unclassified	21. No. of Pages 72	22. Price
"NATIONAL SECURITY INFORMATION" Unauthorized Disclosure Subject to Criminal Sanctions.			

[REDACTED]

EFFECTS OF WING HEIGHT ON LOW-SPEED AERODYNAMIC
CHARACTERISTICS OF A MODEL HAVING A 42° SWEEP WING,
A SUPERCRITICAL AIRFOIL, DOUBLE-SLOTTED FLAPS,
AND A LOW TAIL*

By Paul G. Fournier and William C. Sleeman, Jr.
Langley Research Center

SUMMARY

A low-speed investigation was conducted in the Langley V/STOL tunnel to determine the static longitudinal and lateral stability characteristics of a general research model with the wing in a high position and a low position on the fuselage. The model had a wing with a quarter-chord sweep of 42°, an aspect ratio of 6.78, a supercritical airfoil, and a high-lift system which consisted of a leading-edge slat and a double-slotted flap. Flap deflections of 0°, 20°, and 40° were investigated with corresponding slat deflections of 0° (off), 40°, and 50° to represent clean, take-off, and landing configurations. A 45° swept horizontal tail located slightly below the fuselage center line was investigated with both the low- and high-wing configurations.

Maximum untrimmed lift coefficients (0° tail incidence) obtained for the landing configuration were 2.21 for the low-wing model and 2.54 for the high-wing model. The static longitudinal stability for all the model configurations investigated was positive at low angles of attack and generally decreased at high angles of attack. Severe longitudinal instability at moderate and high angles of attack was indicated for the low-wing model in the clean configuration; whereas, for the high-wing model in the clean configuration, the instability that occurred at high angles of attack was relatively mild. Deflection of the high-lift system increased the static longitudinal stability and delayed the onset of neutral stability to the highest test angles of attack. The static lateral stability derivatives obtained for the complete model showed positive directional stability over the test angle-of-attack range; however, the significant losses in directional stability at high angles of attack indicated that directional instability would be expected for angles somewhat greater than 20°. Positive effective dihedral was generally indicated for all model configurations except the high-wing model in the clean configuration, which showed a reversal and negative effective dihedral at the highest test angles of attack. Lateral-control tests with a partial-span, 75° deflected spoiler on the right wing indicated that the spoiler was effective

* Title, Unclassified.

[REDACTED]

~~CONFIDENTIAL~~

in producing positive rolling moments and that positive yawing moments accompanied the positive rolling moments produced by the spoiler.

INTRODUCTION

Several low-speed research investigations have been conducted by NASA to develop high-lift systems for supercritical airfoils (refs. 1 and 2). Studies of various combinations of flap and slat deflections for a 42° swept high-wing model (unpublished data) were used to define combinations of flap and slat deflections applicable to take-off and landing configurations in the tests of a low-wing version which simulated a transport configuration (ref. 2). The model tested in the investigation of reference 2 was essentially the same as the aforementioned high-wing model, except that the wing was moved to the bottom of the fuselage and the vertical tail and low horizontal tail were replaced by a T-tail.

The relative ease of changing the configuration of the high-wing model permitted an investigation of the effects of wing height, and the results are presented herein. An overall assessment of the low-speed static longitudinal and lateral stability and high-lift system performance was made for both the low- and high-wing configurations. The wing of the model had 42° sweep of the quarter-chord line, an aspect ratio of 6.78, and supercritical airfoil sections. The high-lift system consisted of a partial-span, double-slotted flap which extended from the fuselage side to the 80-percent-wing-semispan station and a leading-edge slat which extended from the outboard edge of the wing-root glove (the 32-percent-wing-semispan station) to the wing tip. Combinations of flap and slat deflections were investigated to represent clean, take-off, and landing configurations.

Tests were conducted in the Langley V/STOL tunnel over an angle-of-attack range from approximately -4° to 20° . Static longitudinal and lateral stability characteristics were determined for the complete models and for the models with the tail surfaces removed. Aerodynamic characteristics in pitch were also obtained for a single spoiler deflection of 75° to determine whether there were significant effects of wing height on the lateral-control capability of an upper-surface spoiler located on one wing panel.


SYMBOLS

The static longitudinal and lateral stability data are presented about the stability-axis system. The positive directions of forces, moments, and angles are indicated in figure 1. The model moment reference point was located longitudinally at the quarter chord of the wing mean aerodynamic chord (theoretical wing) and on the fuselage center line.

The measurements of this investigation are presented in the International System of Units (SI). Details concerning the use of SI units, together with physical constants and conversion factors, are presented in reference 3.

b	wing span, cm
C_D	drag coefficient, $\frac{\text{Drag}}{qS}$
C_L	lift coefficient, $\frac{\text{Lift}}{qS}$
$C_{L,\text{trim}}$	lift coefficient for longitudinal trimmed condition ($C_m = 0$)
C_l	rolling-moment coefficient, $\frac{\text{Rolling moment}}{qSb}$
$C_{l\beta}$	effective dihedral parameter, $\frac{\Delta C_l}{\Delta \beta}$ (for $\beta = \pm 5^\circ$), per deg
C_m	pitching-moment coefficient, $\frac{\text{Pitching moment}}{qS\bar{c}}$
C_n	yawing-moment coefficient, $\frac{\text{Yawing moment}}{qSb}$
$C_{n\beta}$	directional stability parameter, $\frac{\Delta C_n}{\Delta \beta}$ (for $\beta = \pm 5^\circ$), per deg
C_Y	side-force coefficient, $\frac{\text{Side force}}{qS}$
$C_{Y\beta}$	side-force parameter, $\frac{\Delta C_Y}{\Delta \beta}$ (for $\beta = \pm 5^\circ$), per deg
c	wing chord, cm
\bar{c}	wing mean aerodynamic chord (theoretical wing), cm
c'	portion (0.755c) of basic wing ahead of vane, cm
c_f	chord of flap, cm
\bar{c}_H	horizontal-tail mean aerodynamic chord, cm
c_r	wing root chord, cm
c_s	chord of leading-edge slat, cm

c_t	wing tip chord, cm
c_{th}	theoretical wing chord, cm
c_v	chord of vane, cm
\bar{c}_V	vertical-tail mean aerodynamic chord, cm
i_t	incidence of horizontal tail, positive when trailing edge down (see fig. 1), deg
$i_{t,trim}$	horizontal-tail incidence for longitudinal trimmed condition ($C_m = 0$), deg
l_t	distance from $\bar{c}/4$ (moment reference) to $\bar{c}_H/4$, cm
q	free-stream dynamic pressure, N/m^2
R_{le}	leading-edge radius of wing airfoil section, cm
S	wing area (based on theoretical planform, glove not included), m^2
t_{max}	maximum thickness of airfoil section, cm
t_{te}	airfoil trailing-edge thickness, cm
x	distance along chord of selected wing, slat, or flap element, cm
Δx_{le}	distance from glove leading edge to leading edge of theoretical planform at a given spanwise station, cm
y	spanwise distance measured from fuselage center line, cm
z_l	lower coordinate of airfoil section, cm
z_{le}	vertical distance from wing reference line to chord line at leading edge, cm
z_{te}	vertical distance from wing reference line to chord line at trailing edge, cm
z_u	upper coordinate of airfoil section, cm



α	angle of attack of wing chord line, deg
β	angle of sideslip, deg
δ_f	flap deflection angle with respect to wing chord line, deg
δ_s	leading-edge slat deflection angle with respect to wing chord line, deg
$\delta_{spoiler}$	wing upper-surface spoiler deflection angle relative to wing surface, deg
δ_v	vane deflection of double-slotted flap with respect to wing chord line, deg
ϵ	effective downwash angle, deg
ϕ	wing twist, positive when trailing edge is down, deg

MODEL DESCRIPTION

The model used in this investigation was constructed to permit the wing to be mounted in either a high position or a low position. Drawings of the complete model configurations are presented in figure 2(a); details of the wing glove and high-lift system are shown in figures 2(b) and 2(c). A description of the upper-surface spoiler that was installed on only the right wing is presented in figure 2(d). Photographs of the various model configurations are presented in figure 3.

Wing

The basic wing planform was constructed to conform to the theoretical planform shown in figure 2(a); the wing reference area, aspect ratio, taper ratio, and sweep were defined for the theoretical planform. The aluminum wing had 42° sweep of the quarter-chord line, an aspect ratio of 6.78, and a taper ratio of 0.36. The basic wing was fitted with a fiber-glass—resin glove over the inboard part to simulate the planform of the F-8 airplane with a supercritical wing. The chord, twist, and maximum-thickness variation with span for the glove and the wing are shown in figure 2(b). Detailed coordinates for the wing are presented in table I. The basic geometric characteristics are summarized in table II. The wing had a negative dihedral angle of 1.71°. Transition strips, 0.32 cm wide, of No. 80 carborundum were applied to the upper and lower surfaces of the wing 3.81 cm behind the leading edge.

High-Lift System

The high-lift system of the model consisted of a partial-span, double-slotted flap which extended from the wing-body juncture to the 80-percent-wing-semispan station and a slat which extended from the outboard edge of the glove (32-percent-wing-semispan station) to the wing tip. The chord of the double-slotted flap was taken as the aft 35 percent of the basic supercritical airfoil, except at the trailing edge of the inboard portion where the glove was located. The leading edge of the flap was rounded to the nose contour of a modified NACA 4415 airfoil in order to nest within the basic airfoil from 0.650c to 0.755c and to allow 0.159 cm for the upper-surface thickness of the airfoil at 0.755c. The chord of both the leading-edge slat and the vane was 15 percent of the basic wing chord. Both of these elements had St. Cyr 156 airfoil sections modified in thickness ratio at the inboard end and at the tip as shown by the coordinates in tables III and IV.

The geometry of the flap, vane, and slat was defined in a reference deflection position of 50° for the flap and 40° for the slat. The coordinates for the full-span, double-slotted flap (although tested herein as a partial-span, double-slotted flap) are presented in table V, and the coordinates for the leading-edge slat for two spanwise stations parallel to the plane of symmetry are presented in table III. The vane coordinates are presented in table IV. The angle between the vane and flap was fixed at 25° . Deflections of the flap-vane combination and the leading-edge slat were measured in the streamwise plane (fig. 2(c)) relative to their respective reference chord lines. Transition strips, 0.32 cm wide, of No. 60 carborundum were applied to the upper and lower surfaces of the leading-edge slat 2.54 cm behind the leading edge of the slat.

Spoiler

A spoiler was attached to the upper surface of the right wing to investigate its effectiveness as a roll control. The spoiler was made of 0.159-cm-thick metal and was hinged along the 60-percent-chord line from 32 to 80 percent of the wing semispan (fig. 2(d)). A fairly complete selection of spoiler deflection angles up to 75° was investigated on the low-wing model of reference 3, and only the 75° deflection was investigated in the present study of wing-height effects. The spoiler deflection was measured with respect to a plane tangent to the wing surface along the 60-percent-chord line. Part of the wing immediately behind the spoiler was removed when the high-lift system was deflected in order to provide the gap between the wing and vane that would normally occur on an airplane equipped with this type of spoiler and high-lift system.

Fuselage

The fuselage of the model had a modified cylindrical cross section with circular bottom and top portions and flat sides. Overall dimensions of the fuselage are shown in

figure 2(a). A fiber-glass—resin shell, 0.32 cm thick, formed the outer shape of the fuselage and was attached to a metal strongback which housed a six-component strain-gage balance. An electronic angle-of-attack sensor was mounted to the internal strongback to provide the measured geometric angle of attack of the model during the tests.

Tail Surfaces

The location and principal dimensions of the horizontal and vertical tails are given in figure 2(a). Both tail surfaces were made of aluminum and had 45° sweep of the quarter-chord line and NACA 65A006 airfoil sections. The incidence of the horizontal tail could be varied from 5° to -20° in 5° increments.

TESTS AND CORRECTIONS

The investigation was conducted in the Langley V/STOL tunnel; most of the tests were made at a dynamic pressure of 2394 N/m². The test Reynolds number at this dynamic pressure was 2.47×10^6 based on the wing mean aerodynamic chord of 0.579 meter. The test dynamic pressure had to be reduced to about one-half of the usual value for spoiler tests with the high-lift system deflected in order to prevent overloads on the strain-gage balance.

Longitudinal aerodynamic characteristics were obtained from tests conducted through an angle-of-attack range from approximately -4° to 20° in increments of 2°. Configurations with various stabilizer incidence angles and the horizontal tail off were investigated to define trimmed characteristics and effective downwash angles over the test angle-of-attack range.

Lateral stability derivatives were obtained from tests conducted through the angle-of-attack range with the model sideslipped $\pm 5^\circ$. Lateral stability tests were conducted on the complete model configurations and on the models with the horizontal- and vertical-tail surfaces removed to determine the contributions of the tails.

Aerodynamic characteristics were determined for the clean configuration, with the flap undeflected and the leading-edge slat removed. A take-off configuration was simulated by 20° flap deflection with 40° slat deflection; a landing configuration was represented by 40° flap deflection with 50° slat deflection. A fairly complete set of data with various stabilizer settings was obtained on the high-wing model with a 45° flap setting with 50° slat deflection during the flap-slat deflection studies.

Jet-boundary corrections, determined from reference 4, and tunnel-blockage corrections, obtained from reference 5, were applied to the measured data. The drag data were also corrected for the balance-chamber pressure of the fuselage.

PRESENTATION OF RESULTS

The longitudinal and lateral aerodynamic characteristics obtained in the investigation of the effects of wing height are presented in the figures as follows:

Figure

Longitudinal aerodynamic characteristics:

Low-wing model -

Clean configuration	4
Take-off configuration, $\delta_f = 20^\circ$, $\delta_s = 40^\circ$	5
Landing configuration, $\delta_f = 40^\circ$, $\delta_s = 50^\circ$	6

High-wing model -

Clean configuration	7
Take-off configuration, $\delta_f = 20^\circ$, $\delta_s = 40^\circ$	8
Landing configuration, $\delta_f = 40^\circ$, $\delta_s = 50^\circ$	9
Landing configuration, $\delta_f = 45^\circ$, $\delta_s = 50^\circ$	10

Comparison of data for low- and high-wing models -

Clean configuration	11
Take-off configuration, $\delta_f = 20^\circ$, $\delta_s = 40^\circ$	12
Landing configuration, $\delta_f = 40^\circ$, $\delta_s = 50^\circ$	13

Spoiler for roll control:

Clean configuration	14
Take-off configuration, $\delta_f = 20^\circ$, $\delta_s = 40^\circ$	15
Landing configuration, $\delta_f = 40^\circ$, $\delta_s = 50^\circ$	16

Lateral stability derivatives:

Clean configuration	17
Take-off configuration, $\delta_f = 20^\circ$, $\delta_s = 40^\circ$	18
Landing configuration, $\delta_f = 40^\circ$, $\delta_s = 50^\circ$	19

Summary:

Trimmed lift curves	20
Effect of deflection of high-lift system on lift coefficient	21
Trimmed longitudinal stability	22
Flow characteristics at horizontal tail	23

DISCUSSION

Test results obtained for a range of stabilizer settings and tail off are presented separately for the low- and high-wing configurations in order to document the complete longitudinal characteristics obtained for each configuration (figs. 4 to 10). Effects of wing

height on the longitudinal characteristics for the tail off and the $i_t = -10^\circ$ stabilizer setting are taken from the basic data and presented in figures 11 to 13. Effects of spoiler deflection for roll control on the longitudinal and lateral characteristics of the low- and high-wing models are presented in figure 14 for the clean configuration and in figure 15 for the take-off configuration. Tests with the spoiler deflected for roll control in the landing configuration were made only for the low-wing model as presented in figure 16. Basic data obtained for determining effects of wing height on lateral stability derivatives are compared directly in figure 17 for the clean configuration and in figure 18 for the take-off configuration. Lateral stability derivatives for the landing configuration were obtained only for the low-wing model and are presented in figure 19.

Longitudinal Characteristics

Lift performance. - The lift performance obtained for the low- and high-wing model configurations may be summarized as follows:

Configuration	Wing	Maximum untrimmed C_L ($i_t = 0^\circ$)	Trimmed C_L at -		
			$\alpha = 0^\circ$	$\alpha = 5^\circ$	$\alpha = 19^\circ$
Clean ($\delta_f = 0^\circ$, $\delta_s = \text{Off}$)	Low	1.41	0.12	0.53	1.33
	High	1.49	.11	.52	1.31
Take-off ($\delta_f = 20^\circ$, $\delta_s = 40^\circ$)	Low	2.20	0.61	1.04	1.95
	High	2.40	.71	1.15	2.05
Landing ($\delta_f = 40^\circ$, $\delta_s = 50^\circ$)	Low	2.21	1.02	1.38	2.04
	High	2.54	1.33	1.67	2.29

Maximum untrimmed lift coefficients (0° tail incidence) obtained for the landing configuration were 2.21 for the low-wing model and 2.54 for the high-wing model. Values given as maximum lift coefficients generally do not represent the maximum attainable lift for the particular configuration because the test angle of attack was limited to 20° or less, and the reductions in lift that normally accompany wing stall were not indicated except at the highest flap and slat deflections investigated. The maximum untrimmed lift coefficients given do provide an indication of the comparative lift capabilities of the complete model for both the low- and high-wing configurations with and without the high-lift system deflected. Trimmed lift coefficients at angles of attack below the angle for maximum lift are, however, of more interest because the maximum usable operational lift must be lower than the maximum trimmed lift in order to provide the normal flight-safety speed margins.

Trimmed lift coefficients for the clean configuration were about the same for the low- and high-wing configurations; whereas, with the high-lift system deflected, the high-wing model showed consistently higher lift at a given angle of attack. Values of maximum

████████████████████

trimmed lift coefficient for the landing configuration at an angle of attack of 19° were 2.04 for the low wing and 2.29 for the high wing. The increments in trimmed lift coefficient that resulted from deflection of the high-lift system at an angle of attack of 0° were 0.49 (low wing) and 0.60 (high wing) for the take-off configuration and 0.90 (low wing) and 1.22 (high wing) for the landing configuration. A comparison in the above table and figure 20 demonstrates a superior high-lift performance by the high-wing configuration, particularly for the landing configuration.

Effects of longitudinal trimming on the lift performance depend upon the untrimmed condition selected for comparison. Inasmuch as the characteristics of the model with the horizontal tail removed represent the direct effects of deflection of the high-lift system, the tail-off condition was selected as the most logical basis for comparison. The effects of trimming arise, therefore, from indirect effects, which are the magnitude and direction of the tail load required for trim. A summary of the effects of deflection of the high-lift system for trimmed and untrimmed conditions is presented in figure 21. These results at a flap deflection of 0° show that the effects of trimming on the lift were fairly small and favorable only at high angles of attack. Deflection of the high-lift system produced negative pitching-moment increments that required increasing negative tail deflections for trim and attendant loss in lift as the flap deflections increased. At the highest flap deflections investigated, the loss in lift coefficient caused by trimming amounted to a maximum of about 0.3 at low angles of attack. The results obtained at high angles of attack showed a decrease in flap effectiveness for the low-wing configuration for flap deflections greater than 20° , and for these conditions, the changes in lift due to trimming were almost insignificant because the tail load for trim was relatively small (see pitching moments of fig. 6). For the high-wing configuration (fig. 21), some flap effectiveness was maintained up to 40° deflection, and the tail download for trim caused a reduction in lift for trimmed conditions.

The overall levels of both trimmed and untrimmed lift presented in figure 21 indicate that significantly better flap performance was achieved on the high-wing configuration than on the low-wing configuration throughout the test angle-of-attack range. This favorable effect of the high wing on performance of the high-lift system can be attributed to the favorable endplate effect of the fuselage on lift carryover at the inboard ends of the deflected flaps and to the fact that the upper surface of the wing in the high position was not interrupted by the body.

Longitudinal stability of low-wing model. - The pitching-moment data for the low-wing model presented in figures 4 to 6 indicated positive static longitudinal stability at low and moderate angles of attack, but longitudinal instability was indicated at high angles of attack for all flap deflections investigated. The pitching-moment slope $\partial C_m / \partial C_L$ at a given value of C_L generally varied with stabilizer incidence; the angle of attack and

lift coefficient at which instability occurred also varied with stabilizer incidence. In view of the nature of these results, it was considered appropriate to determine the static longitudinal stability characteristics for trimmed conditions; the trimmed pitching-moment slopes are presented in figure 22 as a function of trimmed lift coefficient. The results of figure 22 show that the low-wing model was longitudinally unstable for trimmed lift coefficients above 0.9 for the clean configuration and 1.9 for the take-off and landing configurations. The instability of the clean configuration was particularly severe; this instability can be attributed to both the high level of instability of the wing-body combination and a loss in the tail contribution to stability at high angles of attack (fig. 4).

Effective downwash for low-wing model.- The downwash and stabilizer effectiveness are of interest in assessing the contribution of the tail to longitudinal stability, which can be expressed as the product $\frac{\partial C_m}{\partial i_t} \left(1 - \frac{\partial \epsilon}{\partial \alpha} \right)$. The downwash and stabilizer effectiveness presented in figure 23(a) were obtained from the pitching-moment data of figures 4 to 6. The results in figure 23(a) for the low-wing model in the clean configuration show a significant destabilizing increase in downwash for angles of attack from 4° to 18° . Although the horizontal tail continued to provide some contribution to stability over this angle-of-attack range, the tail contribution was decreasing ($\partial \epsilon / \partial \alpha$ increasing) while the instability of the wing-body was increasing (tail-off C_m curve of fig. 4). The stabilizer effectiveness ($\partial C_m / \partial i_t$) for the clean configuration remained constant throughout the angle-of-attack range (fig. 23(a)) and, therefore, did not influence the variations of stability over the angle-of-attack range.

The results for the low-wing model with the high-lift system deflected (fig. 23(a)) showed large increases in downwash angle at a given angle of attack that were caused by deflection of the flaps. The downwash gradient $\partial \epsilon / \partial \alpha$ was significantly lower with the high-lift system deflected than for the clean configuration; however, some increases in $\partial \epsilon / \partial \alpha$ occurred at moderate angles of attack (8° to 12°). These increases in $\partial \epsilon / \partial \alpha$, however, combined with about 35 percent reduction in stabilizer effectiveness and the high instability of the wing-body to cause the complete model to become longitudinally unstable at the highest angles of attack (fig. 22).

Comparison of stability characteristics of low- and high-wing models.- The basic longitudinal characteristics of the high-wing model are presented in figures 7 to 10; however, the discussion of these results will be limited to a comparison of data for the low- and high-wing models (figs. 11 to 13).

Both the pitching-moment coefficients (figs. 11 to 13) and the trimmed pitching-moment slopes (fig. 22) show more favorable longitudinal stability characteristics for the high wing than for the low wing. Although there were losses in stability at high lift for both the high- and low-wing arrangements, these losses were delayed to a higher lift coef-

efficient and were generally less severe for the high wing than for the low wing. The results presented in figure 23(b) for the high wing show higher downwash increments due to flap deflection at low angles of attack than for the low wing (fig. 23(a)); however, there were no large destabilizing increases in downwash at higher angles of attack for the high-wing model. In comparison with the low-wing model, the tail-off pitching moments for the high-wing model (figs. 11 to 13) showed relatively small changes in stability with lift coefficient at low and moderate lift coefficients, followed by an abrupt loss in stability at the highest lift coefficients attained. This abrupt increase in instability of the tail-off configuration was primarily responsible for the loss in stability shown for the clean and landing configurations of the high-wing model.

Test results for the take-off configuration of the high-wing model did not indicate longitudinal instability over the angle-of-attack range investigated (figs. 12 and 23(b)) primarily because the tail-off instability did not increase as abruptly at high angles of attack as for the clean and landing configurations. Wake effects (decrease in $\partial C_m / \partial i_t$ at high angles of attack) for the high-wing model in the landing configuration (fig. 23(b)) along with the tail-off characteristics (fig. 9) caused the stability loss of the complete model at high angles of attack.

Stabilizer effectiveness for low- and high-wing models. - The stabilizer effectiveness results presented in figure 23(b) for the high-wing model show some characteristics that are not typical of the results obtained for either the low-wing model of this investigation or the low-wing transport configuration of reference 2. Values of $\partial C_m / \partial i_t$ at low angles of attack were about -0.040 both with and without the high-lift system deflected. At high angles of attack for the landing configuration, values of $\partial C_m / \partial i_t$ showed the decrease that is expected when the tail is immersed in the wake that trails from the wing flaps. For both the clean and landing configurations, there was an increase in $\partial C_m / \partial i_t$ to a value about 13 percent larger than the value at an angle of attack of 0° . The maximum increase occurred at about 16° for the clean configuration and about 8° for the landing configuration. Reasons for this increase in stabilizer effectiveness are not apparent on the basis of the limited data obtained, and detailed wake surveys would be needed to define the flow-field characteristics that caused these results.

Detailed analysis of the present data revealed that unusual flow characteristics were evident, and a discussion of these characteristics and consequent limitations of the present data may be helpful. The technique used for determining effective downwash angles from pitching-moment data involves linear interpolation for the stabilizer setting for zero tail lift at each model angle of attack. The interpolation accuracy is greater for a range of stabilizer settings near zero tail load, and the values of $\partial C_m / \partial i_t$ presented in figure 23 were obtained insofar as possible for these conditions. In most cases, for both the low- and high-wing models in the clean configuration (figs. 4 and 7), the variation of

pitching moment with stabilizer incidence (at a given angle of attack) was linear between $i_t = 0^\circ$ and -10° , except at the lowest and highest angle of attack, where tail stall was being approached. The test results presented in figure 10 for $\delta_f = 45^\circ$ and $\delta_s = 50^\circ$, on the other hand, show a large difference in the pitching-moment increment caused by a -5° change in stabilizer angle between 0° and -5° and between -5° and -10° . At the higher negative stabilizer angles, the stabilizer effectiveness was significantly lower than the effectiveness at small incidence angles.

The highly nonlinear nature of the stabilizer effectiveness for the high-wing model with $\delta_f = 45^\circ$ and $\delta_s = 50^\circ$ suggests that for the angle-of-attack range up to about 12° , the horizontal tail was close to a region where the flow characteristics varied appreciably with rather small variation in vertical distance. For stabilizer angles of 0° and -5° (fig. 10), the stabilizer effectiveness was about the same as for all the other flap angles at low angles of attack for both the low- and high-wing configurations. For incidence angles much greater than -5° , the stabilizer effectiveness was reduced significantly, this result suggests that the leading edge of the horizontal tail may have become progressively immersed in the wake, and at angles of attack greater than 12° , the tail was in a region of decreased dynamic pressure for all incidence angles tested.

The large variation of stabilizer effectiveness with stabilizer angles encountered on the high-wing model with $\delta_f = 45^\circ$ and $\delta_s = 50^\circ$ indicated the need for more data at low stabilizer angles. Data for the landing configuration (fig. 9) with $\delta_f = 40^\circ$ and $\delta_s = 50^\circ$ did not include the -5° angle; therefore, no downwash or stabilizer effectiveness results have been included for this configuration in the present report.

Lateral Stability Characteristics

Directional stability. - The static lateral stability derivatives presented in figures 17 to 19 showed positive values of the directional stability parameter C_{n_β} for the high- and low-wing complete model configurations throughout the angle-of-attack range investigated. Significant losses in directional stability were generally evident at high angles of attack for both the low- and high-wing configurations (figs. 17 and 18), and the data trends indicate that directional instability for the complete model would be expected to occur for angles of attack somewhat greater than 20° .

Values of the directional stability parameter C_{n_β} were higher at low angles of attack for the low-wing model than for the high-wing model; however, at moderate and high angles of attack, there was little significant effect of wing position on C_{n_β} . Deflection of the high-lift system generally caused appreciable increases in the directional stability of the model, both with and without the vertical tail, throughout the test angle-of-attack range. For the low-wing model in the landing configuration, the tail-off configuration became directionally stable at angles of attack between 14° and 19° (fig. 19).

[REDACTED]

edge slat and a double-slotted trailing-edge flap. A 45° swept horizontal tail was located slightly below the fuselage center line. The results of this investigation may be summarized as follows:

1. Significantly better high-lift system performance was obtained with the high-wing configuration than with the low-wing configuration throughout the test angle-of-attack range. Maximum untrimmed lift coefficients (0° tail incidence) obtained for the landing configuration were 2.21 for the low-wing model and 2.54 for the high-wing model.

2. The static longitudinal stability at low and moderate angles of attack was positive for all the model configurations investigated. For the low-wing model in the clean configuration, there was a large loss of stability above an angle of attack of 10° , and the model was unstable throughout the high angle-of-attack range. Deflecting the high-lift system increased the static longitudinal stability of the low-wing model throughout the angle-of-attack range and delayed the onset of neutral stability to the highest angles of attack investigated. The high-wing model in the clean configuration showed a small range of longitudinal instability at high lift, but the level of instability was very low in comparison with that for the low-wing model. Deflection of the high-lift system increased the longitudinal stability of the high-wing model throughout the angle-of-attack range except for the landing configuration at the highest angle of attack, where the longitudinal stability was neutral.

3. Static lateral stability derivatives obtained for both the low- and high-wing models showed positive values of directional stability parameter ($C_{n\beta}$) throughout the angle-of-attack range investigated. Significant decreases in $C_{n\beta}$ occurred, however, at high angles of attack; the data trends indicate that directional instability would be expected for angles of attack somewhat greater than 20° . Negative values of the effective dihedral parameter ($C_{l\beta}$) were generally obtained for positive lifting conditions. For the high-wing model in the clean configuration, there was a significant loss in effective dihedral for angles of attack above 12° , and negative effective dihedral was indicated for angles of attack above 16.5° . Deflections of the high-lift system caused large increases in effective dihedral ($-C_{l\beta}$) at moderate and high angles of attack for both the low- and high-wing model.

4. Lateral-control tests indicated that a partial-span spoiler on the right wing was effective in producing positive rolling moments for a deflection angle of 75° . Positive yawing moments and negative side force accompanied the positive rolling moments produced by the spoiler.

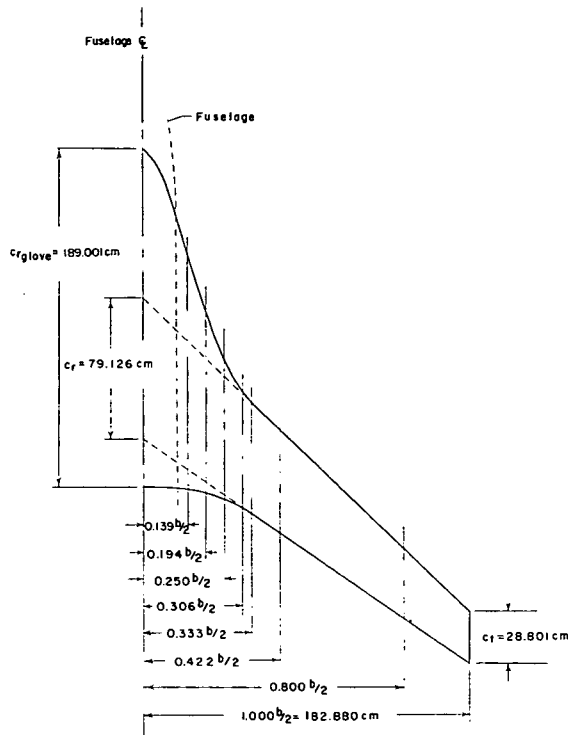
Langley Research Center,
National Aeronautics and Space Administration,
Hampton, Va., June 4, 1973.

[REDACTED]

REFERENCES

1. Goodson, Kenneth W.: Low-Speed Aerodynamic Characteristics of a Rectangular, Aspect-Ratio-6, Slotted Supercritical Airfoil Wing Having Several High-Lift Flap Systems. NASA TM X-2317, 1971.
2. Fournier, Paul G.; and Sleeman, William C., Jr.: Low-Speed Aerodynamic Characteristics of a Model Having a 42° Swept Low Wing With a Supercritical Airfoil, Double-Slotted Flaps, and a T-Tail. NASA TM X-2582, 1972.
3. Mechtly, E. A.: The International System of Units - Physical Constants and Conversion Factors (Revised). NASA SP-7012, 1969.
4. Gillis, Clarence L.; Polhamus, Edward C.; and Gray, Joseph L., Jr.: Charts for Determining Jet-Boundary Corrections for Complete Models in 7- by 10-Foot Closed Rectangular Wind Tunnels. NACA WR L-123, 1945. (Formerly NACA ARR L5G31.)
5. Herriot, John G.: Blockage Corrections for Three-Dimensional-Flow Closed-Throat Wind Tunnels, With Considerations of the Effect of Compressibility. NACA Rep. 995, 1950. (Supersedes NACA RM A7B28.)

TABLE I.- BASIC WING COORDINATES



$\frac{y}{b/2}$	0.139		0.194		0.250		0.306		0.333		0.422		0.800		1.000	
c, cm	128.270		99.314		77.724		65.430		62.329		57.874		38.867		28.801	
$\frac{x}{c}$	$\frac{z_U}{c}$	$\frac{z_L}{c}$	$\frac{z_U}{c}$	$\frac{z_L}{c}$	$\frac{z_U}{c}$	$\frac{z_L}{c}$	$\frac{z_U}{c}$	$\frac{z_L}{c}$	$\frac{z_U}{c}$	$\frac{z_L}{c}$	$\frac{z_U}{c}$	$\frac{z_L}{c}$	$\frac{z_U}{c}$	$\frac{z_L}{c}$	$\frac{z_U}{c}$	$\frac{z_L}{c}$
0	.0317	.0317	.0281	.0281	.0327	.0327	.0291	.0291	.0294	.0294	.0225	.0225	-.0185	-.0185	-.0635	-.0635
.0025	.0418	.0213	.0432	.0233	.0415	.0235	.0388	.0190	.0367	.0204	.0318	.0132	-.0129	-.0260	-.0595	-.0717
.0050	.0450	.0182	.0471	.0197	.0464	.0186	.0437	.0155	.0408	.0163	.0351	.0103	-.0098	-.0294	-.0573	-.0732
.0100	.0497	.0137	.0531	.0148	.0523	.0144	.0474	.0122	.0448	.0131	.0395	.0073	-.0065	-.0327	-.0539	-.0755
.0200	.0558	.0083	.0596	.0096	.0598	.0092	.0538	.0066	.0490	.0082	.0437	.0033	-.0002	-.0384	-.0502	-.0802
.0300	.0602	.0044	.0639	.0059	.0654	.0057	.0582	.0031	.0530	.0054	.0472	.0000	.0019	-.0414	-.0471	-.0838
.0400	.0636	.0012	.0673	.0031	.0693	.0023	.0609	-.0006	.0557	.0036	.0494	-.0020	.0039	-.0435	-.0441	-.0850
.0500	.0667	-.0012	.0701	.0008	.0719	-.0010	.0631	-.0023	.0579	.0015	.0516	-.0041	.0064	-.0439	-.0440	-.0855
.0750	.0735	-.0065	.0750	-.0041	.0771	-.0049	.0672	-.0066	.0623	-.0020	.0557	-.0075	.0098	-.0441	-.0379	-.0838
.1000	.0778	-.0101	.0788	-.0079	.0794	-.0088	.0695	-.0089	.0660	-.0051	.0595	-.0102	.0146	-.0454	-.0340	-.0836
.1500	.0851	-.0152	.0836	-.0141	.0835	-.0123	.0749	-.0120	.0718	-.0089	.0653	-.0143	.0212	-.0454	-.0264	-.0794
.2000	.0901	-.0190	.0867	-.0179	.0858	-.0141	.0776	-.0144	.0758	-.0108	.0691	-.0154	.0262	-.0438	-.0195	-.0764
.2500	.0923	-.0208	.0885	-.0199	.0876	-.0147	.0804	-.0151	.0775	-.0116	.0724	-.0157	.0325	-.0425	-.0123	-.0713
.3000	.0931	-.0218	.0893	-.0205	.0879	-.0144	.0815	-.0146	.0795	-.0117	.0746	-.0149	.0359	-.0393	-.0066	-.0672
.3500	.0929	-.0220	.0887	-.0192	.0882	-.0137	.0829	-.0136	.0807	-.0105	.0755	-.0140	.0393	-.0370	-.0008	-.0617
.4000	.0917	-.0218	.0872	-.0169	.0873	-.0118	.0823	-.0116	.0811	-.0082	.0762	-.0118	.0432	-.0337	.0052	-.0559
.4500	.0899	-.0200	.0854	-.0143	.0863	-.0092	.0815	-.0093	.0810	-.0061	.0759	-.0096	.0457	-.0306	.0113	-.0508
.5000	.0877	-.0160	.0831	-.0110	.0853	-.0057	.0811	-.0062	.0803	-.0038	.0757	-.0060	.0479	-.0256	.0172	-.0442
.5500	.0842	-.0105	.0806	-.0070	.0833	-.0013	.0800	-.0023	.0795	.0000	.0757	-.0017	.0505	-.0199	.0228	-.0386
.6000	.0807	-.0059	.0780	-.0028	.0807	.0033	.0788	.0027	.0784	.0057	.0755	.0028	.0523	-.0133	.0284	-.0317
.6500	.0758	.0008	.0749	.0026	.0783	.0068	.0776	.0089	.0774	.0133	.0746	.0110	.0545	-.0055	.0340	-.0220
.7000	.0716	.0071	.0739	.0090	.0748	.0144	.0747	.0163	.0761	.0217	.0737	.0204	.0564	.0060	.0381	-.0086
.7500	.0670	.0137	.0668	.0161	.0714	.0219	.0718	.0248	.0741	.0319	.0717	.0300	.0581	.0174	.0425	.0044
.8000	.0626	.0192	.0624	.0226	.0667	.0286	.0681	.0326	.0711	.0408	.0691	.0389	.0575	.0263	.0441	.0150
.8500	.0560	.0253	.0568	.0279	.0614	.0343	.0637	.0388	.0672	.0473	.0658	.0455	.0566	.0344	.0441	.0237
.9000	.0497	.0275	.0504	.0294	.0556	.0373	.0586	.0427	.0622	.0503	.0612	.0483	.0523	.0388	.0439	.0294
.9500	.0418	.0267	.0427	.0281	.0487	.0350	.0524	.0404	.0557	.0412	.0541	.0441	.0458	.0356	.0382	.0289
.9700	.0384	.0255	.0394	.0269	.0458	.0340	.0493	.0384	.0530	.0409	.0509	.0408	.0422	.0326	.0344	.0244
.9800	.0364	.0246	.0381	.0258	.0444	.0327	.0479	.0373	.0511	.0404	.0491	.0384	.0408	.0314	.0301	.0212
.9900	.0347	.0236	.0361	.0253	.0425	.0320	.0462	.0357	.0489	.0376	.0467	.0364	.0388	.0278	.0282	.0184
.9950	.0335	.0232	.0353	.0251	.0422	.0317	.0458	.0349	.0475	.0367	.0455	.0351	.0376	.0262	.0258	.0159
1.0000	.0332	.0226	.0345	.0243	.0415	.0310	.0450	.0344	.0463	.0360	.0444	.0342	.0359	.0250	.0247	.0143
R_{le}/c	.0198		.0210		.0212		.0186		.0155		.0149		.0091		.0031	

TABLE II.- GEOMETRIC CHARACTERISTICS

Wing:

Area, m ²	1.97
Mean aerodynamic chord, cm	57.86
Span, cm	365.76
Aspect ratio	6.78
Taper ratio	0.36
Dihedral angle, deg	-1.71

Horizontal tail:

Area, m ²	0.76
Mean aerodynamic chord, cm	54.87
Span, cm	164
Aspect ratio	3.55
Dihedral angle, deg	5.41

Vertical tail:

Area, m ²	0.50
Mean aerodynamic chord, cm	66.80
Span, cm	81

TABLE III.- LEADING-EDGE SLAT COORDINATES

x/c_s	z_u/c_s	z_l/c_s	z_u/c_s	z_l/c_s
	$\frac{y}{b/2} = 0.320; c_s = 9.455 \text{ cm}$		$\frac{y}{b/2} = 1.000; c_s = 4.321 \text{ cm}$	
0	-0.0122	-0.0122	-0.0837	-0.0837
.0125	.0217	-.0351	-.0564	-.1000
.0250	.0366	-.0429	-.0444	-.1041
.0500	.0574	-.0505	-.0270	-.1064
.0750	.0740	-.0538	-.0134	-.1073
.1000	.0887	-.0542	-.0012	-.1061
.1500	.1109	-.0495	.0176	-.0998
.2000	.1277	-.0417	.0326	-.0897
.3000	.1467	-.0238	.0514	-.0682
.4000	.1506	-.0062	.0607	-.0485
.5000	.1461	.0110	.0647	-.0300
.6000	.1320	.0237	.0620	-.0129
.7000	.1076	.0281	.0531	-.0015
.8000	.0776	.0261	.0400	.0031
.9000	.0436	.0170	.0234	.0035
.9500	.0254	.0094	.0138	.0021
1.0000	.0062	0	.0043	0

TABLE IV. - VANE COORDINATES

x/c_v	z_u/c_v	z_l/c_v	z_u/c_v	z_l/c_v	z_u/c_v	z_l/c_v
	$c_v = 10.795 \text{ cm}; \frac{y}{b/2} = 0.0139$		$c_v = 9.455; \frac{y}{b/2}$	$c_v = 0.320 \frac{y}{b/2}$	$c_v = 4.321 \text{ cm}; \frac{y}{b/2}$	$c_v = 1.000 \frac{y}{b/2}$
0	-0.0049	-0.0049	-0.0122	-0.0122	-0.0837	-0.0837
.0125	.0300	-.0280	.0217	-.0351	-.0564	-.1000
.0250	.0450	-.0366	.0366	-.0429	-.0444	-.1041
.0500	.0663	-.0446	.0574	-.0505	-.0270	-.1064
.0750	.0832	-.0480	.0740	-.0538	-.0134	-.1073
.1000	.0982	-.0487	.0887	-.0542	-.0012	-.1061
.1500	.1210	-.0442	.1109	-.0495	.0176	-.0998
.2000	.1379	-.0366	.1277	-.0417	.0326	-.0897
.3000	.1547	-.0190	.1467	-.0238	.0514	-.0682
.4000	.1600	-.0016	.1506	-.0062	.0607	-.0485
.5000	.1546	.0150	.1461	.0110	.0647	-.0300
.6000	.1394	.0275	.1320	.0237	.0620	-.0129
.7000	.1135	.0312	.1076	.0281	.0531	-.0015
.8000	.0815	.0295	.0776	.0261	.0400	.0031
.9000	.0457	.0187	.0436	.0170	.0234	.0035
.9500	.0267	.0102	.0254	.0094	.0138	.0021
1.0000	.0065	0	.0062	0	.0043	0

TABLE V.- FLAP COORDINATES

x/c_f	z_u/c_f	z_l/c_f	z_u/c_f	z_l/c_f	z_u/c_f	z_l/c_f
	$c_f = 34.392 \text{ cm}; \frac{y}{b/2} = 0.139$	$c_f = 22.060 \text{ cm}; \frac{y}{b/2} = 0.320$	$c_f = 10.081 \text{ cm}; \frac{y}{b/2} = 1.000$			
0	0.0754	0.0754	0.0903	0.0903	-0.0252	-0.0252
.0100	.1012	.0572	.1184	.0708	-.0016	-.0393
.0200	.1130	.0535	.1296	.0651	.0072	-.0423
.0400	.1307	.0499	.1456	.0596	.0211	-.0452
.0600	.1433	.0499	.1570	.0576	.0317	-.0450
.1000	.1647	.0554	.1741	.0594	.0496	-.0380
.1500	.1824	.0613	.1900	.0669	.0675	-.0244
.2000	.1950	.0679	.1984	.0751	.0821	-.0115
.2500	.2016	.0727	.2030	.0843	.0950	.0006
.3000	.2053	.0790	.2048	.0938	.1046	.0124
.3517	.2072	.0857	.2054	.1035	.1115	.0233
.4189	.2049	.0931	.2030	.1155	.1179	.0373
.4851	.2001	.0982	.1991	.1255	.1228	.0495
.5458	.1950	.1016	.1947	.1336	.1260	.0605
.6160	.1869	.1033	.1890	.1395	.1264	.0706
.6811	.1758	.1033	.1820	.1424	.1256	.0787
.7451	.1669	.1016	.1745	.1414	.1229	.0830
.8089	.1569	.0997	.1668	.1365	.1160	.0816
.8717	.1455	.0975	.1572	.1279	.1061	.0763
.9337	.1352	.0923	.1459	.1166	.0906	.0631
1.0000	.1237	.0842	.1312	.1028	.0691	.0403

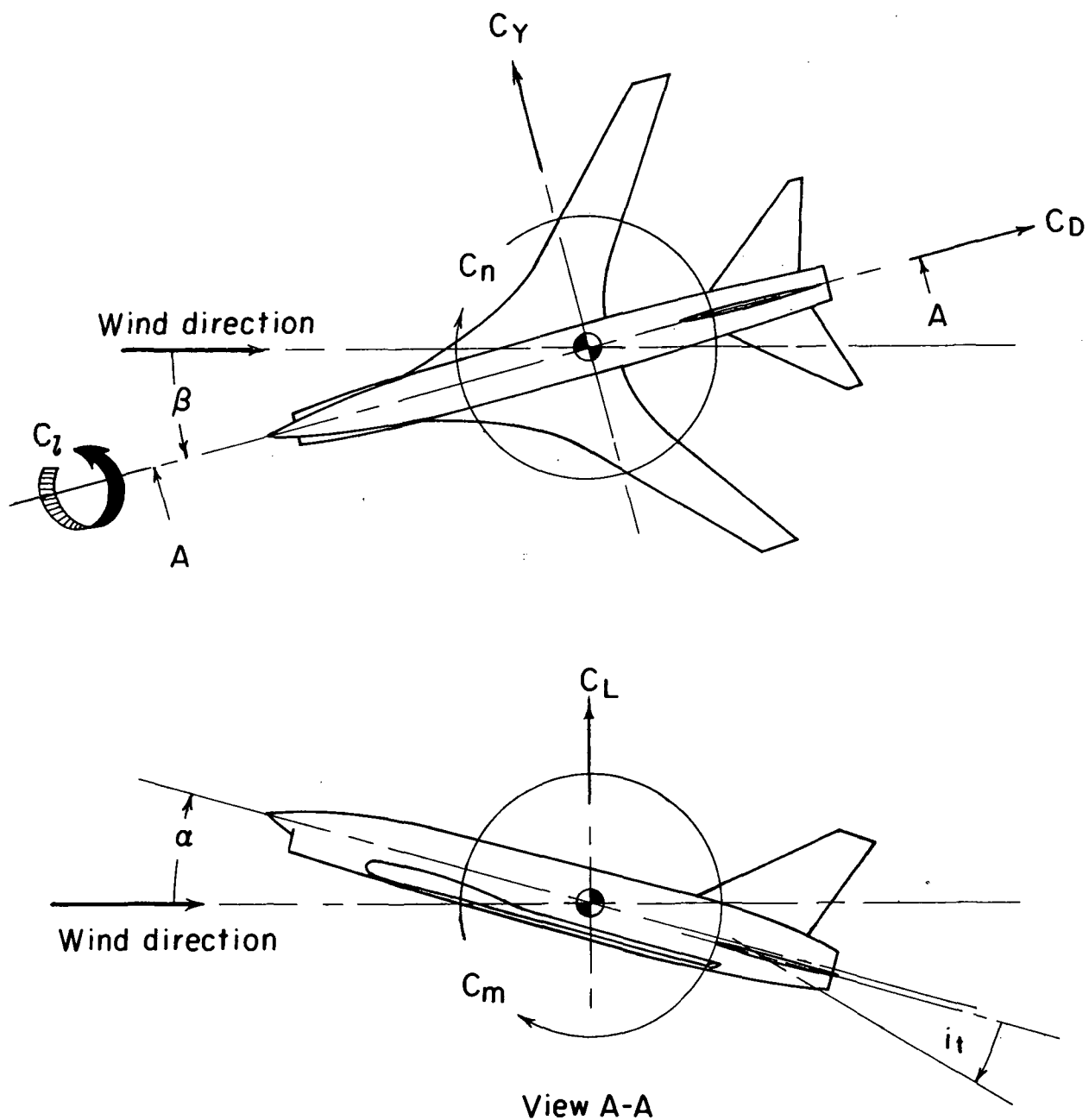
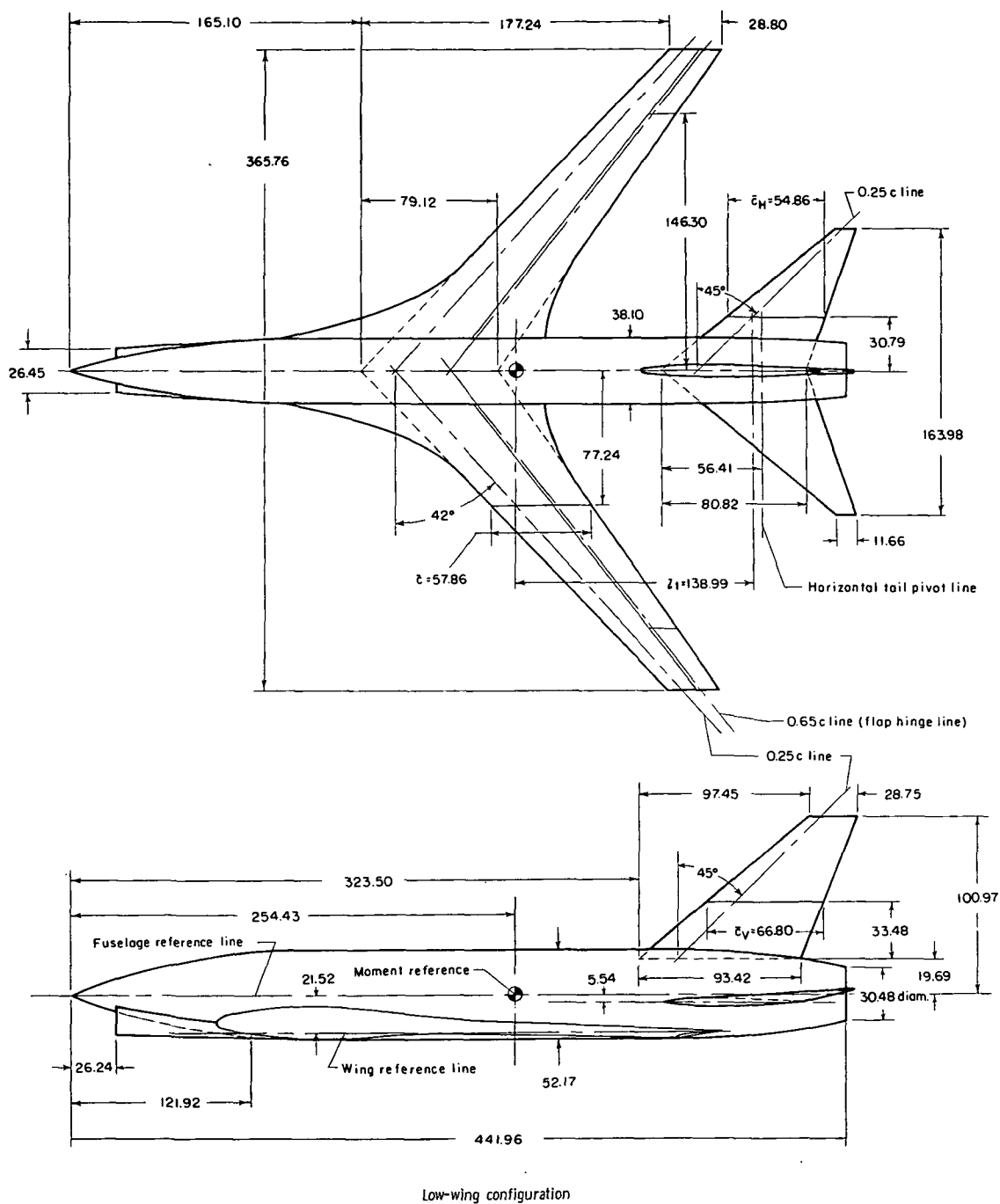
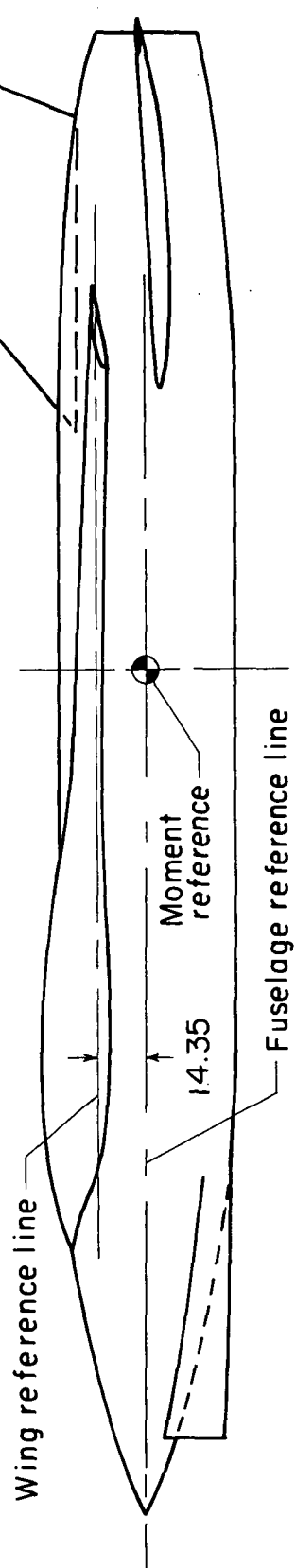


Figure 1.- System of axes. Positive directions of forces, moments, and angles are indicated by arrows.



(a) Complete model geometric characteristics.

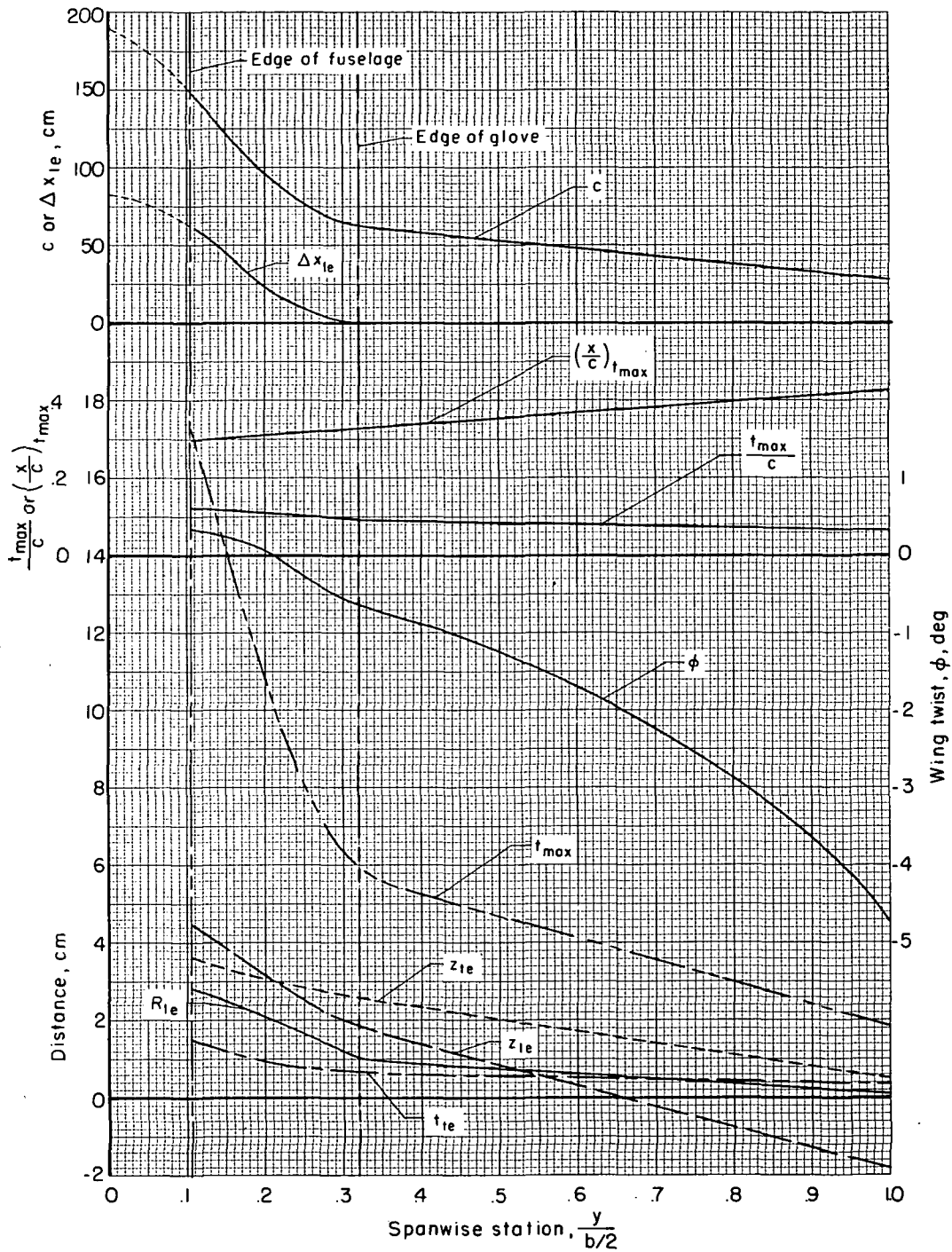
Figure 2.- Details of model. All dimensions are given in centimeters.



High-wing configuration

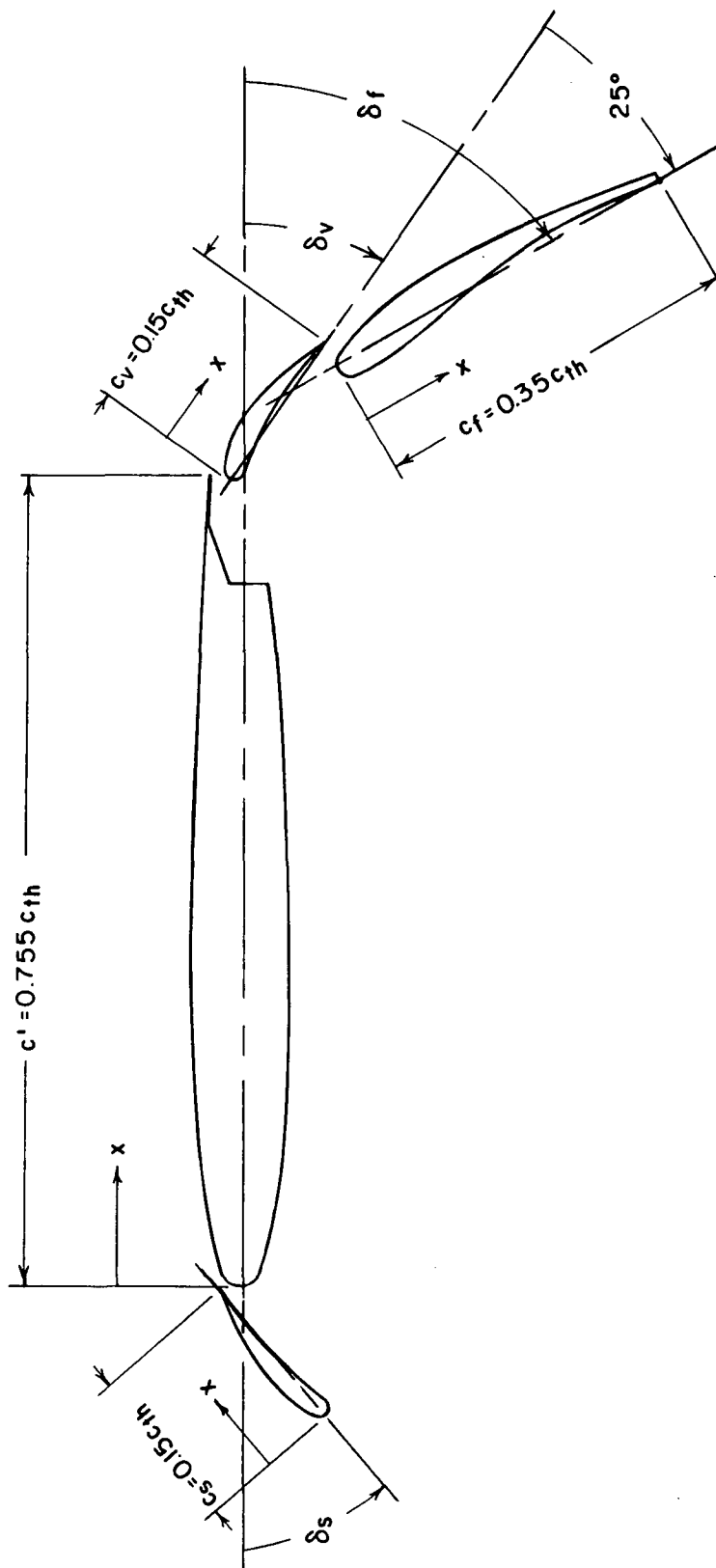
(a) Concluded.

Figure 2.- Continued.



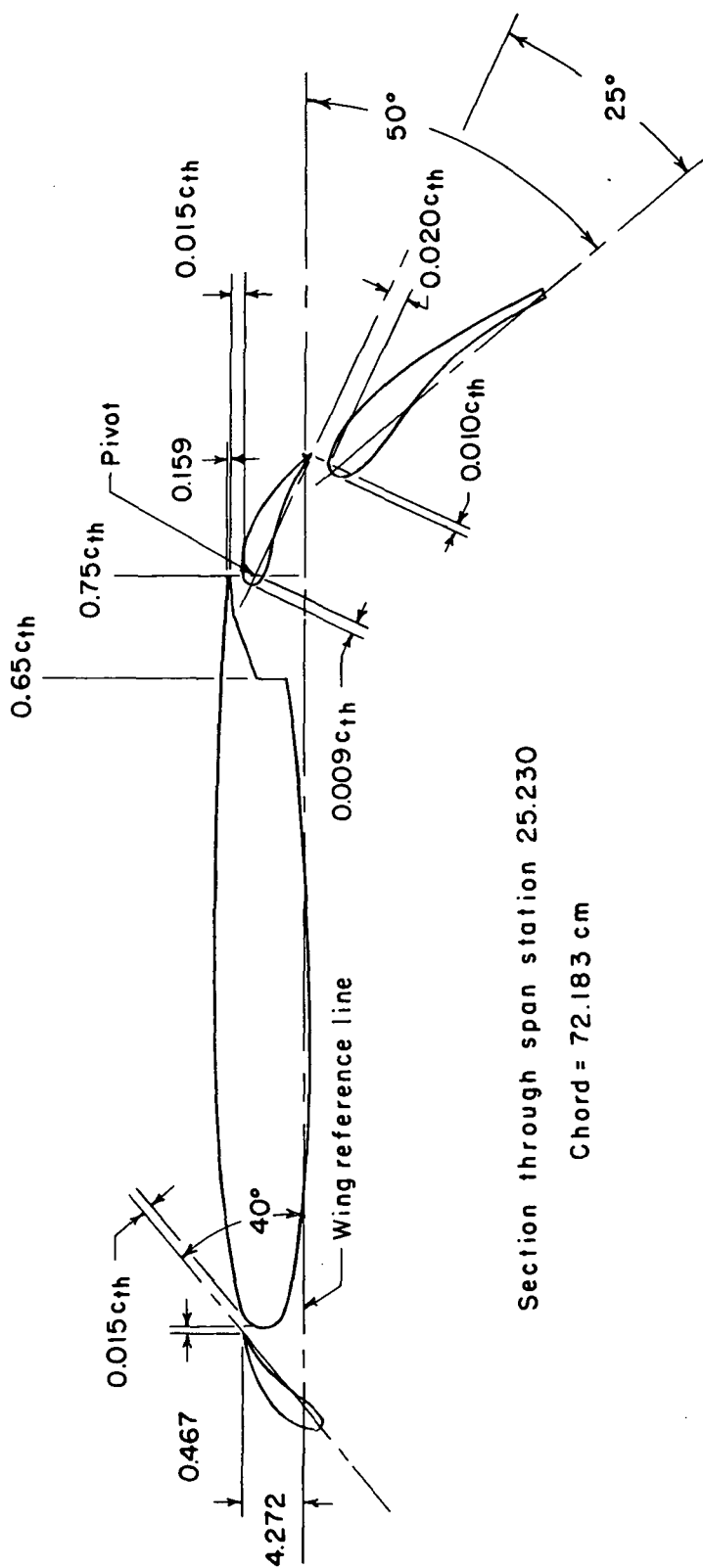
(b) Wing spanwise details.

Figure 2.- Continued.



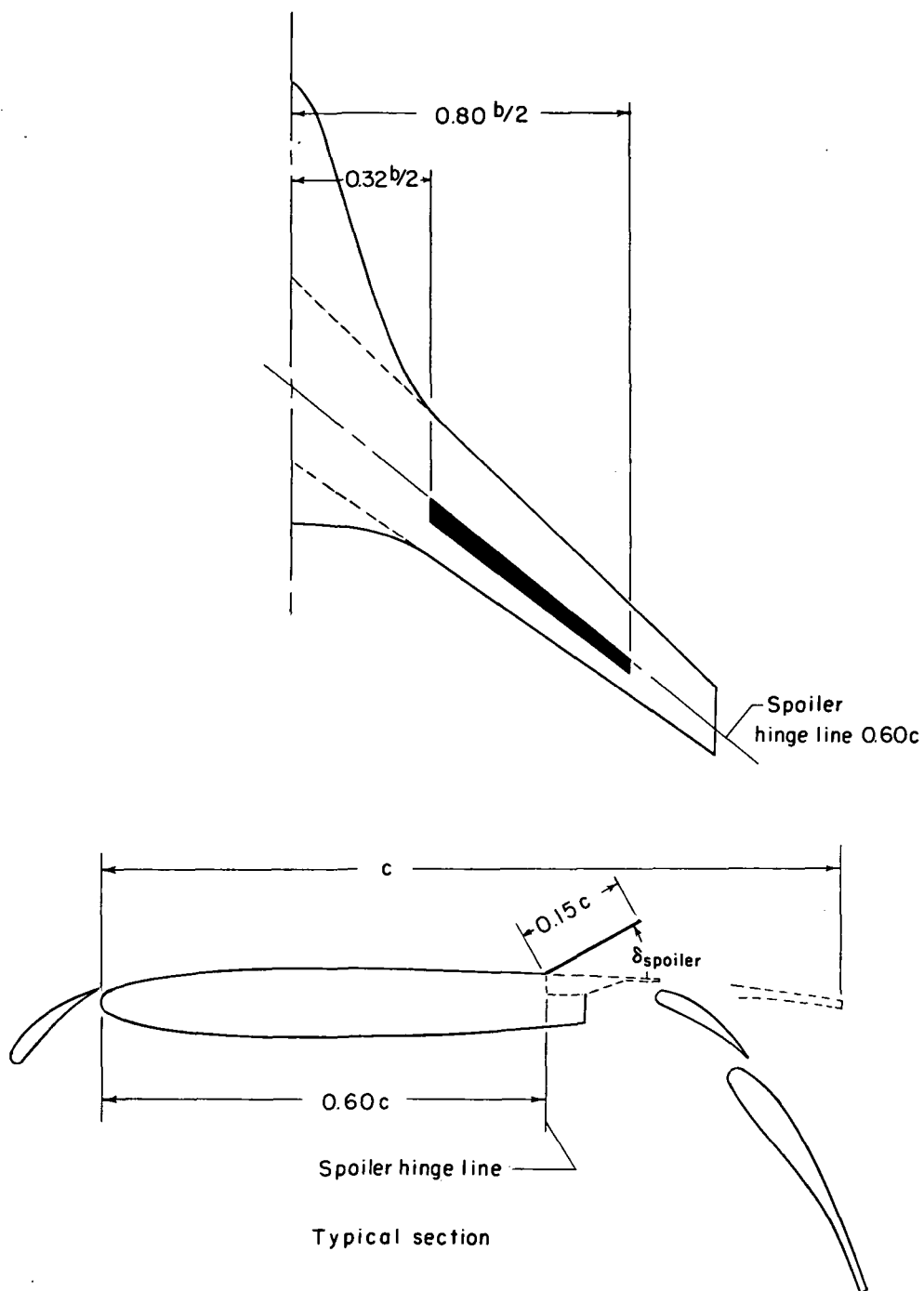
(c) Details of flap and slat system.

Figure 2.- Continued.



(c) Concluded.

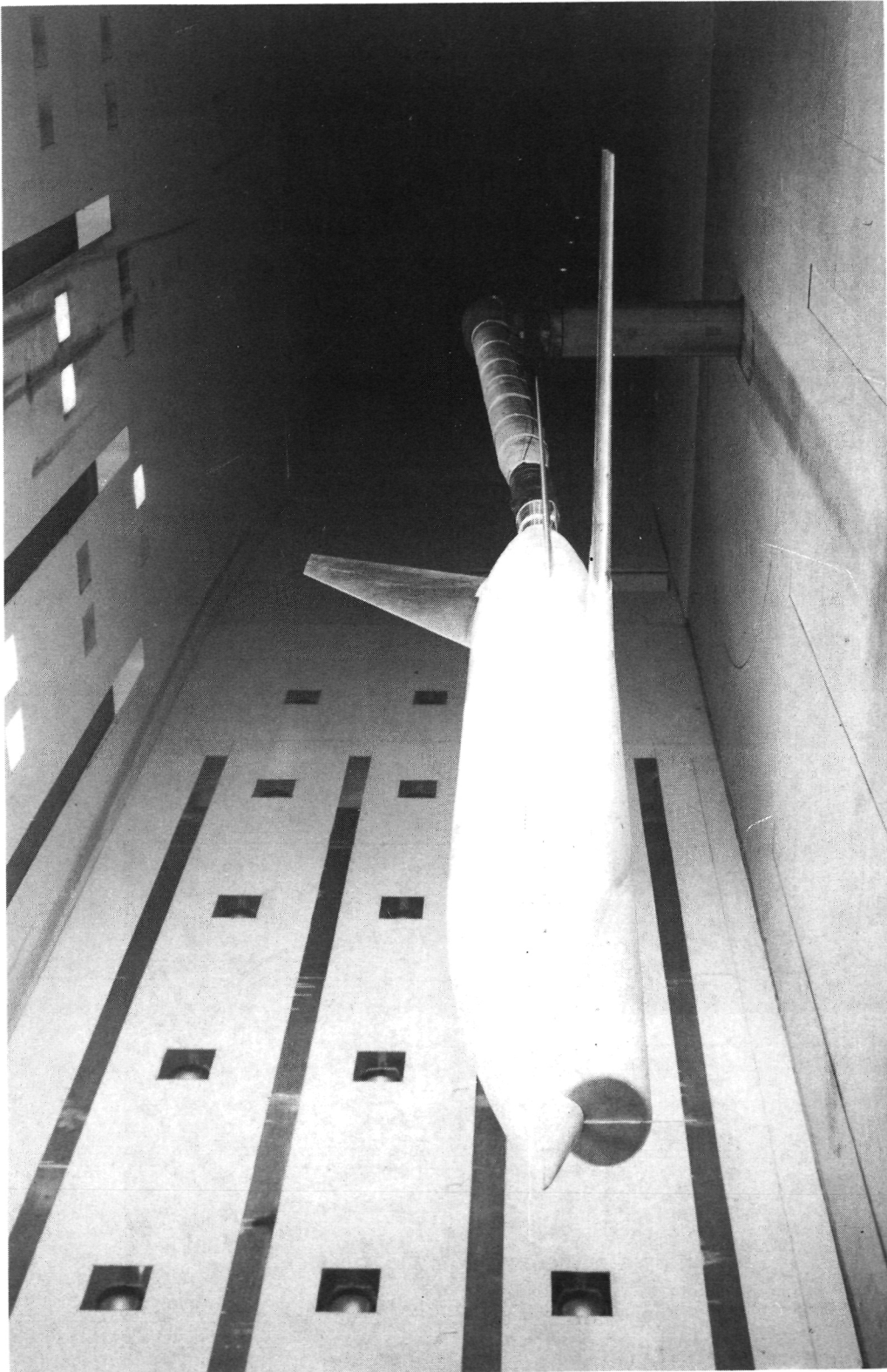
Figure 2. - Continued.



(d) Spoiler description and location.

Figure 2.- Concluded.

~~CONFIDENTIAL~~



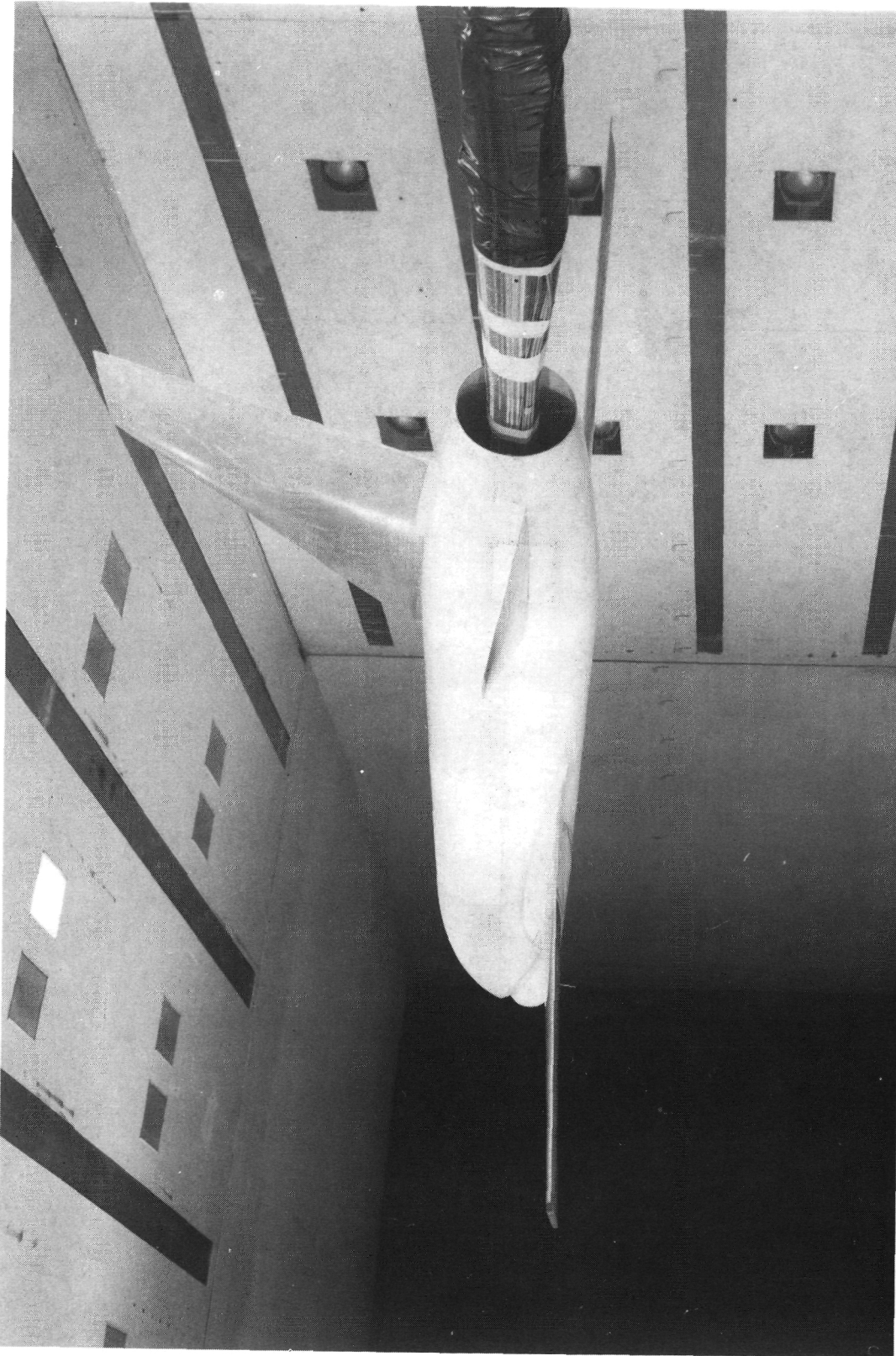
L-71-7558

(a) Low-wing model in clean configuration.

Figure 3.- Photographs of various model configurations.

~~CONFIDENTIAL~~

~~CONFIDENTIAL~~



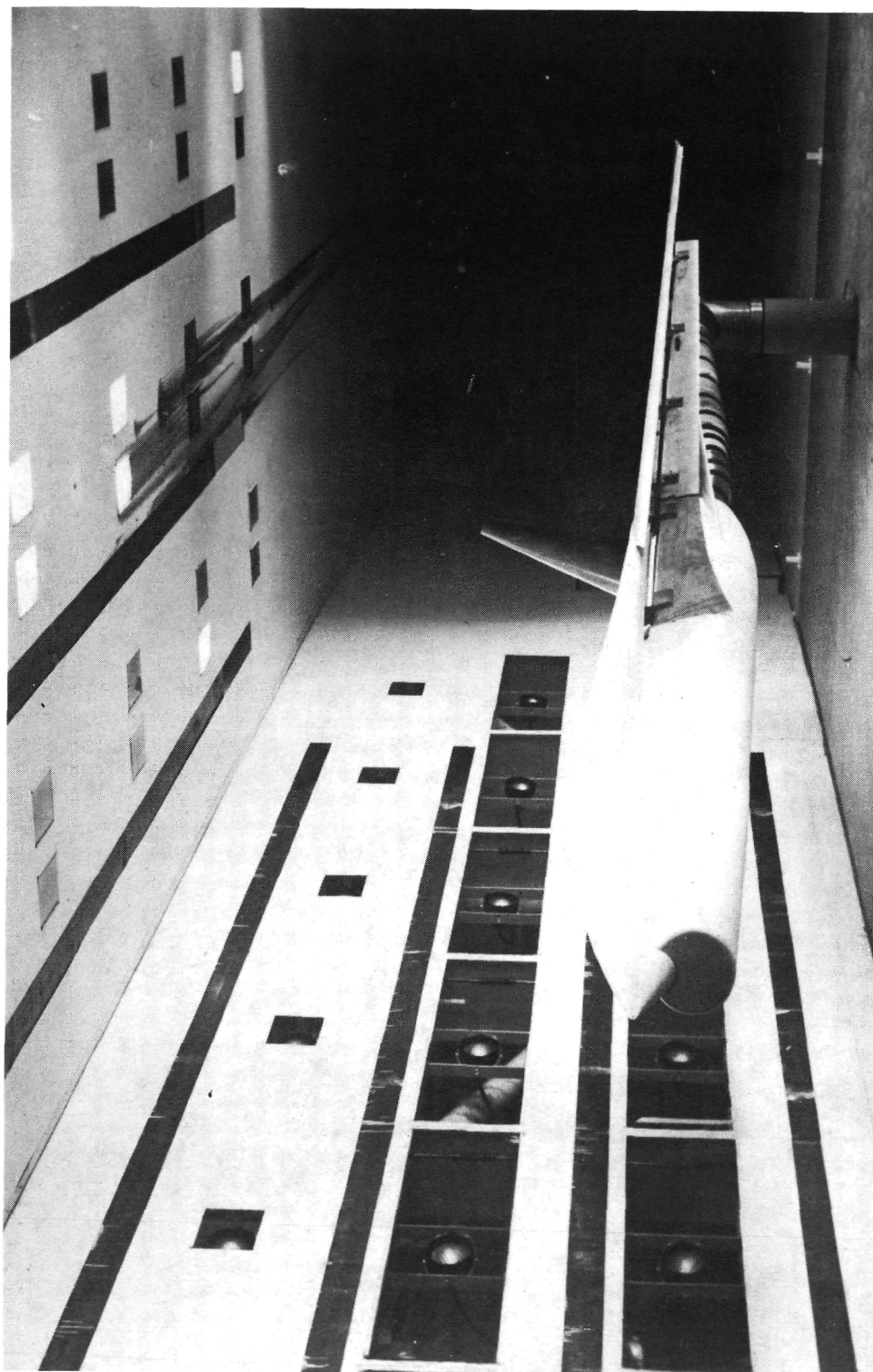
L-71-7560

(a) Concluded.

Figure 3.- Continued.

~~CONFIDENTIAL~~

~~CONFIDENTIAL~~

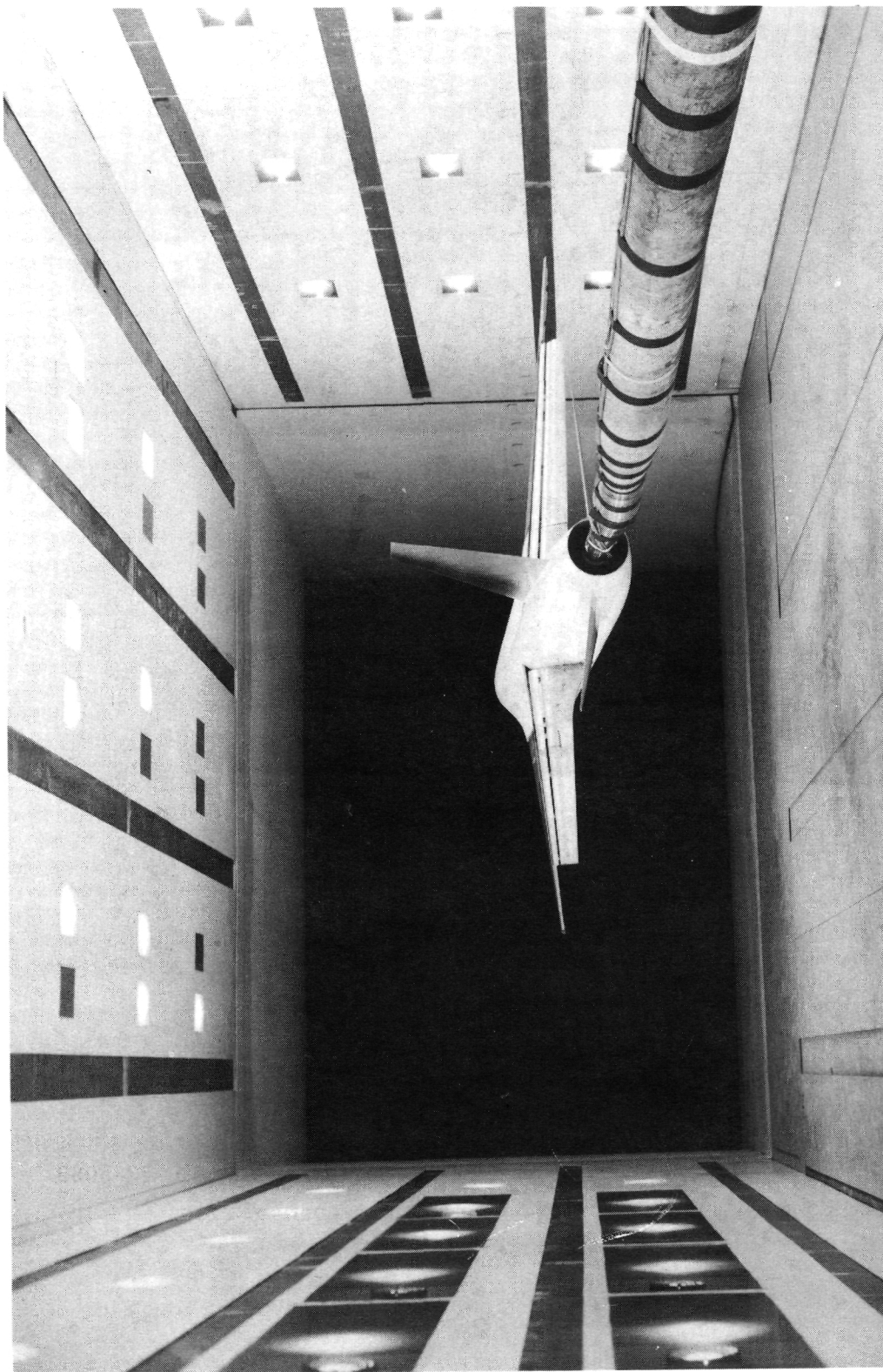


L-70-8828

(b) High-wing model in landing configuration.

Figure 3.- Continued.

~~CONFIDENTIAL~~

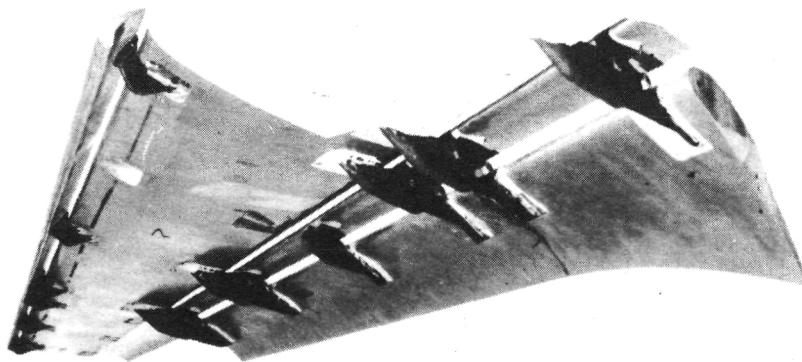
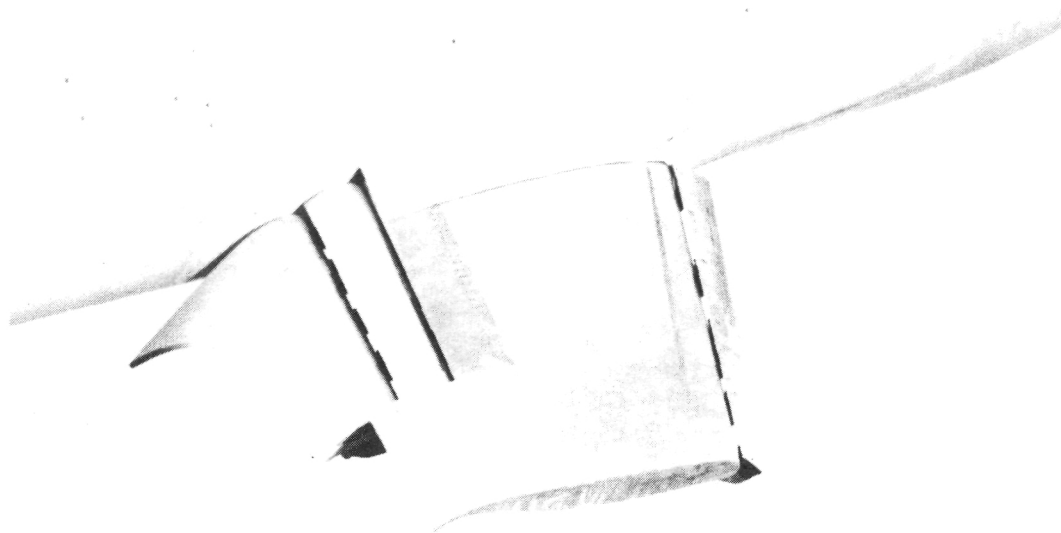


L-70-8831

(b) Concluded.

Figure 3.- Continued.

~~CONFIDENTIAL~~



L-73-3089

(c) Closeup of high-lift system for take-off configuration.

Figure 3.- Concluded.

~~CONFIDENTIAL~~

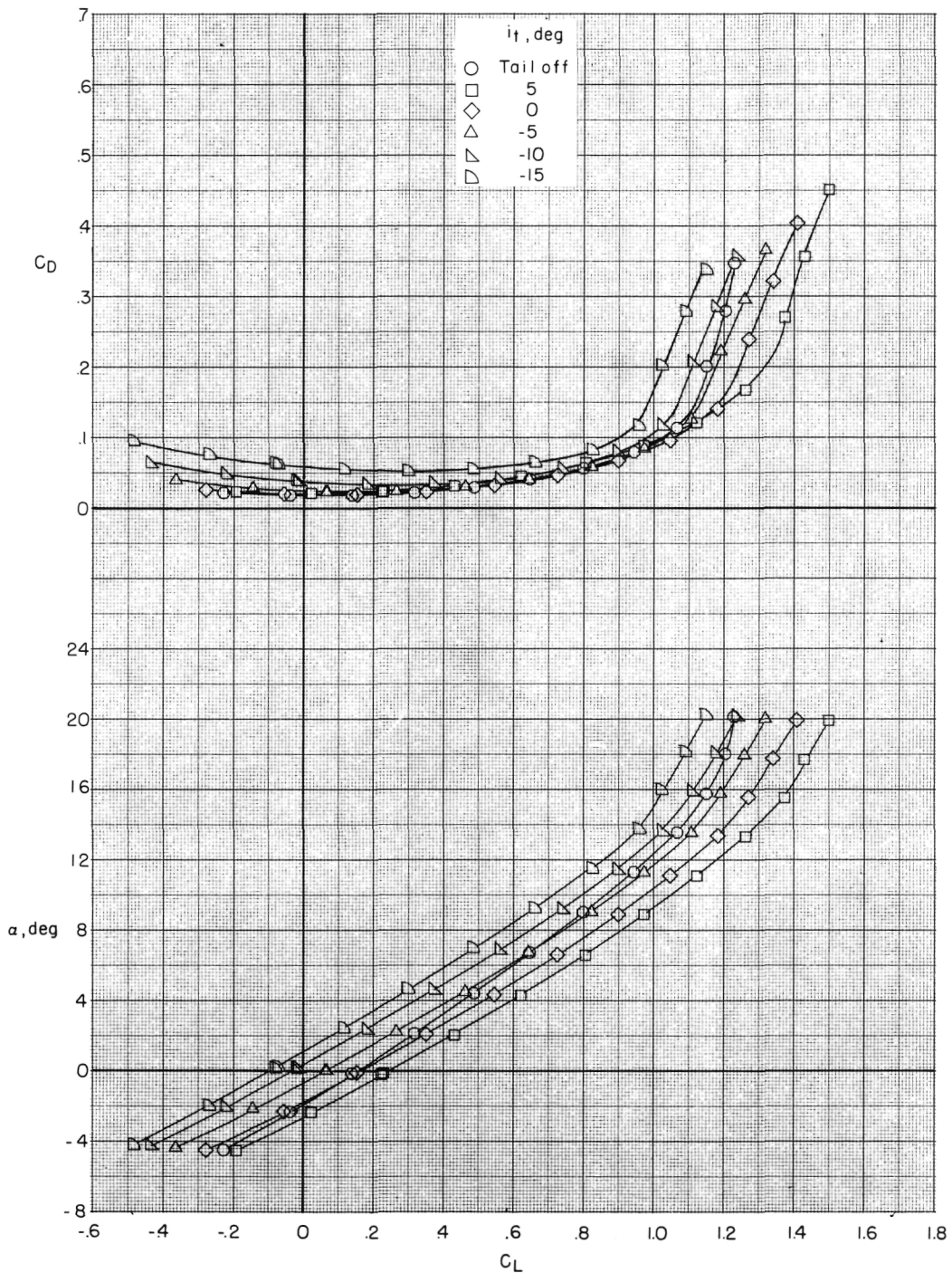


Figure 4.- Effect of horizontal-stabilizer deflection on longitudinal aerodynamic characteristics of low-wing model in clean configuration. $\delta_f = 0^\circ$; $\delta_s = \text{Off}$.

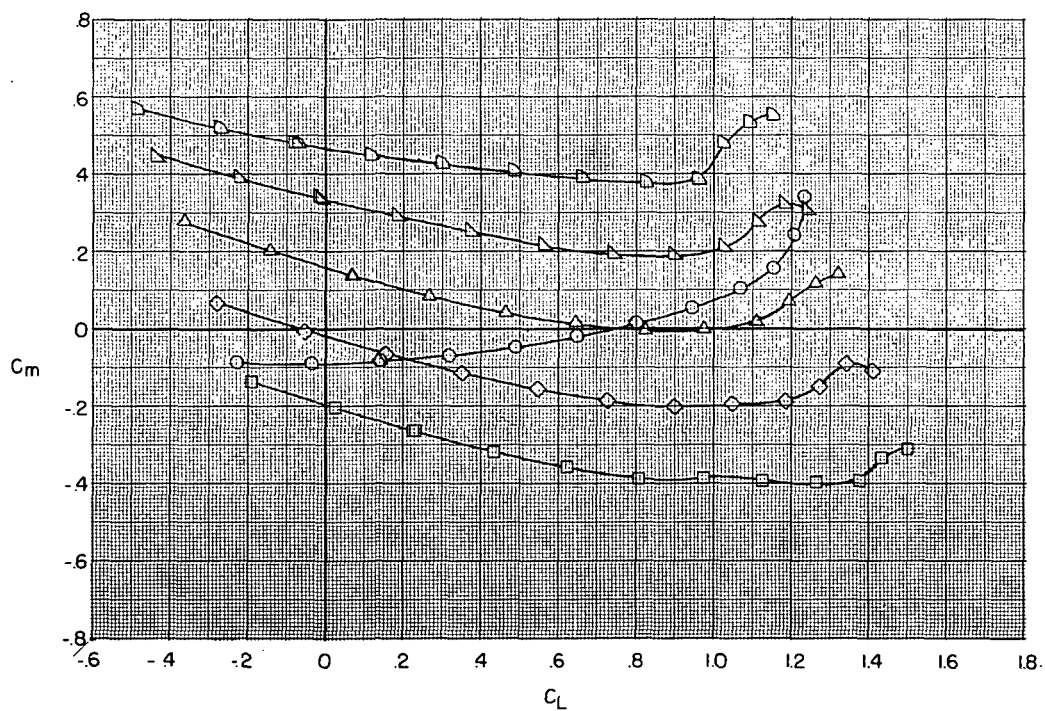
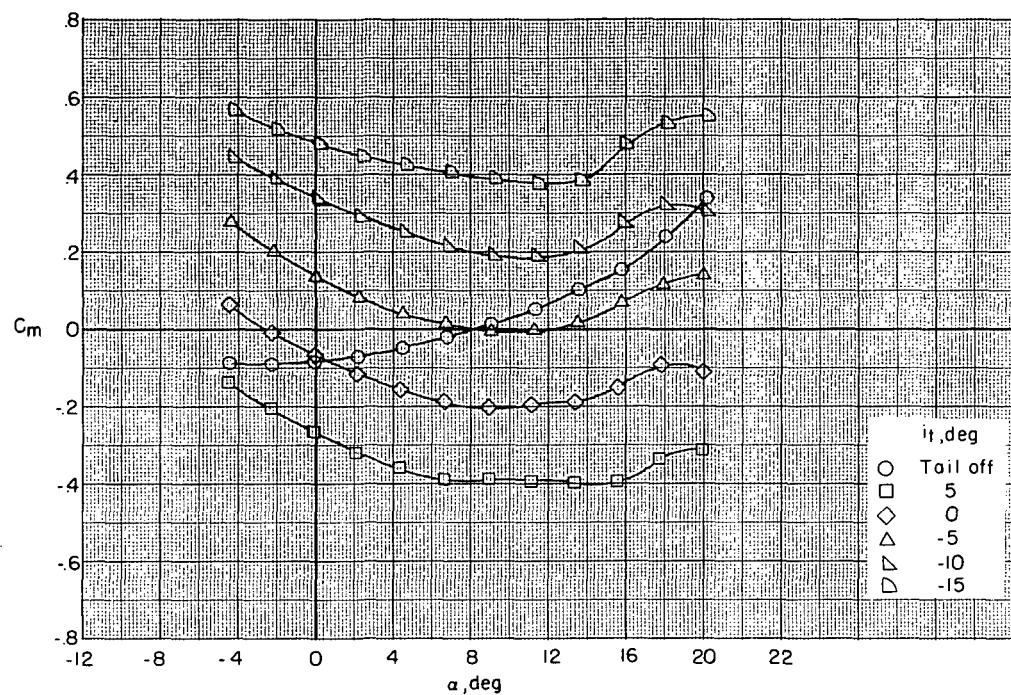


Figure 4.- Concluded.

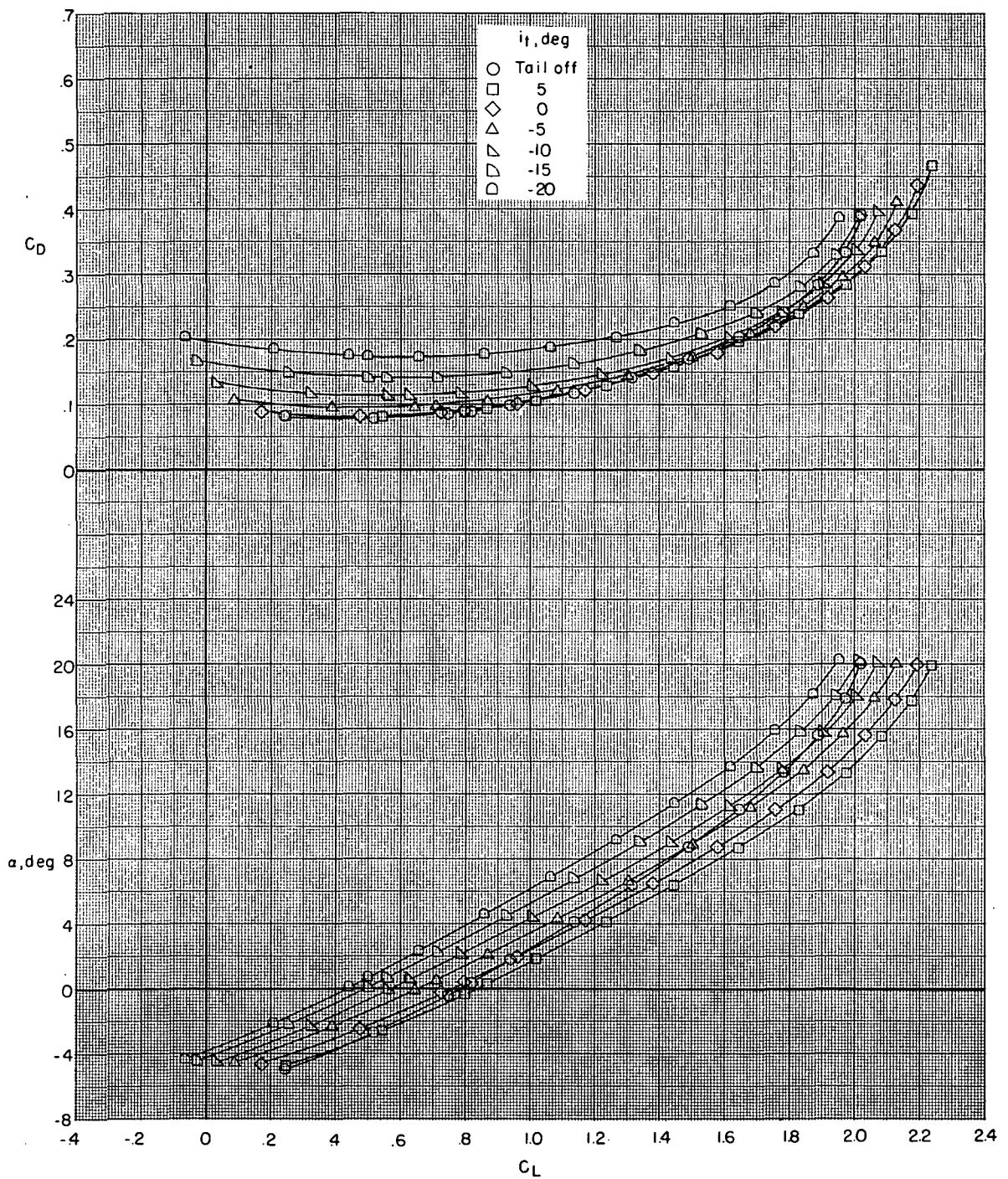


Figure 5.- Effect of horizontal-stabilizer deflection on longitudinal aerodynamic characteristics of low-wing model in take-off configuration. $\delta_f = 20^\circ$; $\delta_s = 40^\circ$.

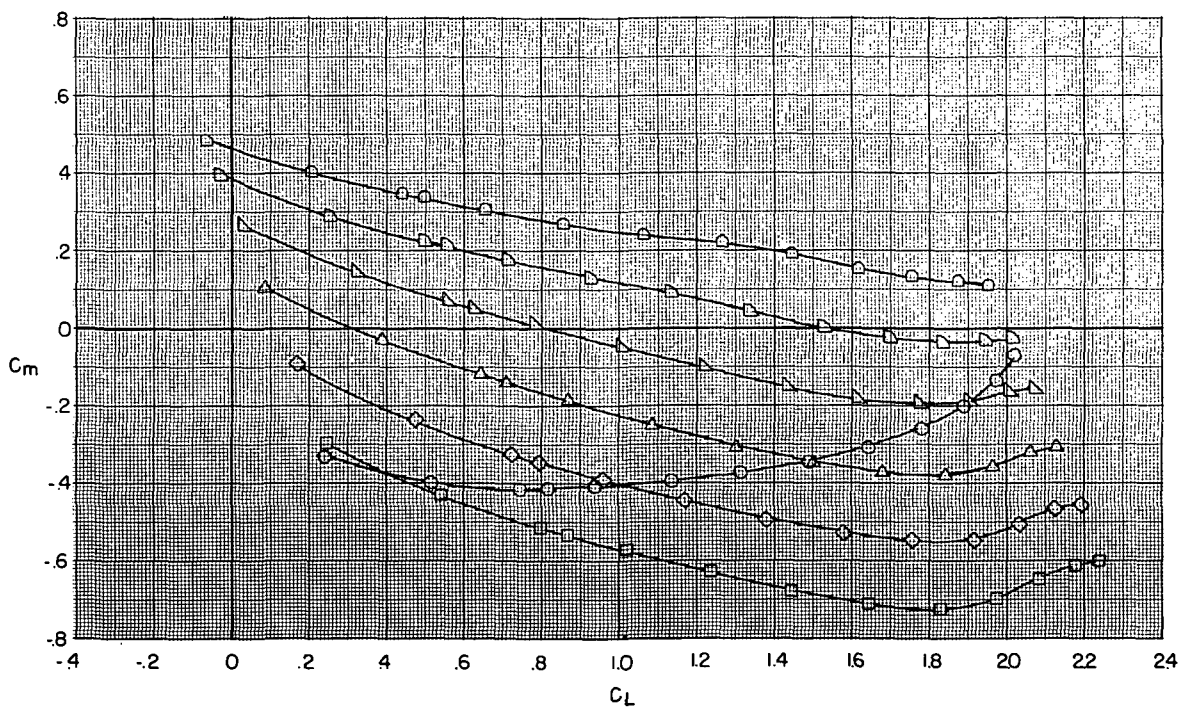
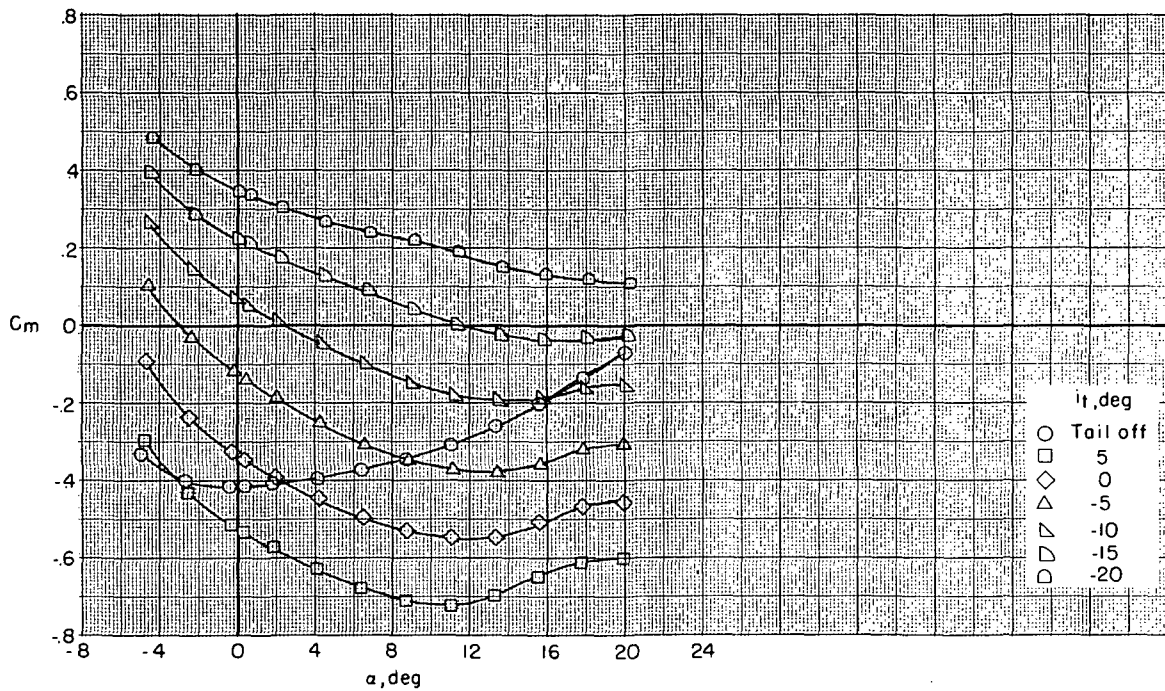


Figure 5.- Concluded.

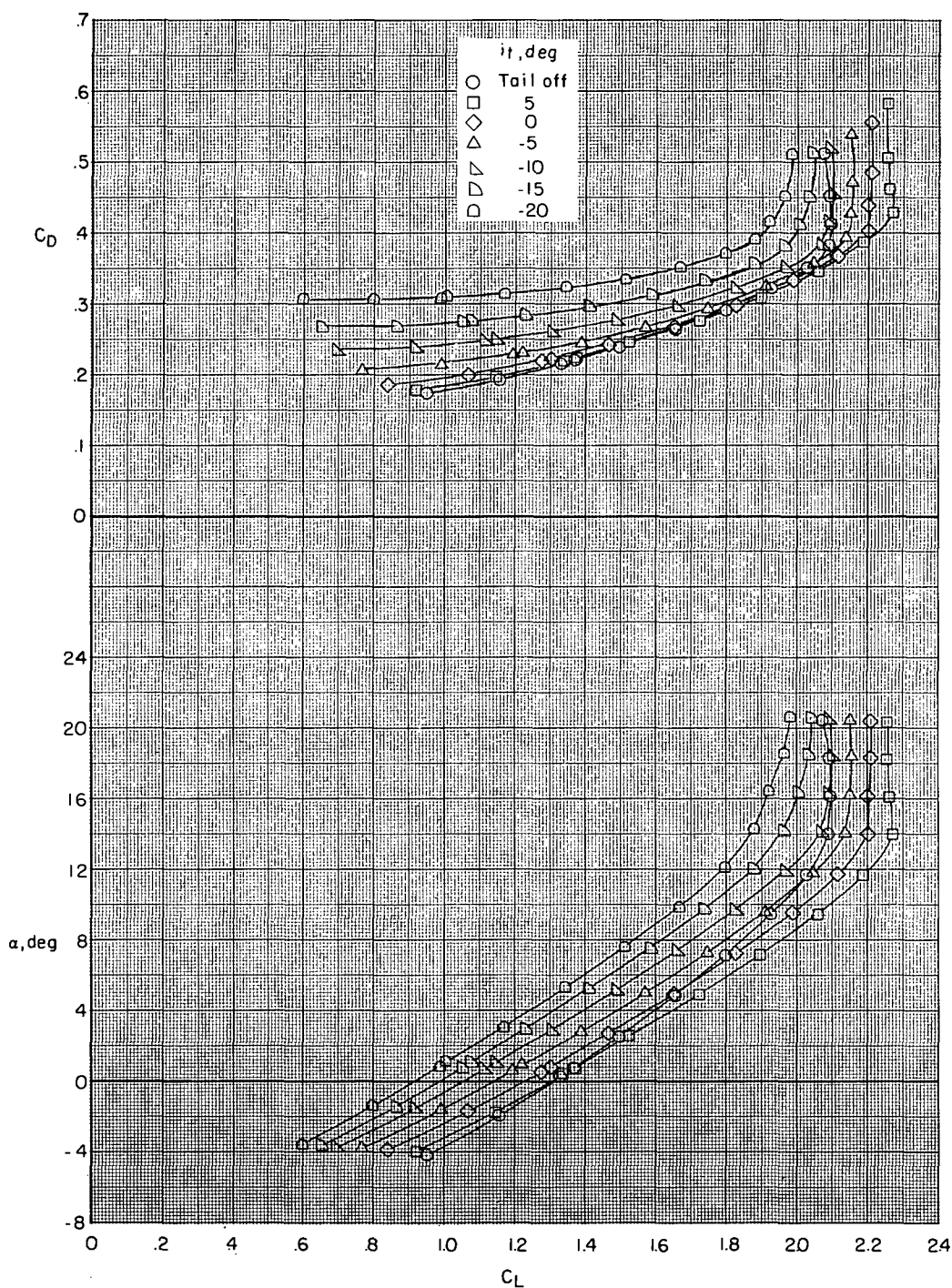


Figure 6.- Effect of horizontal-stabilizer deflection on longitudinal aerodynamic characteristics of low-wing model in landing configuration. $\delta_f = 40^\circ$; $\delta_s = 50^\circ$.

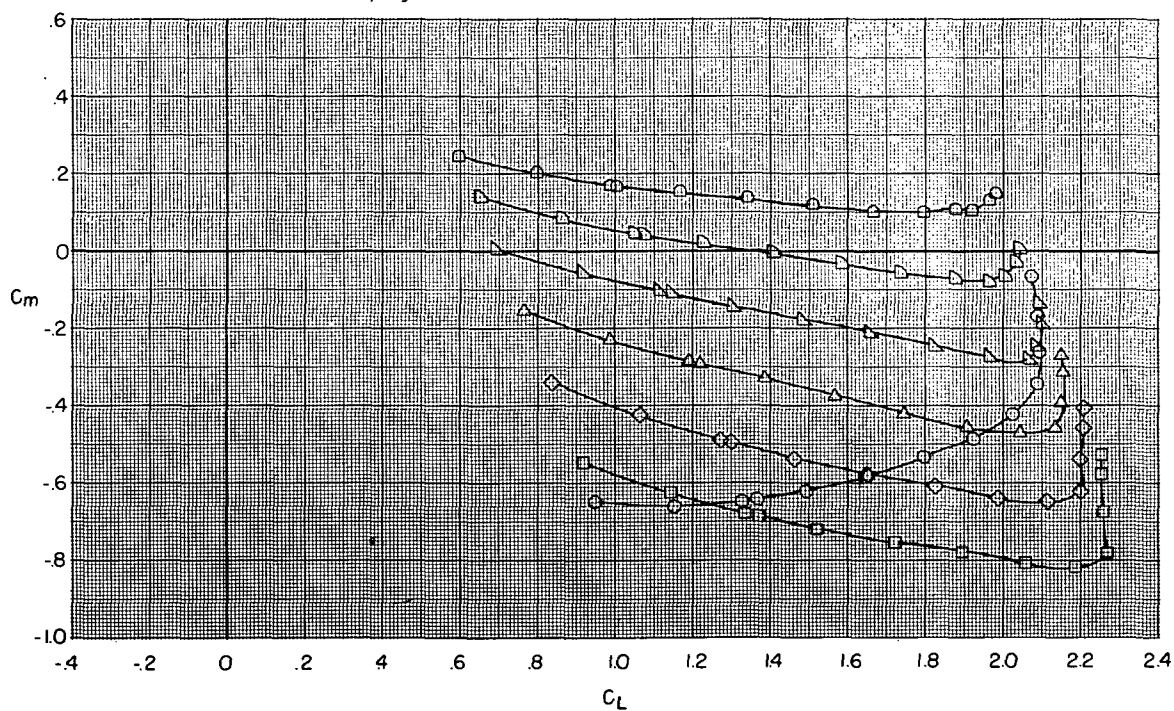
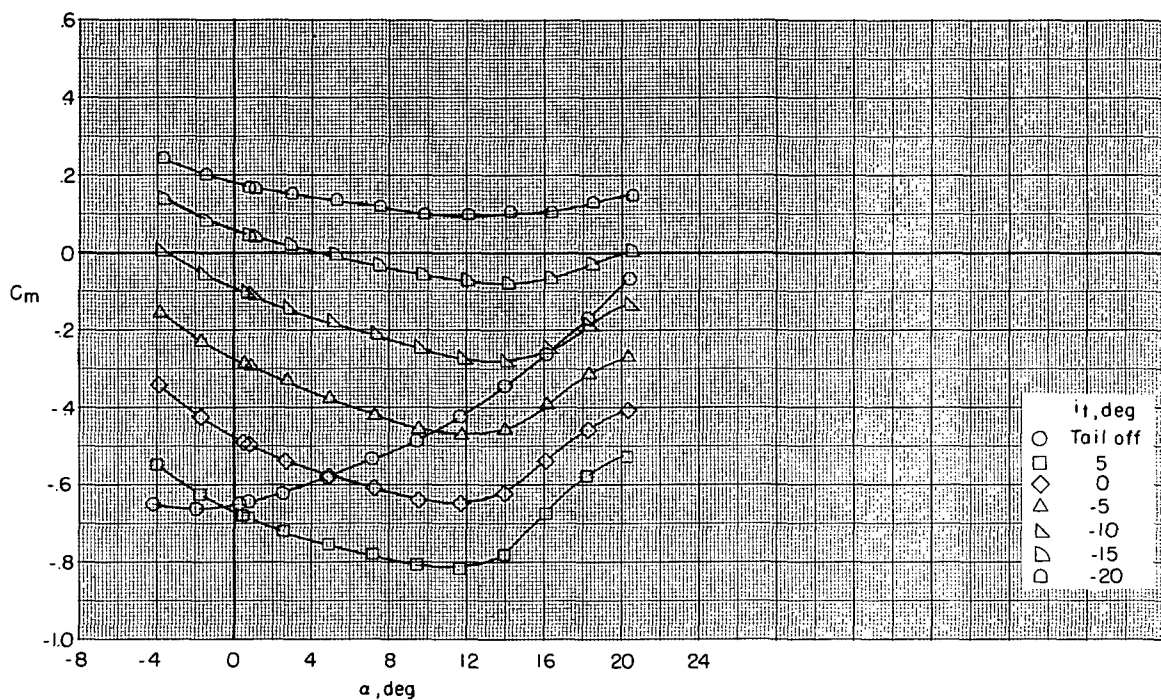


Figure 6. - Concluded.

~~CONFIDENTIAL~~

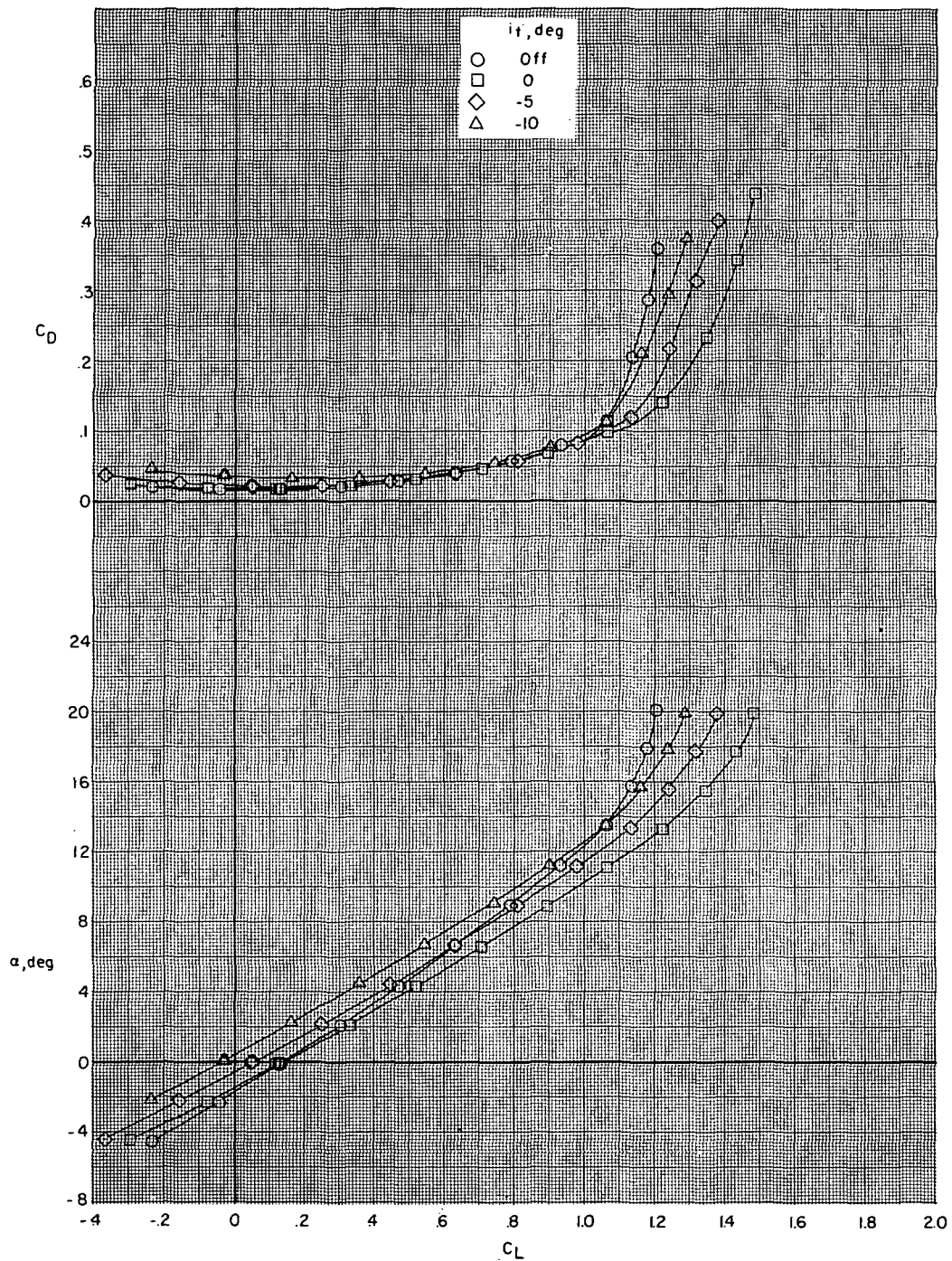


Figure 7.- Effect of horizontal-stabilizer deflection on longitudinal aerodynamic characteristics of high-wing model in clean configuration. $\delta_f = 0^\circ$; $\delta_s = \text{Off}$.

~~CONFIDENTIAL~~

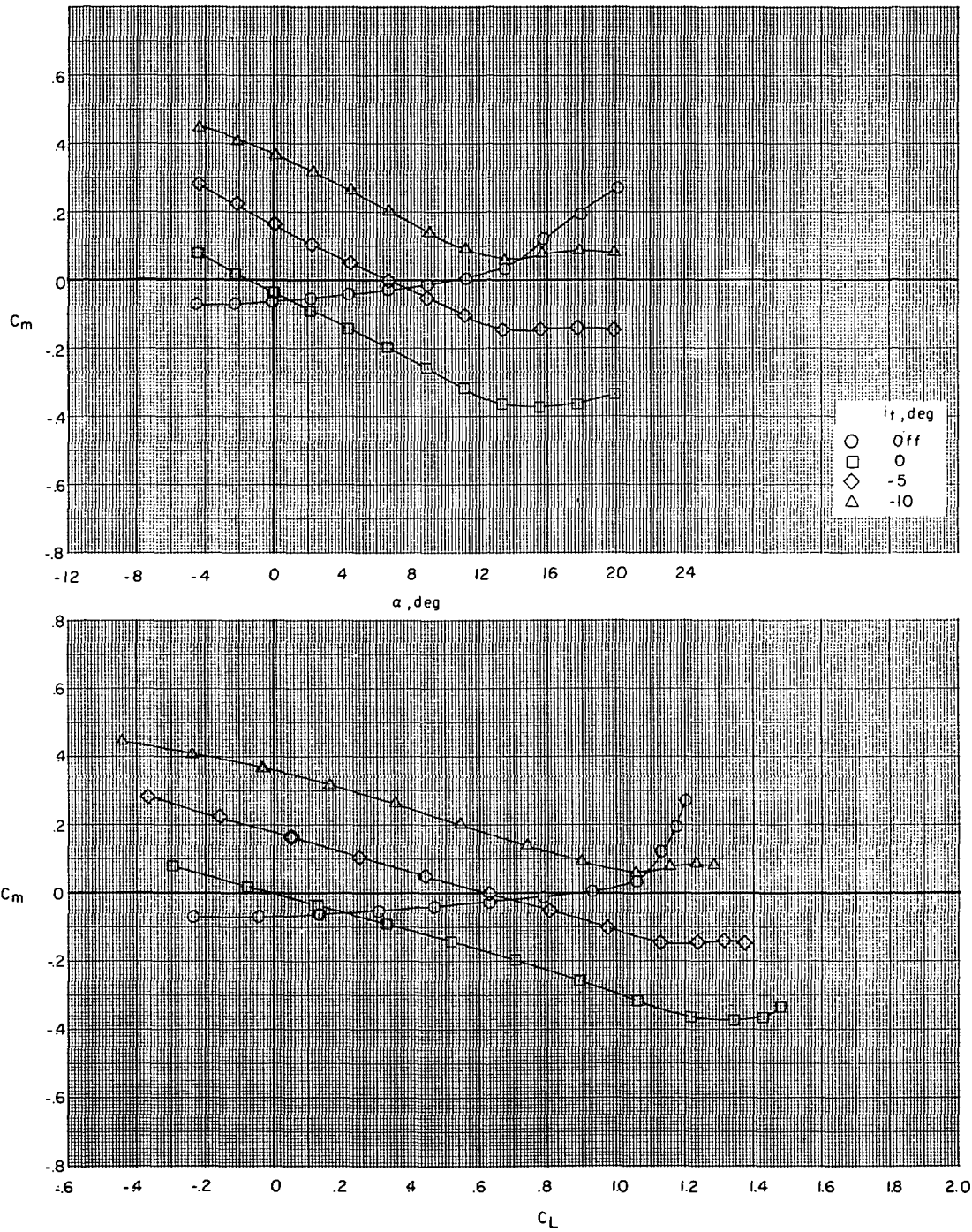


Figure 7.- Concluded.

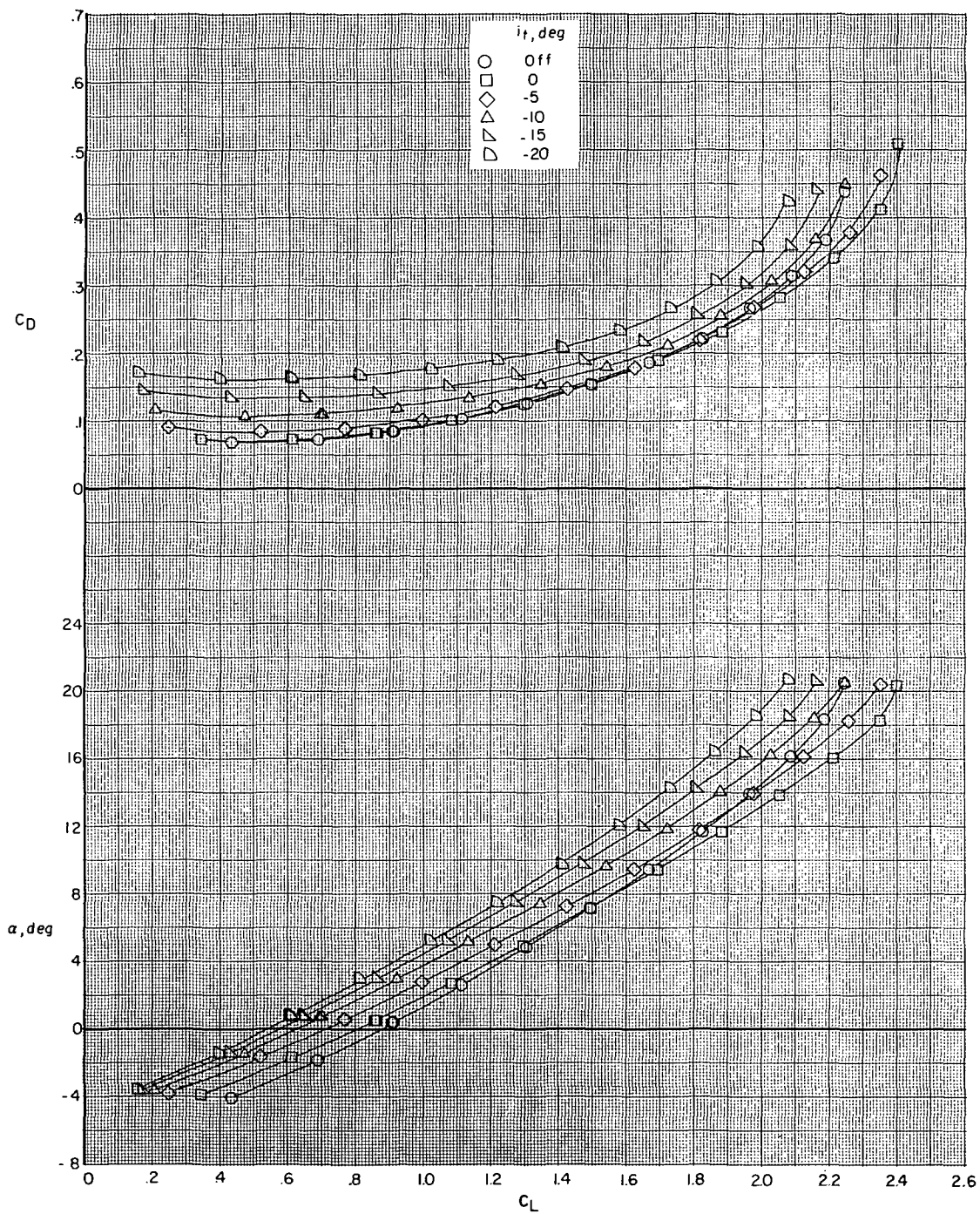


Figure 8.- Effect of horizontal-stabilizer deflection on longitudinal aerodynamic characteristics of high-wing model in take-off configuration. $\delta_f = 20^\circ$; $\delta_s = 40^\circ$.

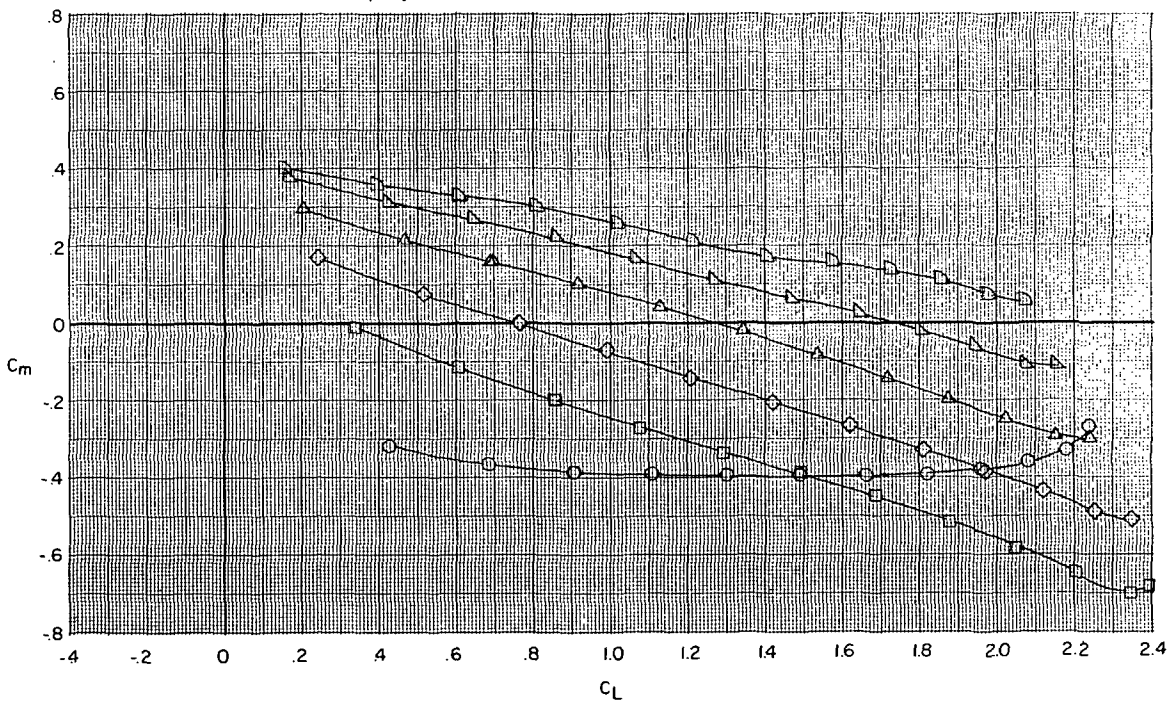
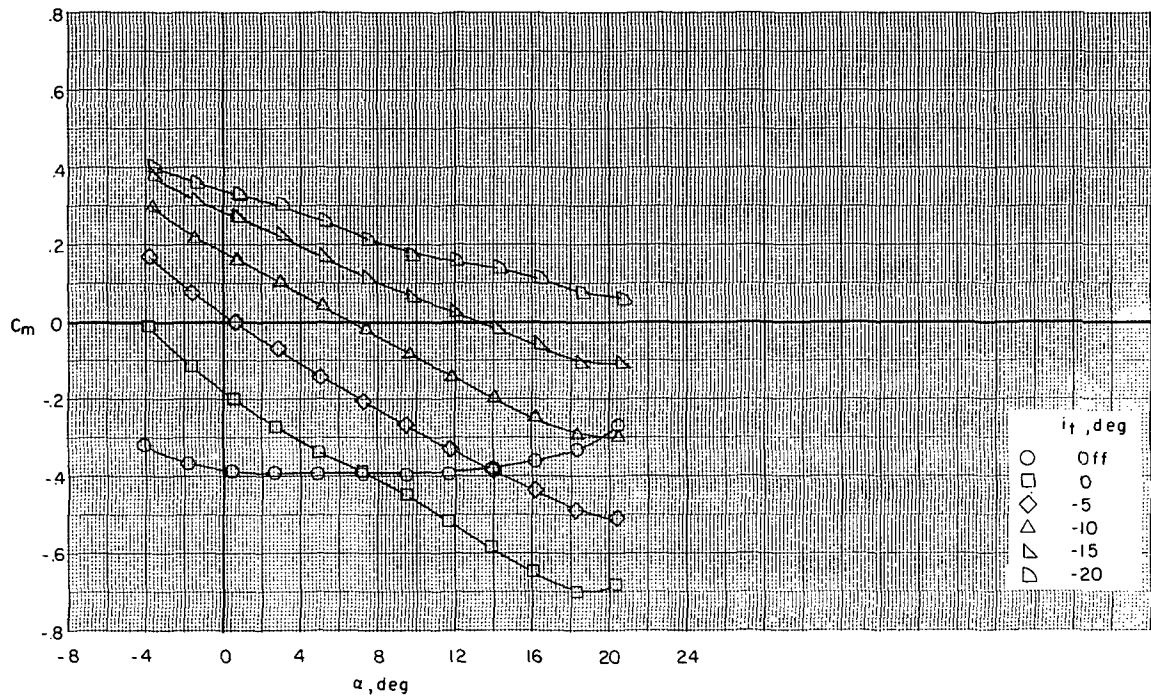


Figure 8.- Concluded.

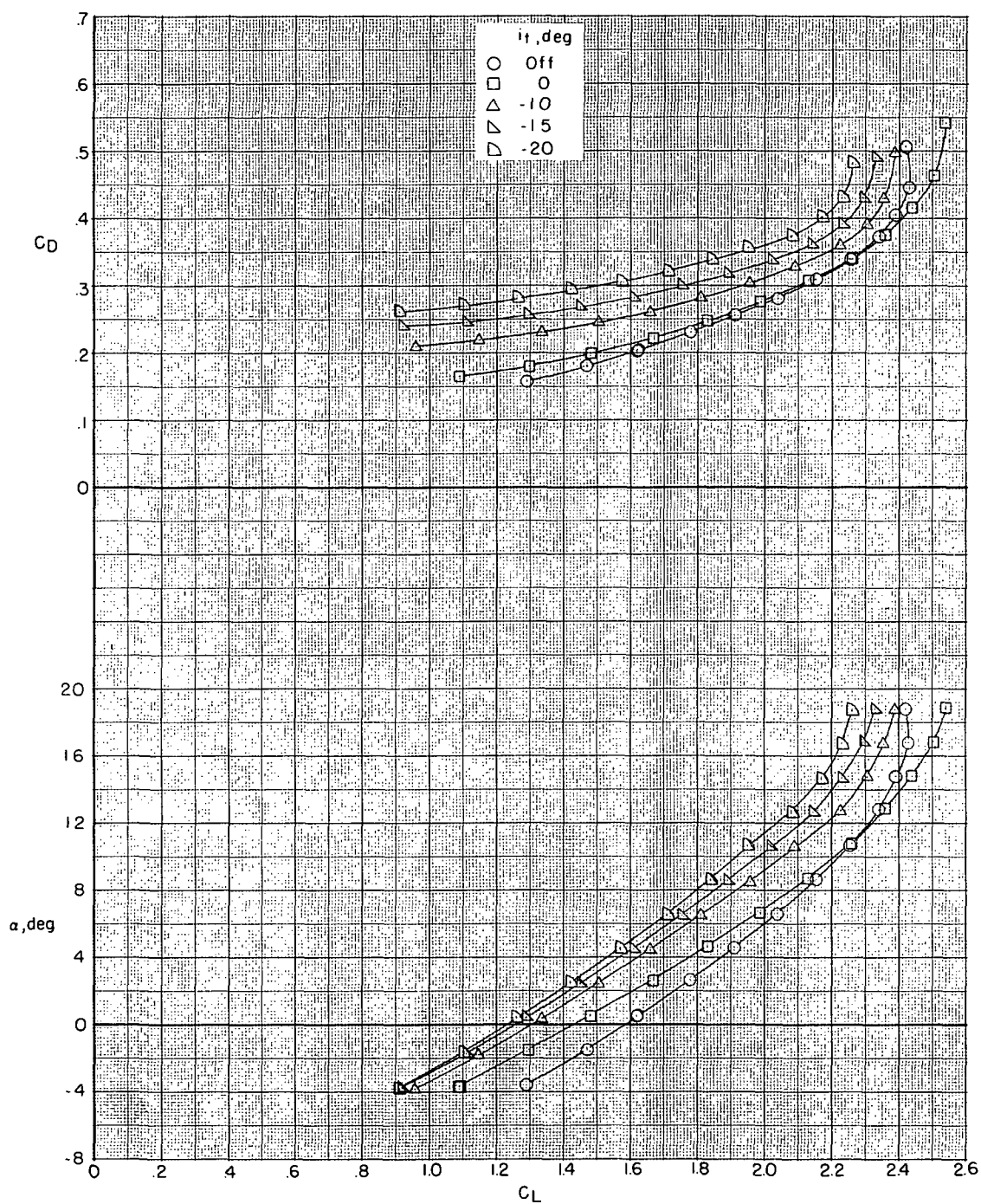


Figure 9.- Effect of horizontal-stabilizer deflection on longitudinal aerodynamic characteristics of high-wing model in landing configuration. $\delta_f = 40^\circ$; $\delta_s = 50^\circ$.

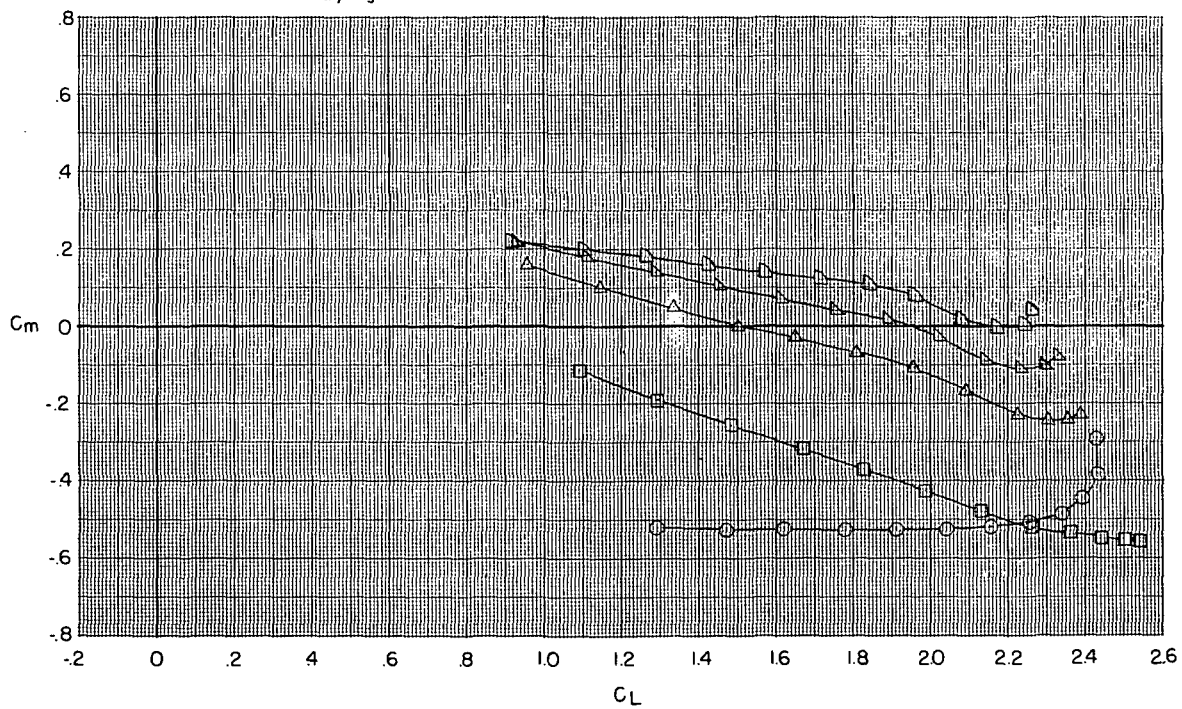
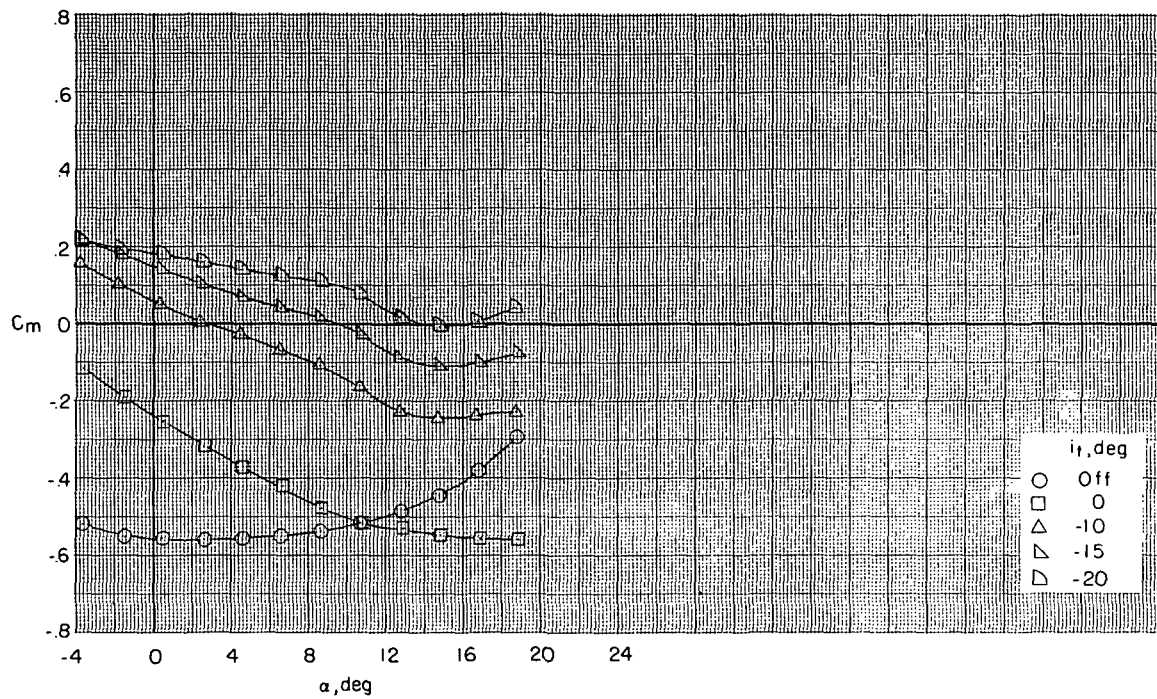


Figure 9.- Concluded.

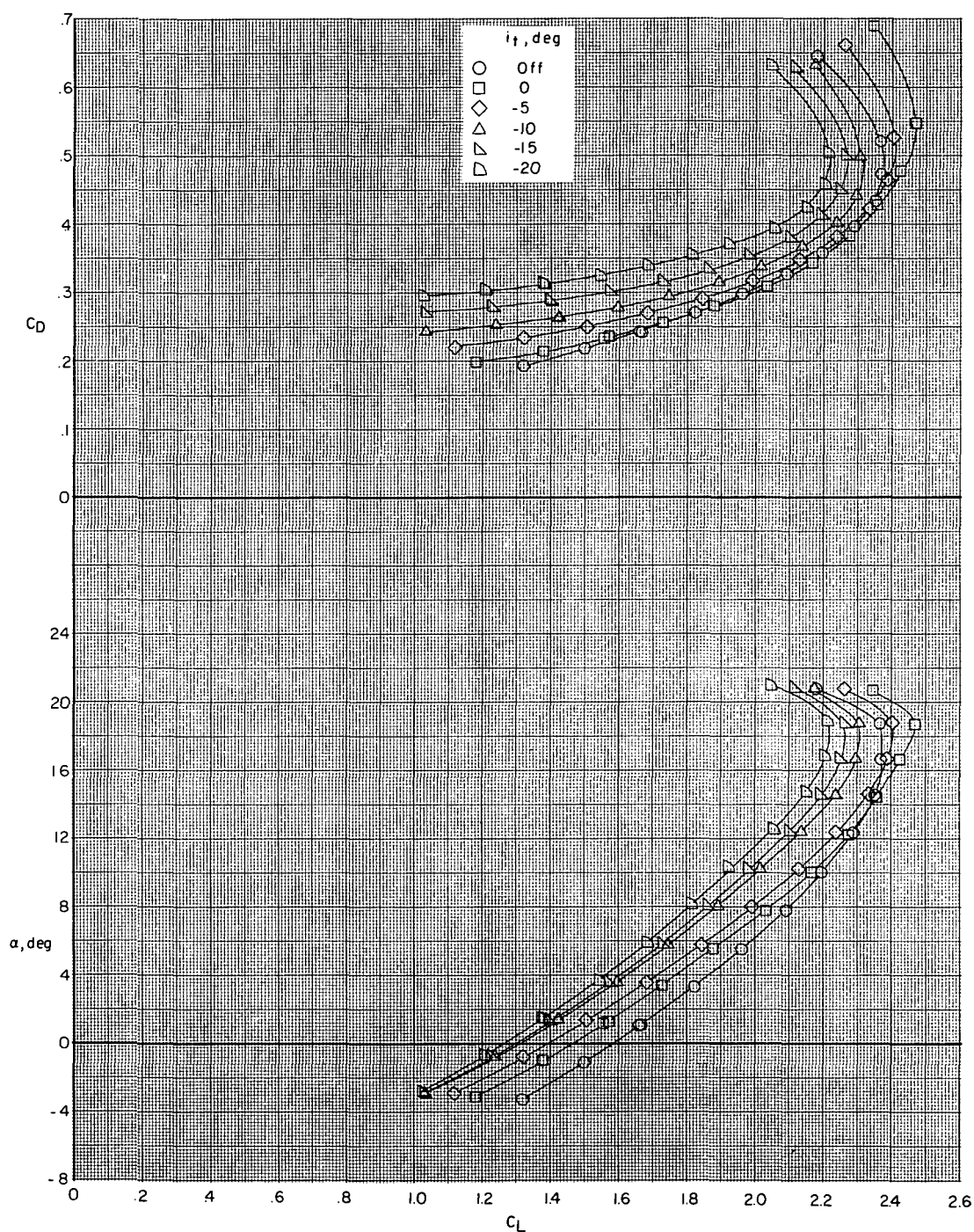


Figure 10.- Effect of horizontal-stabilizer deflection on longitudinal aerodynamic characteristics of high-wing model in landing configuration. $\delta_f = 45^\circ$; $\delta_s = 50^\circ$.

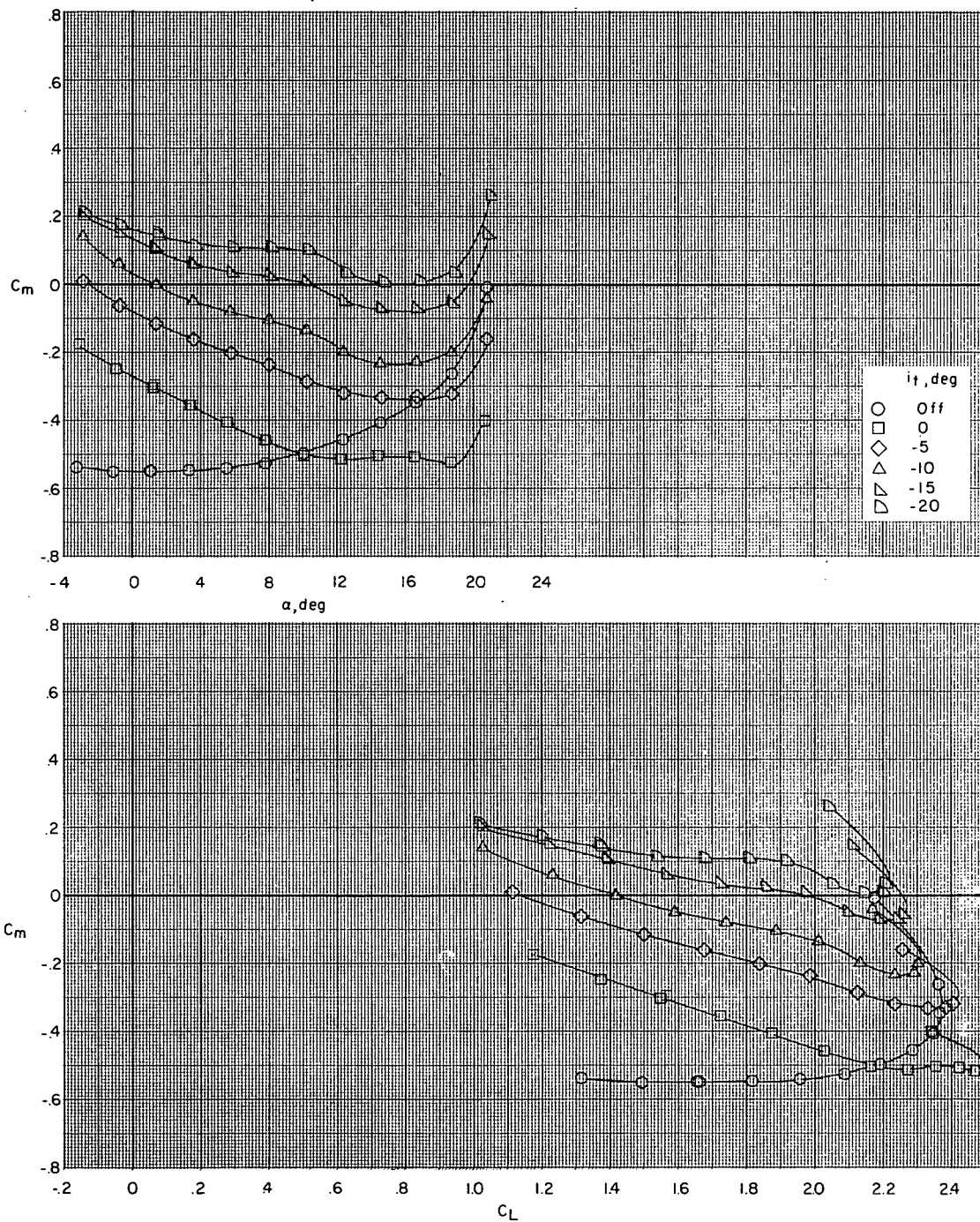


Figure 10.- Concluded.

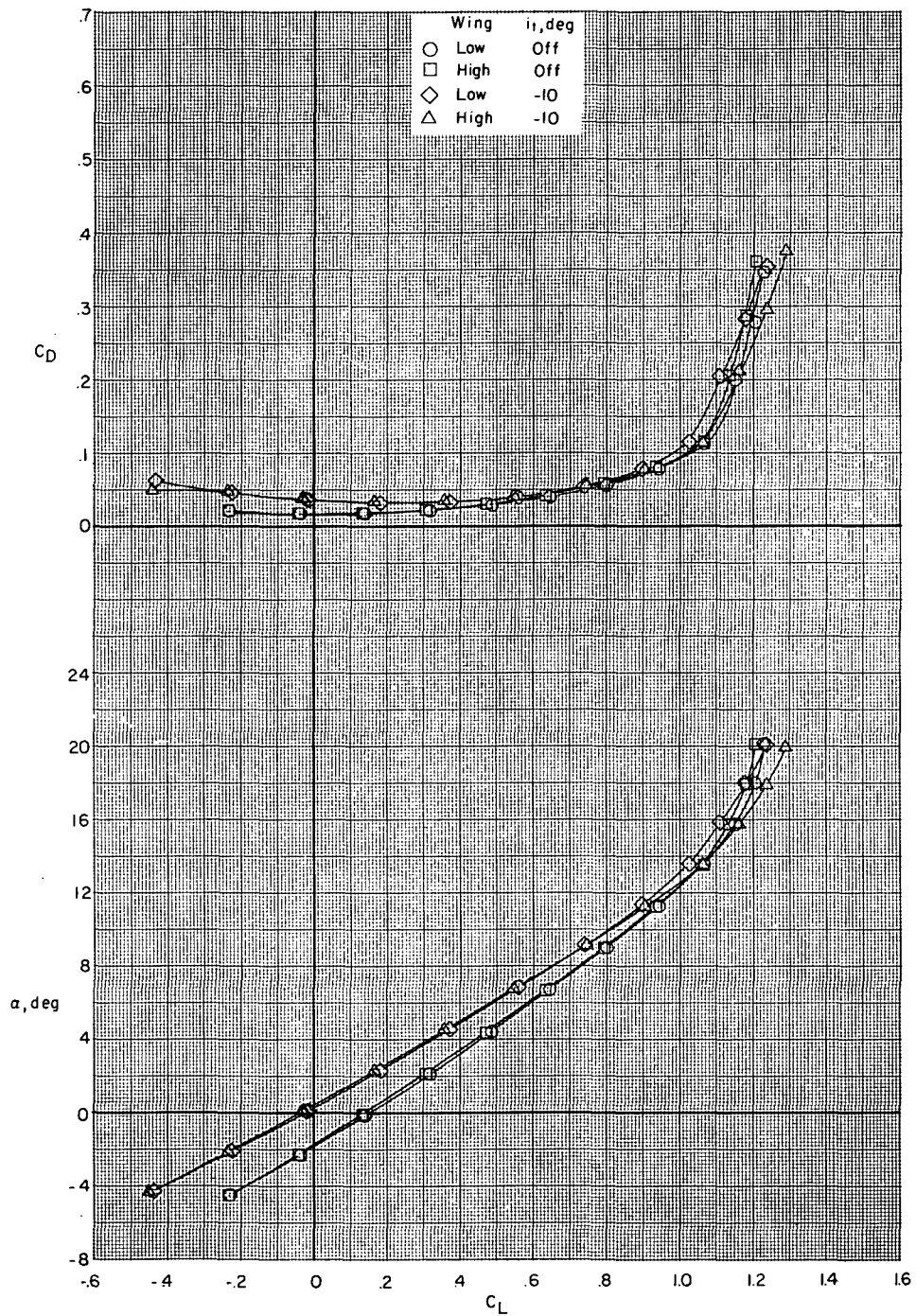


Figure 11.- Effect of wing height on longitudinal aerodynamic characteristics of clean configuration with and without horizontal tail. $\delta_f = 0^\circ$; $\delta_s = \text{Off}$.

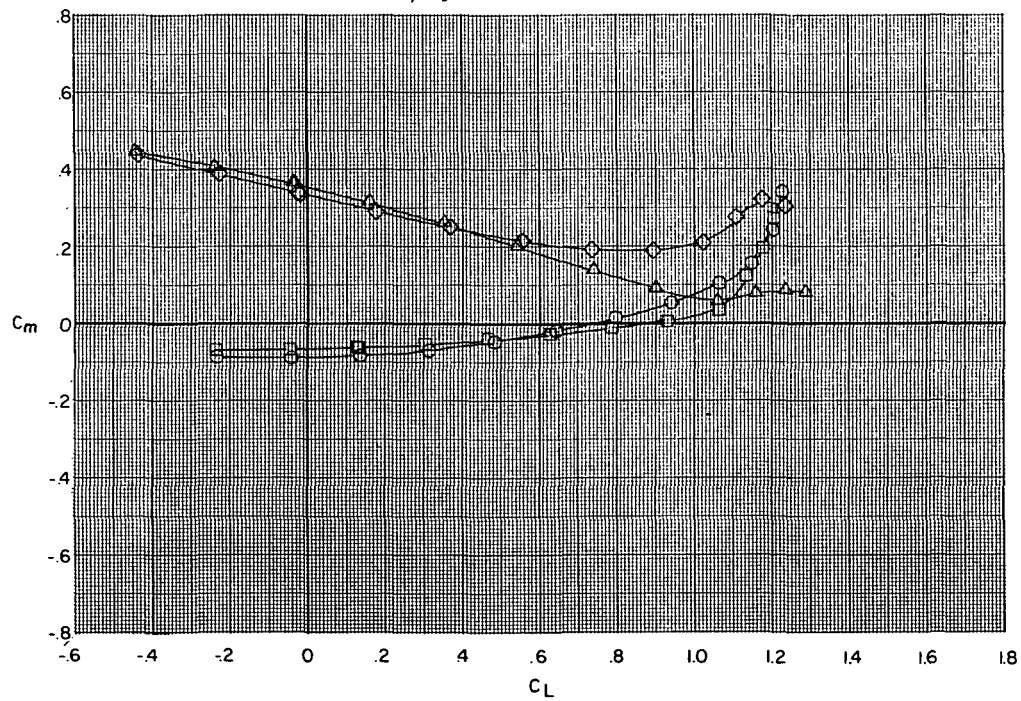
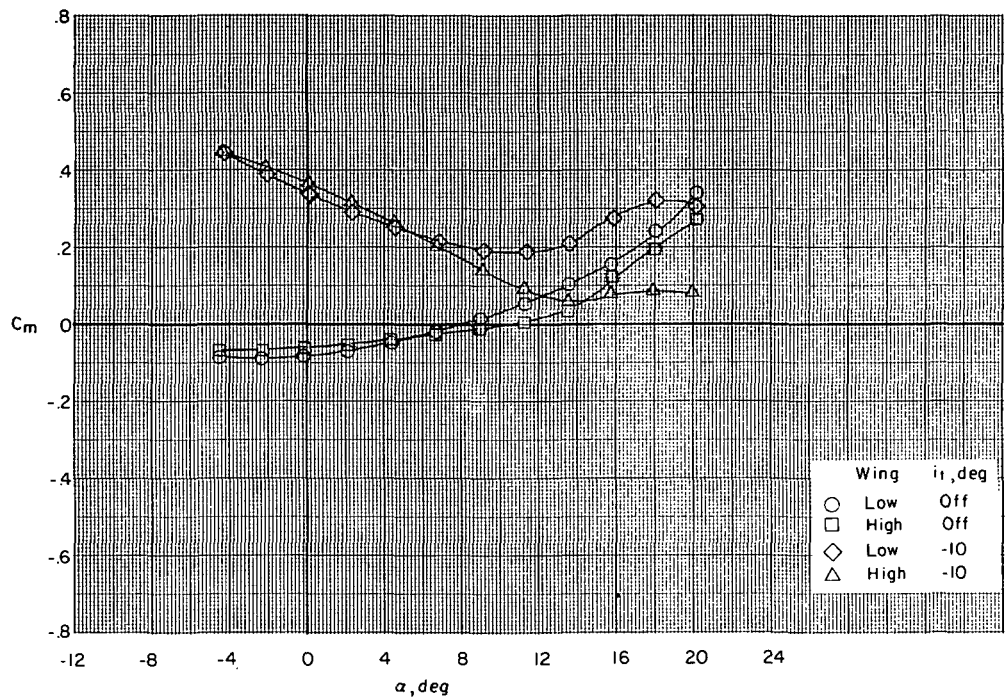


Figure 11.- Concluded.

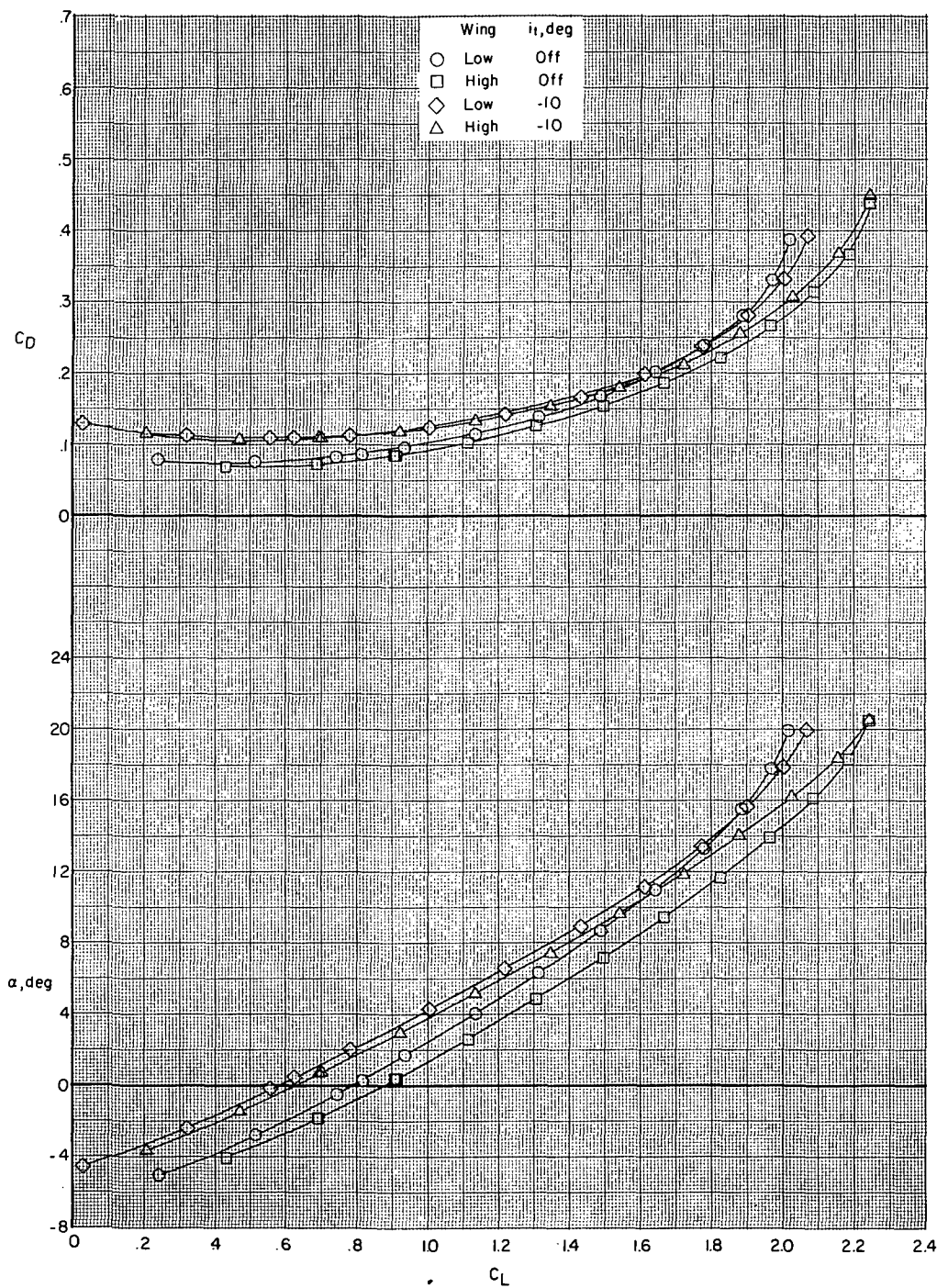


Figure 12.- Effect of wing height on longitudinal aerodynamic characteristics of take-off configuration with and without horizontal tail. $\delta_f = 20^\circ$; $\delta_s = 40^\circ$.

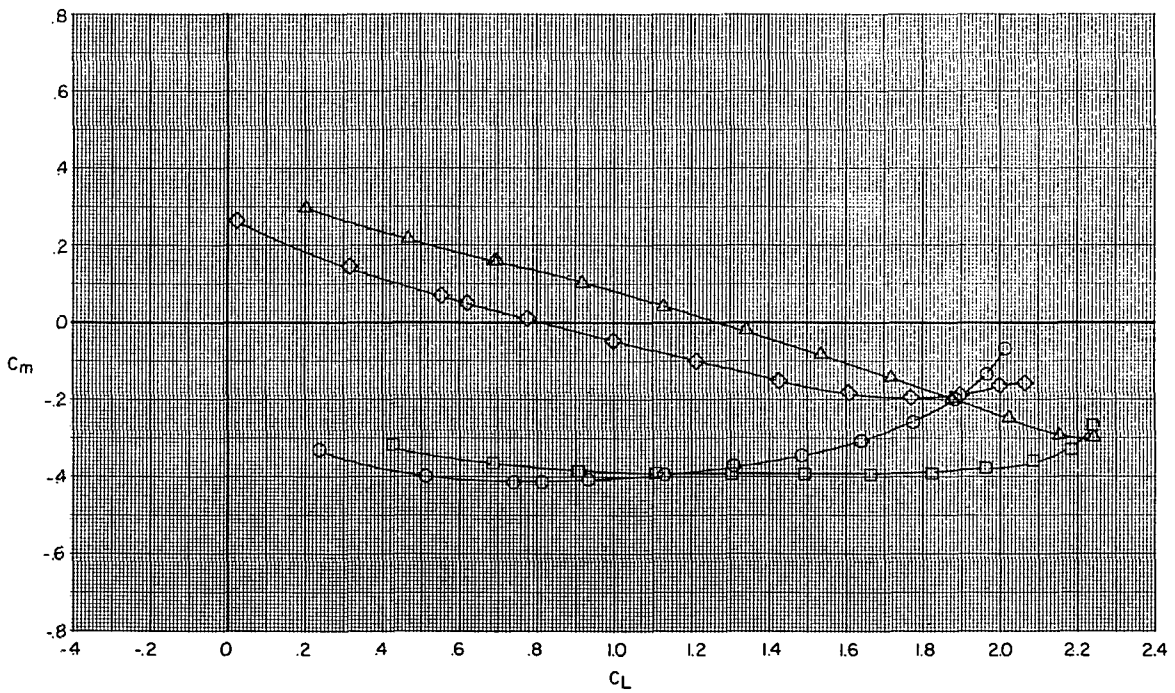
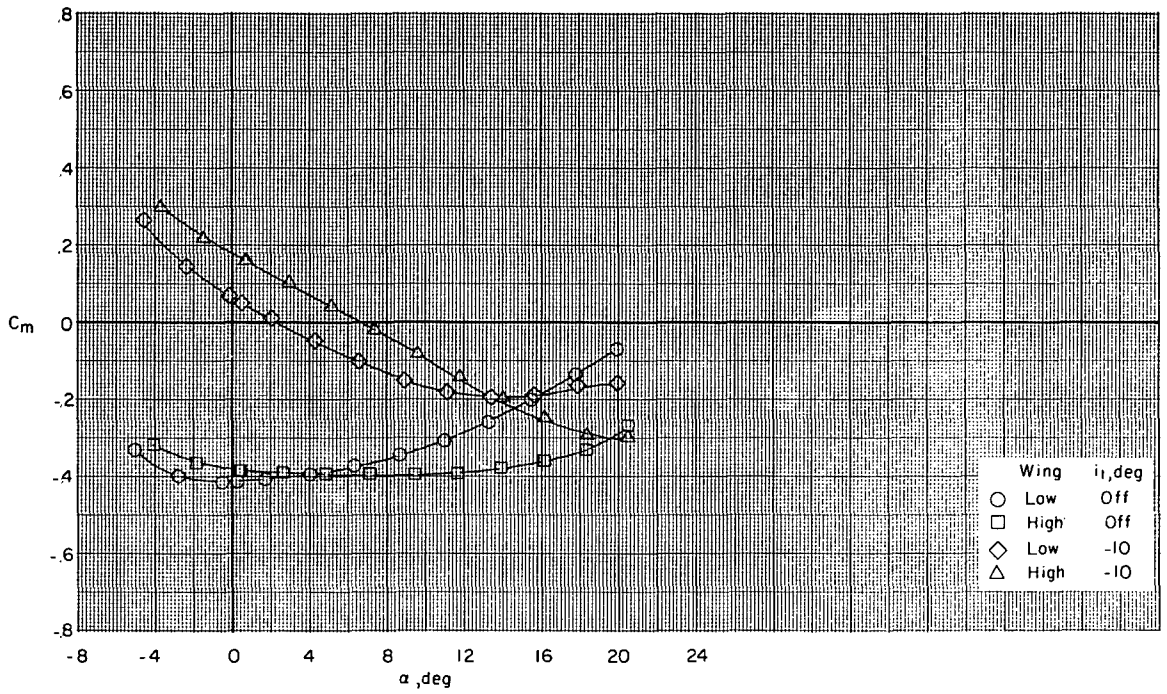


Figure 12.- Concluded.

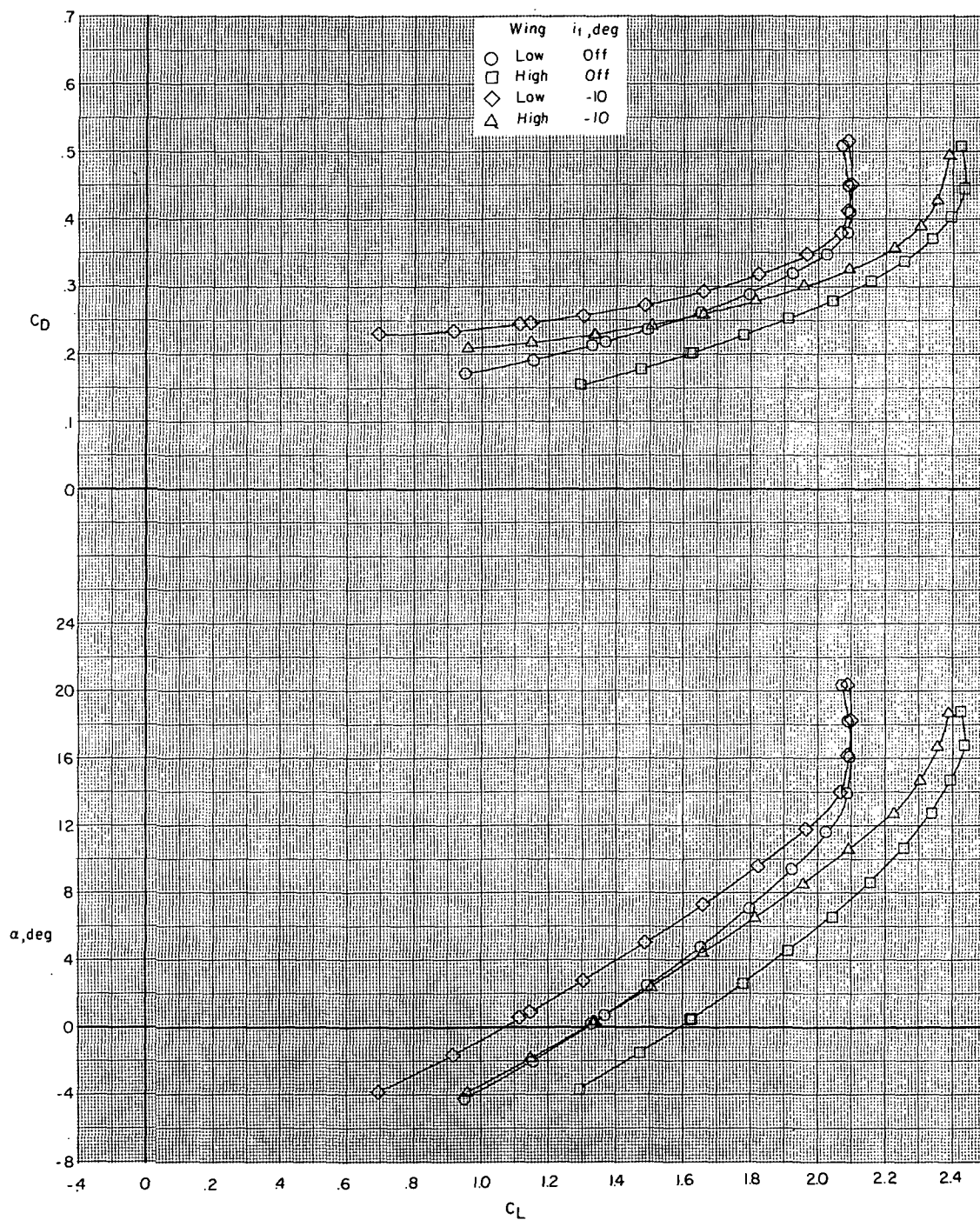


Figure 13.- Effect of wing height on longitudinal aerodynamic characteristics of landing configuration with and without horizontal tail. $\delta_f = 40^\circ$; $\delta_s = 50^\circ$.

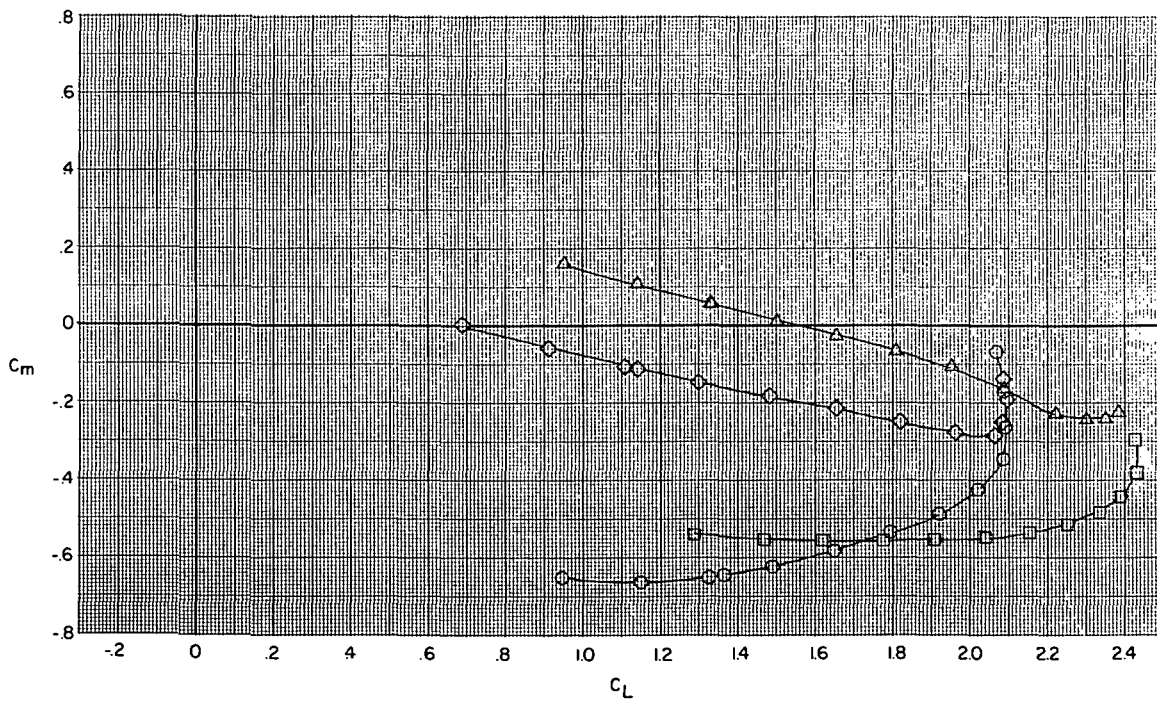
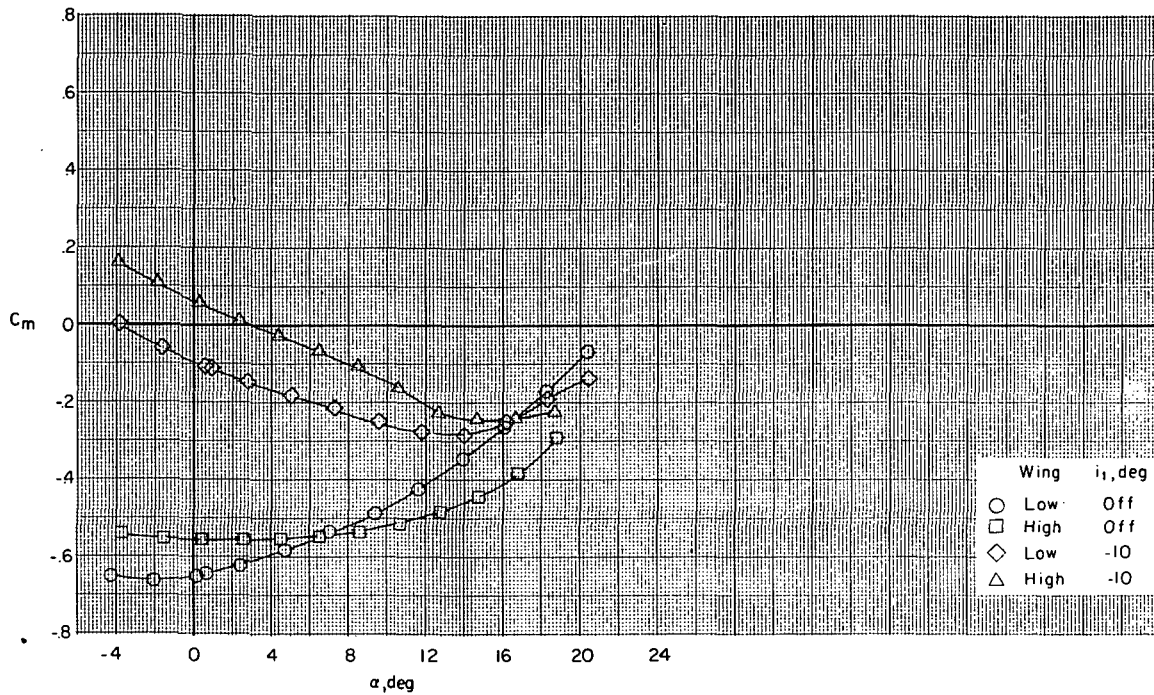


Figure 13.- Concluded.

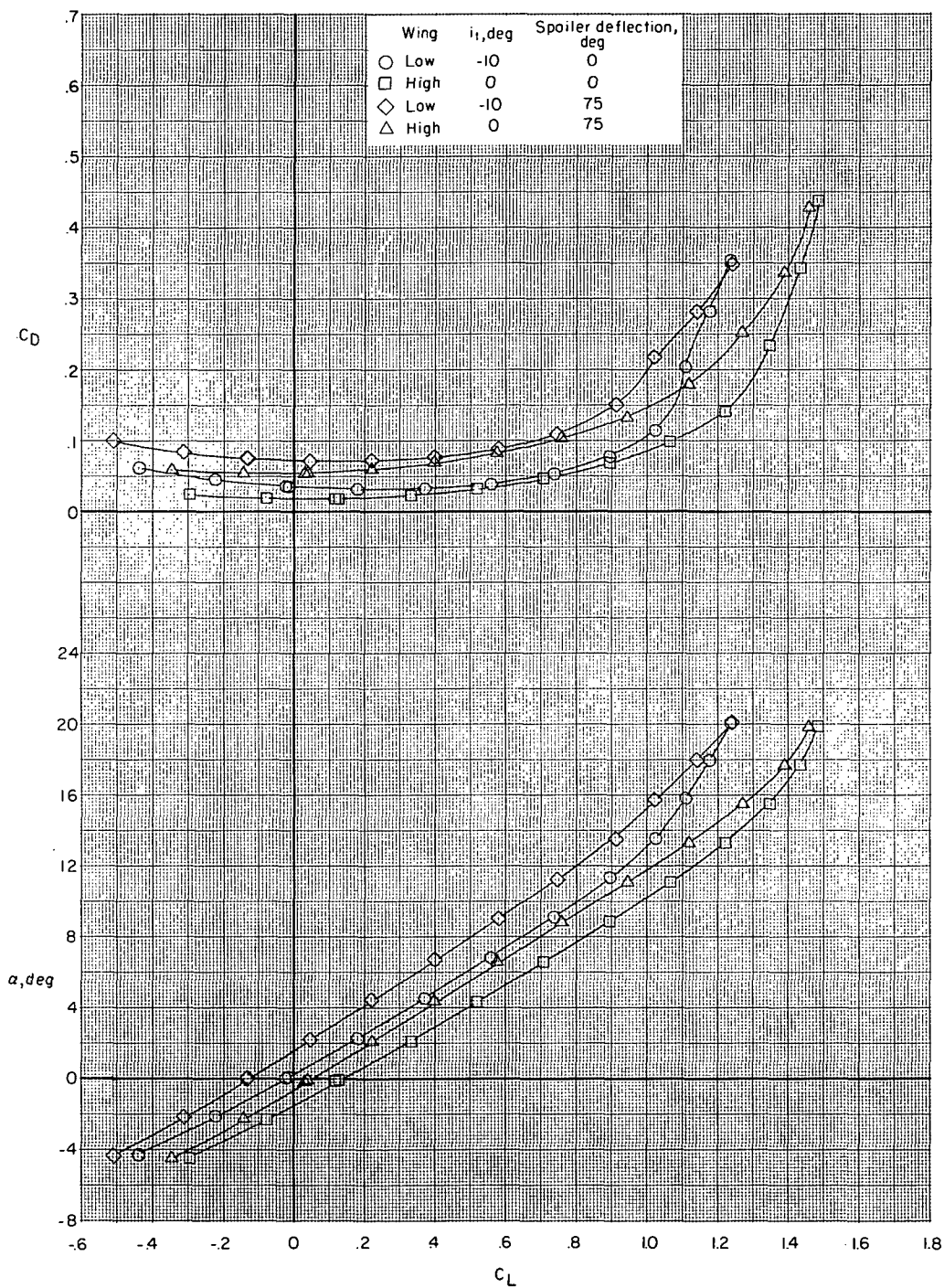


Figure 14.- Effect of wing upper-surface spoiler for roll control for clean configuration.
 $\delta_f = 0^\circ$; $\delta_s = \text{Off}$.

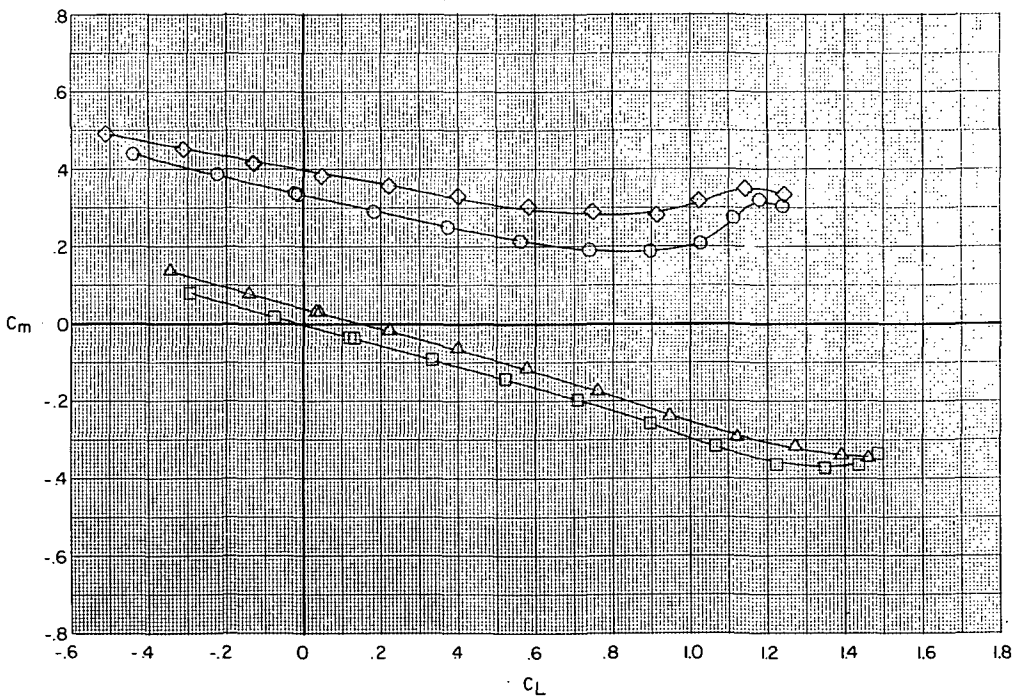
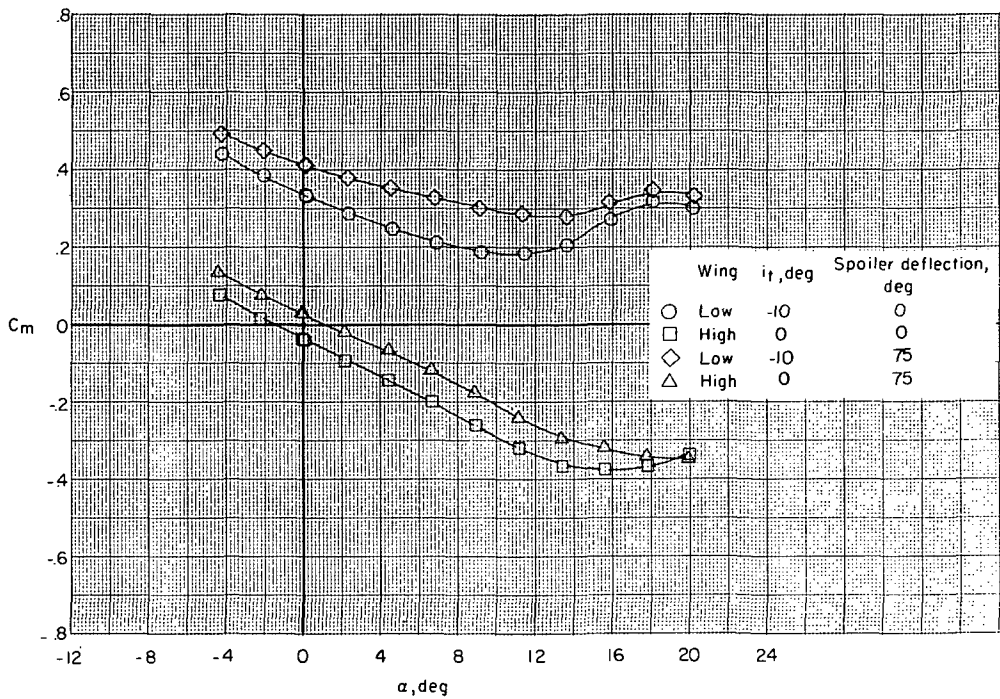


Figure 14.- Continued.

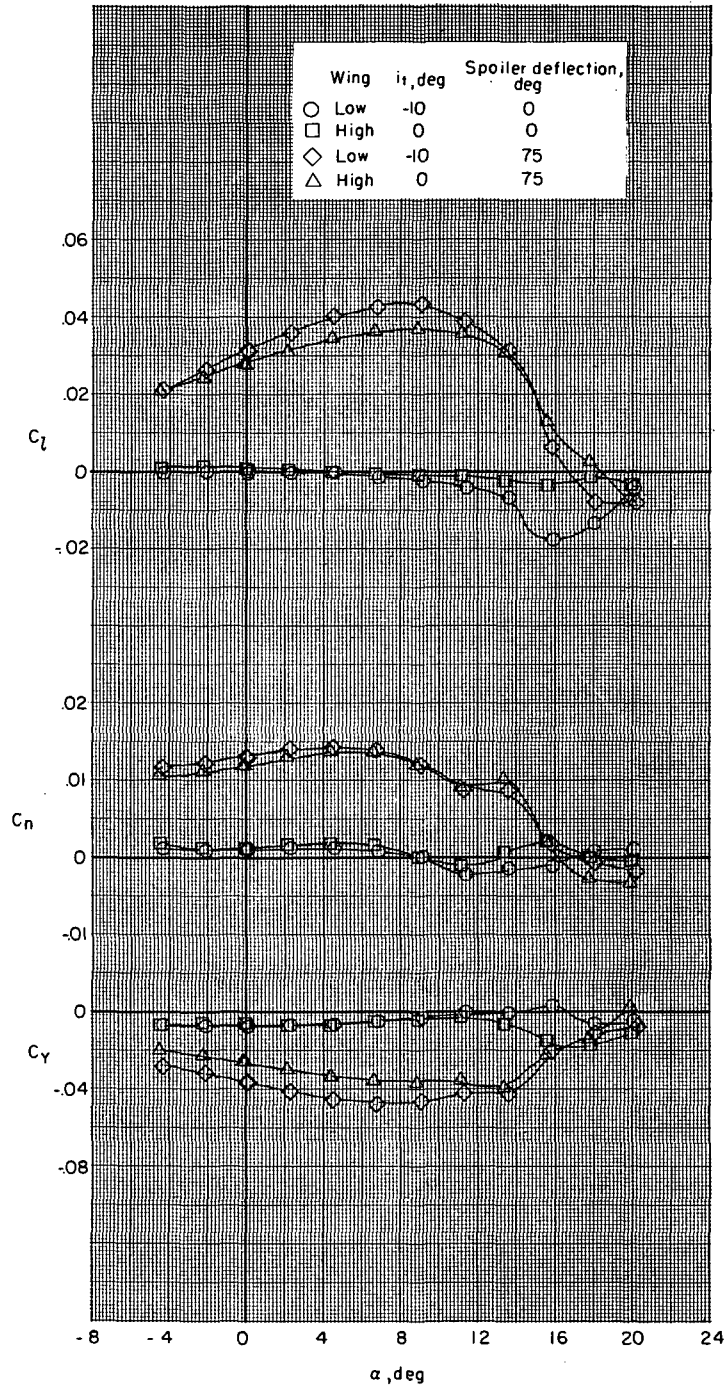


Figure 14.- Concluded.

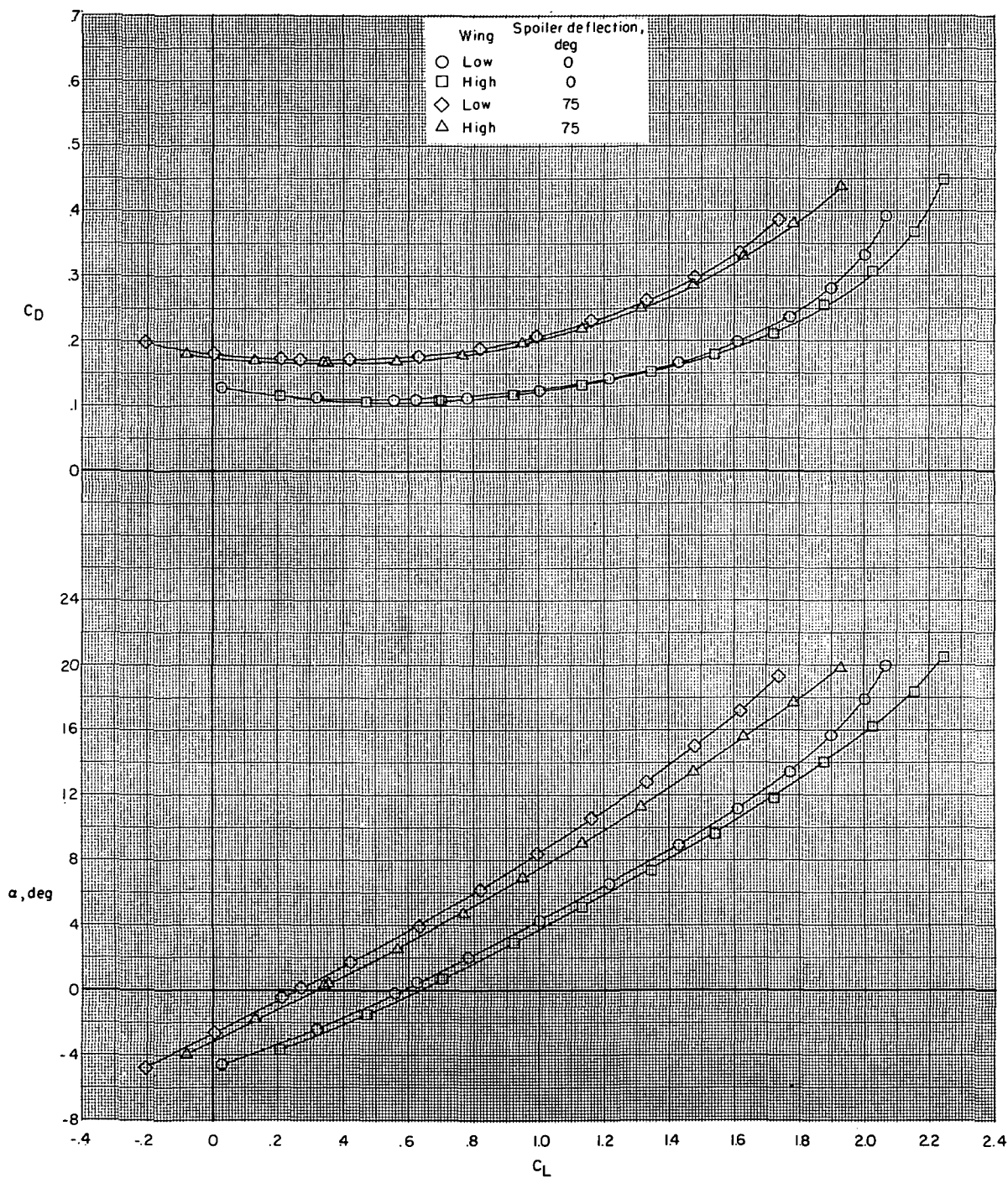


Figure 15.- Effect of wing upper-surface spoiler for roll control for take-off configuration. $\delta_f = 20^\circ$; $\delta_s = 40^\circ$; $i_t = -10^\circ$.

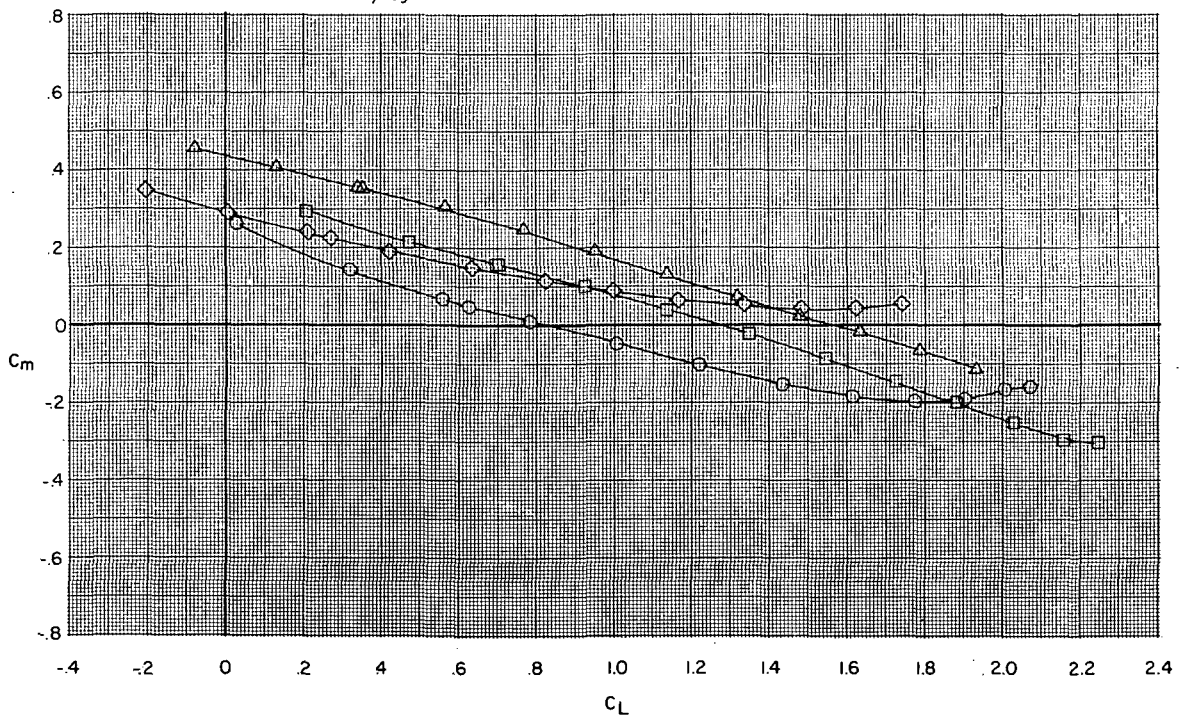
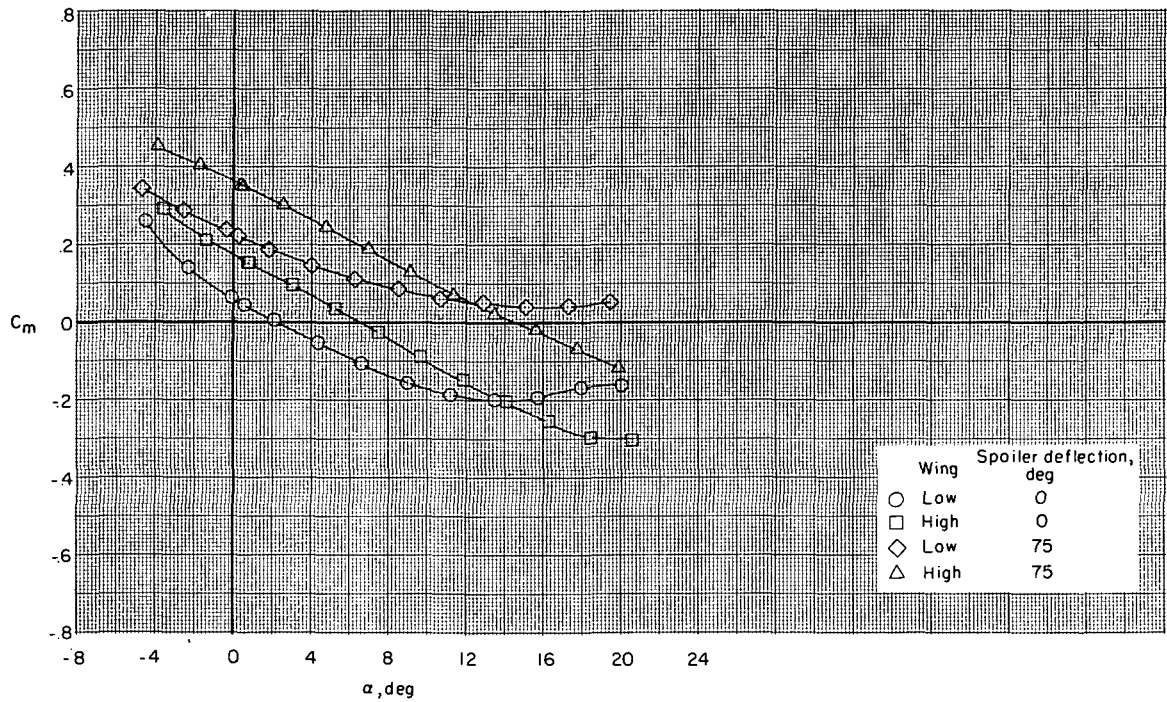


Figure 15.- Continued.

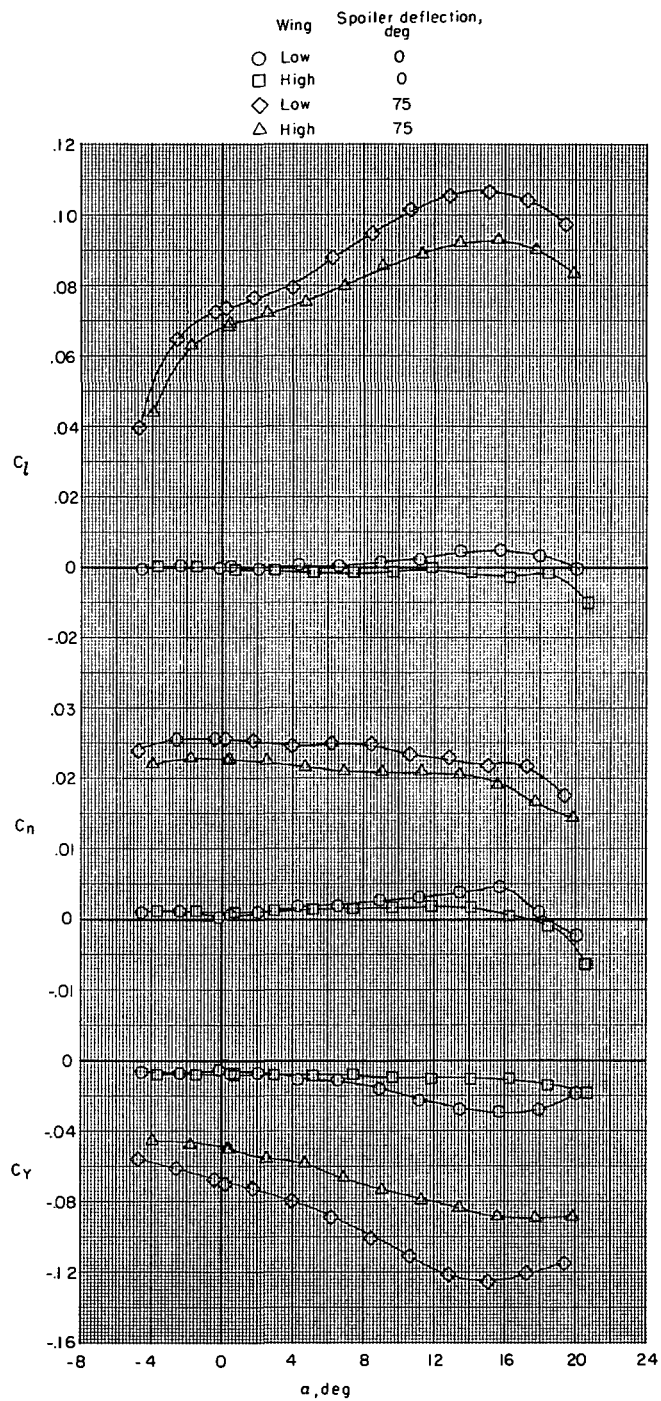


Figure 15.- Concluded.

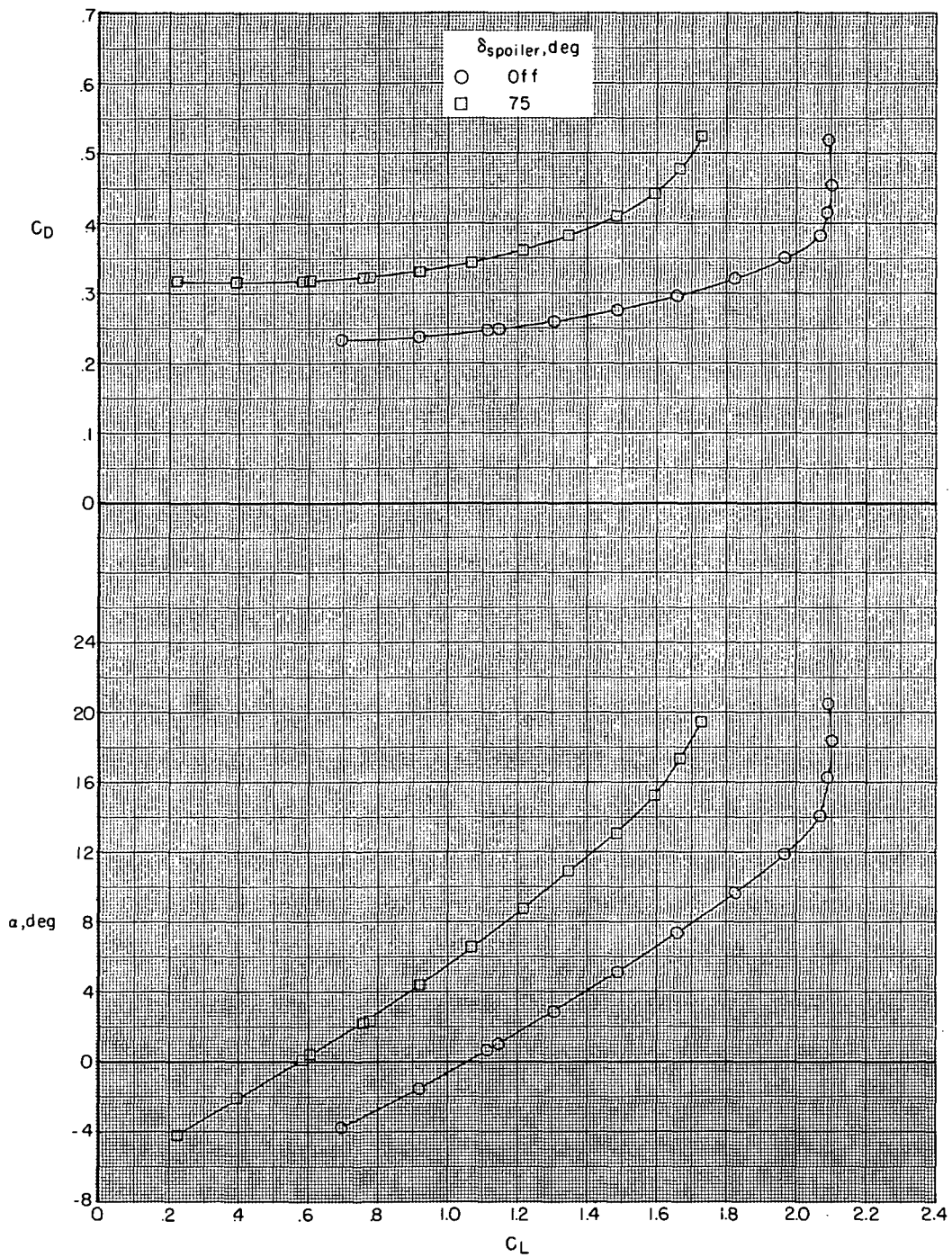


Figure 16.- Effect of wing upper-surface spoiler for roll control for low-wing model in landing configuration. $\delta_f = 40^\circ$; $\delta_s = 50^\circ$; $i_t = -10^\circ$.

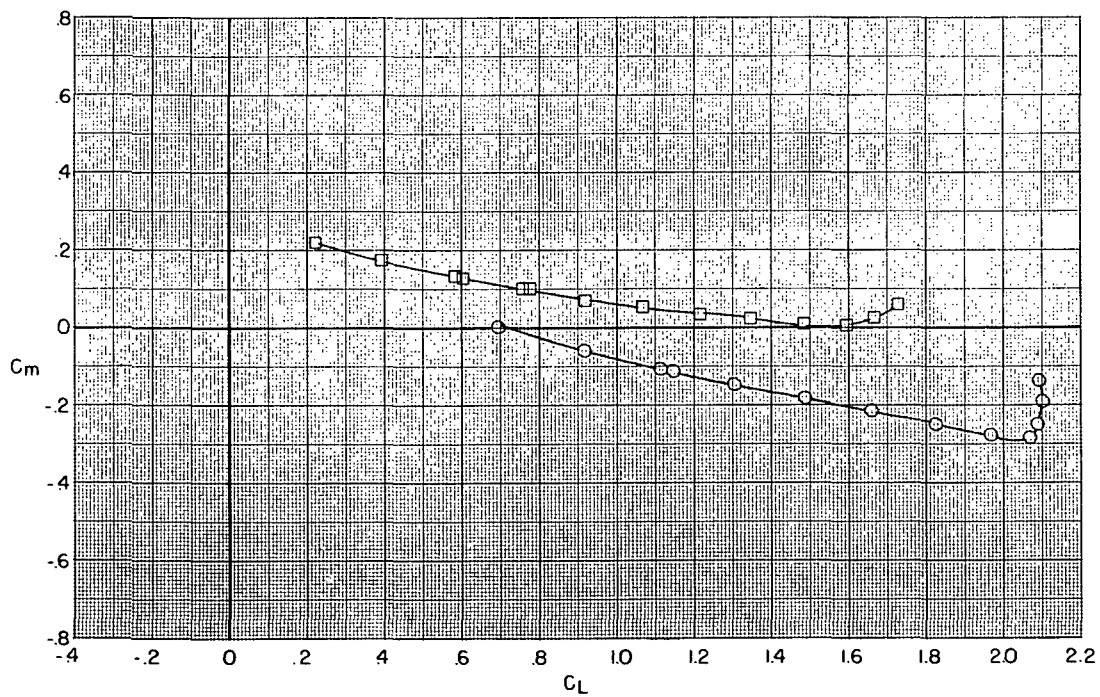
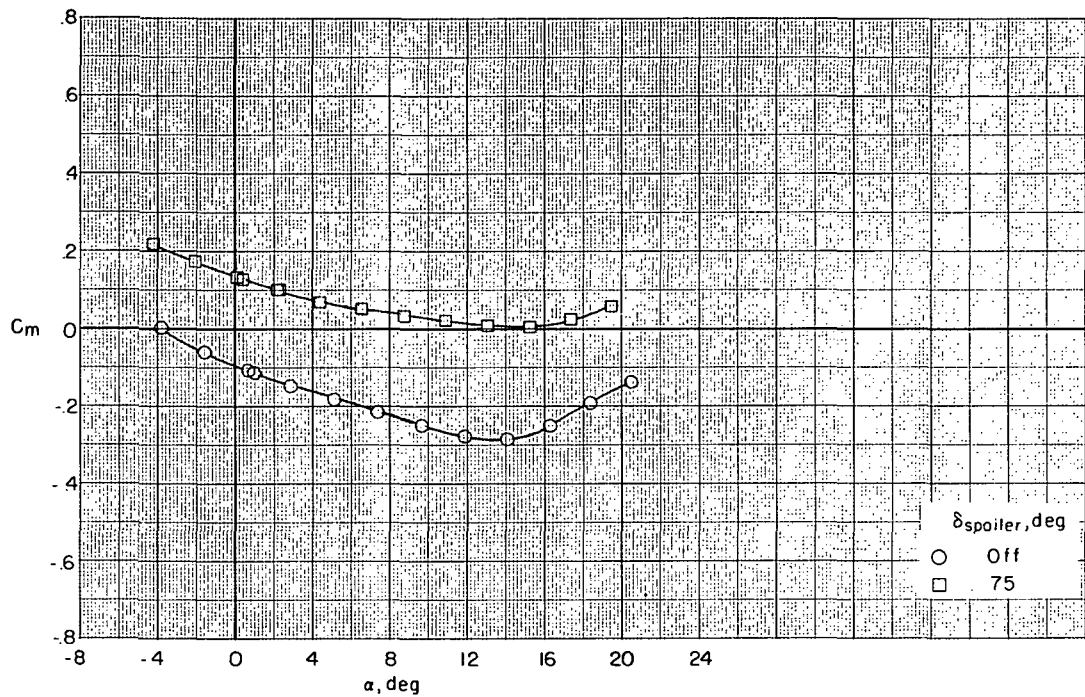


Figure 16.- Continued.

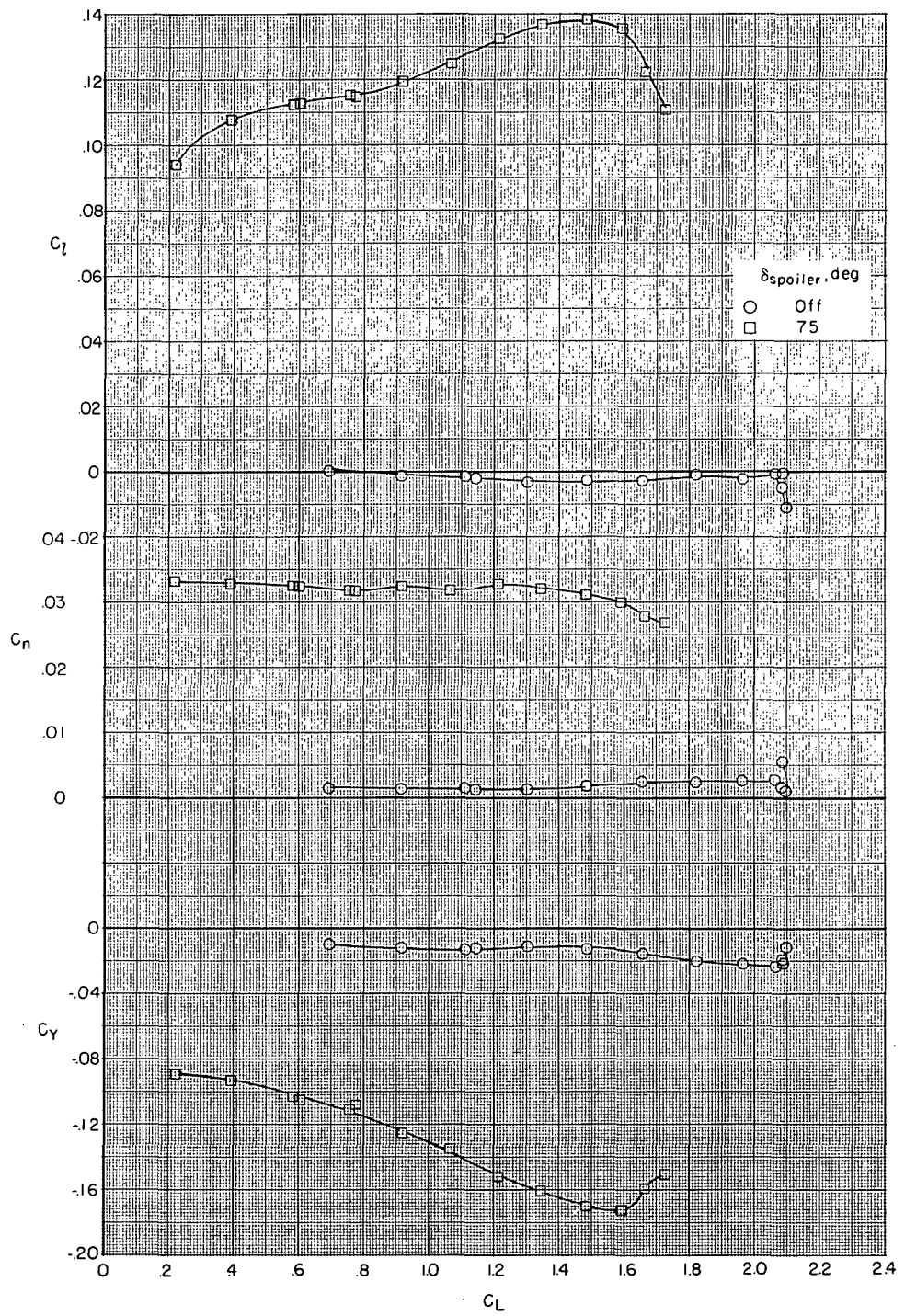


Figure 16.- Continued.

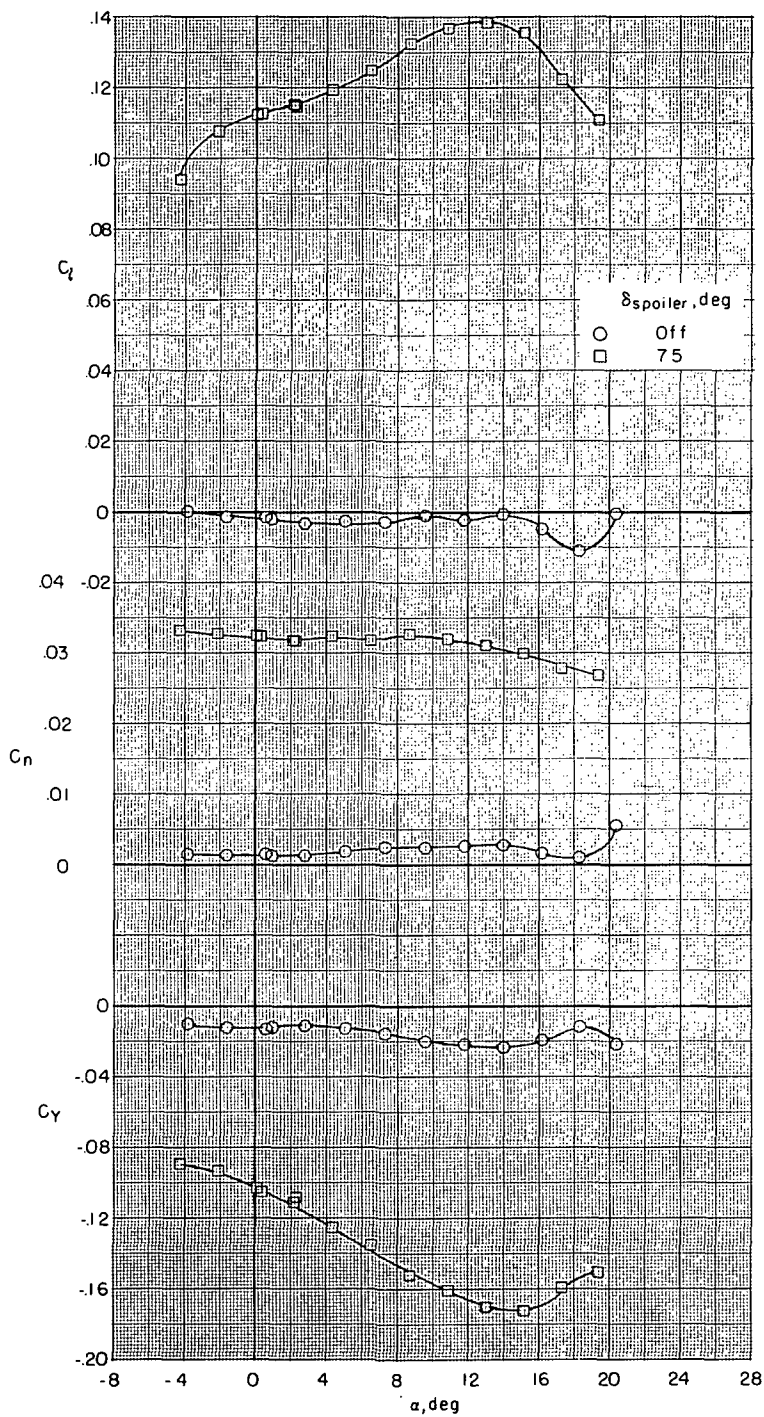


Figure 16. - Concluded.

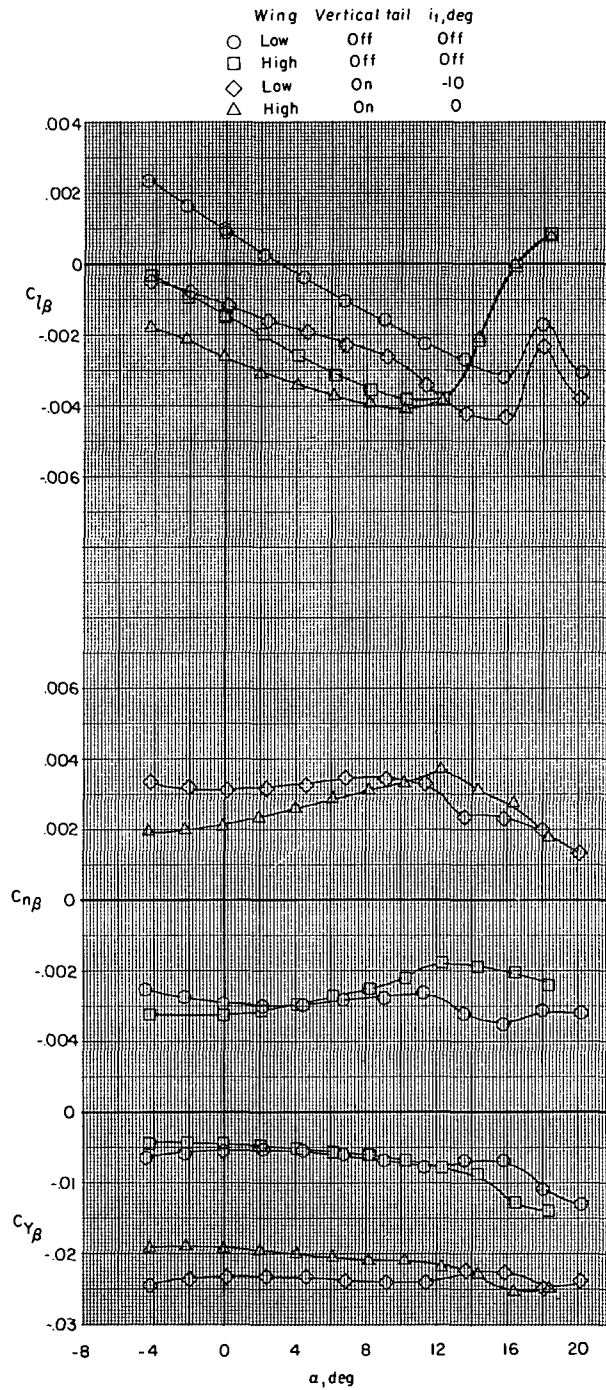


Figure 17.- Effect of wing height on static lateral stability derivatives of clean configuration with and without horizontal tail and vertical tail. $\delta_f = 0^\circ$; $\delta_s = \text{Off}$.

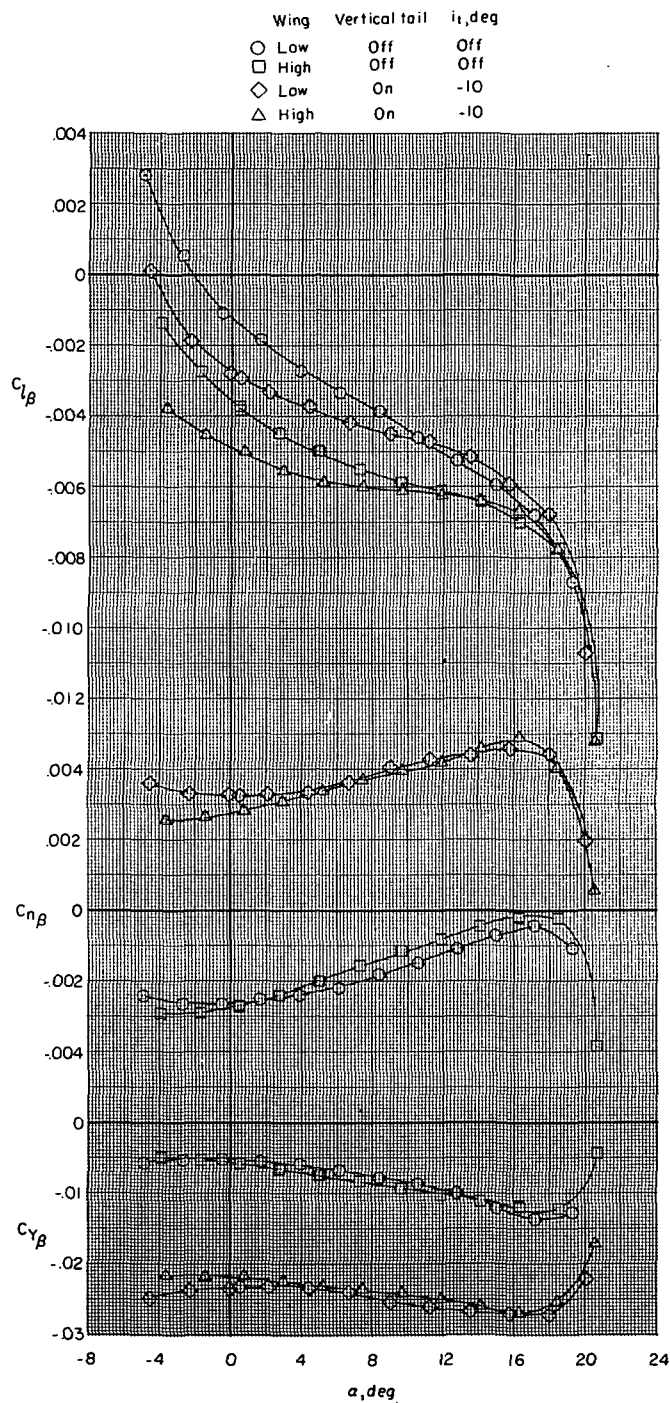


Figure 18.- Effect of wing height on static lateral stability derivatives of take-off configuration with and without horizontal tail and vertical tail. $\delta_f = 20^\circ$; $\delta_s = 40^\circ$.

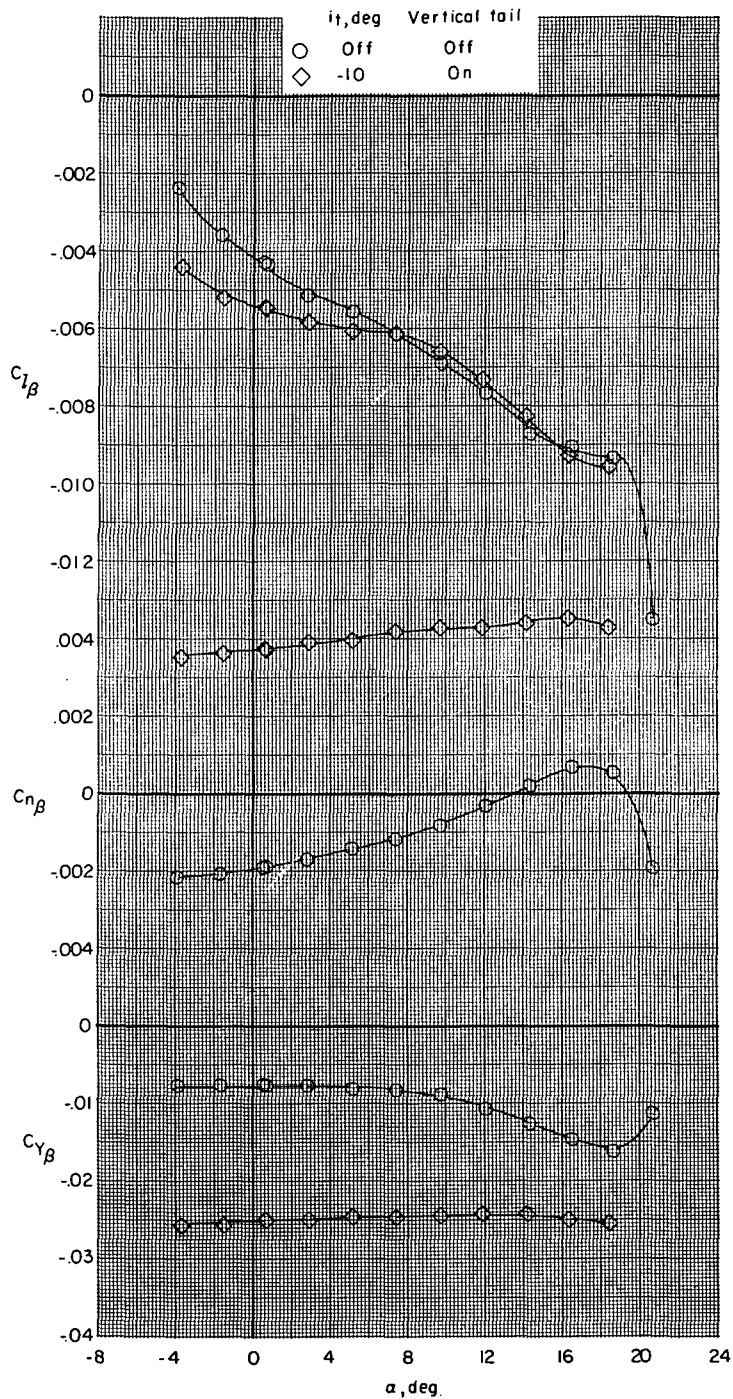
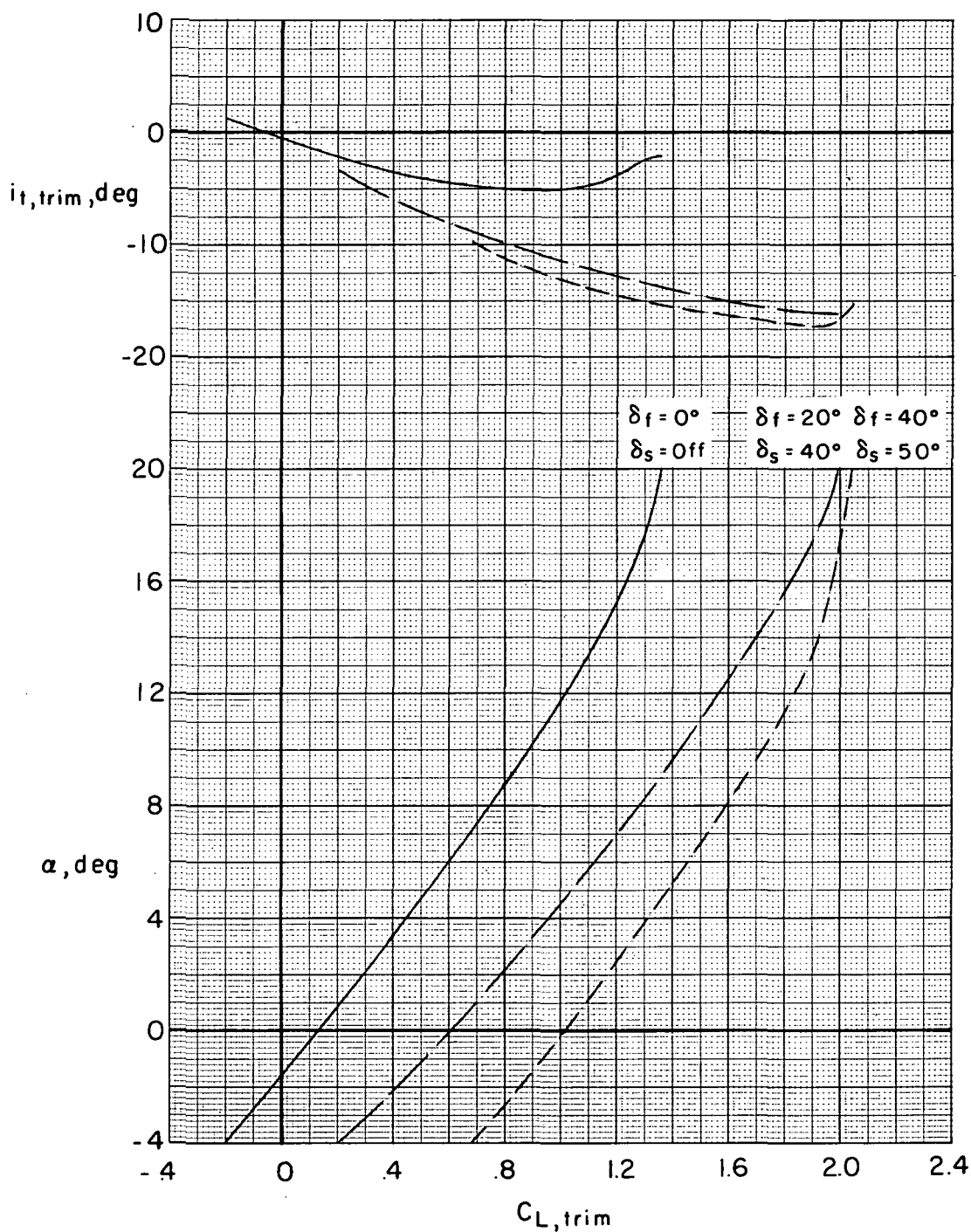
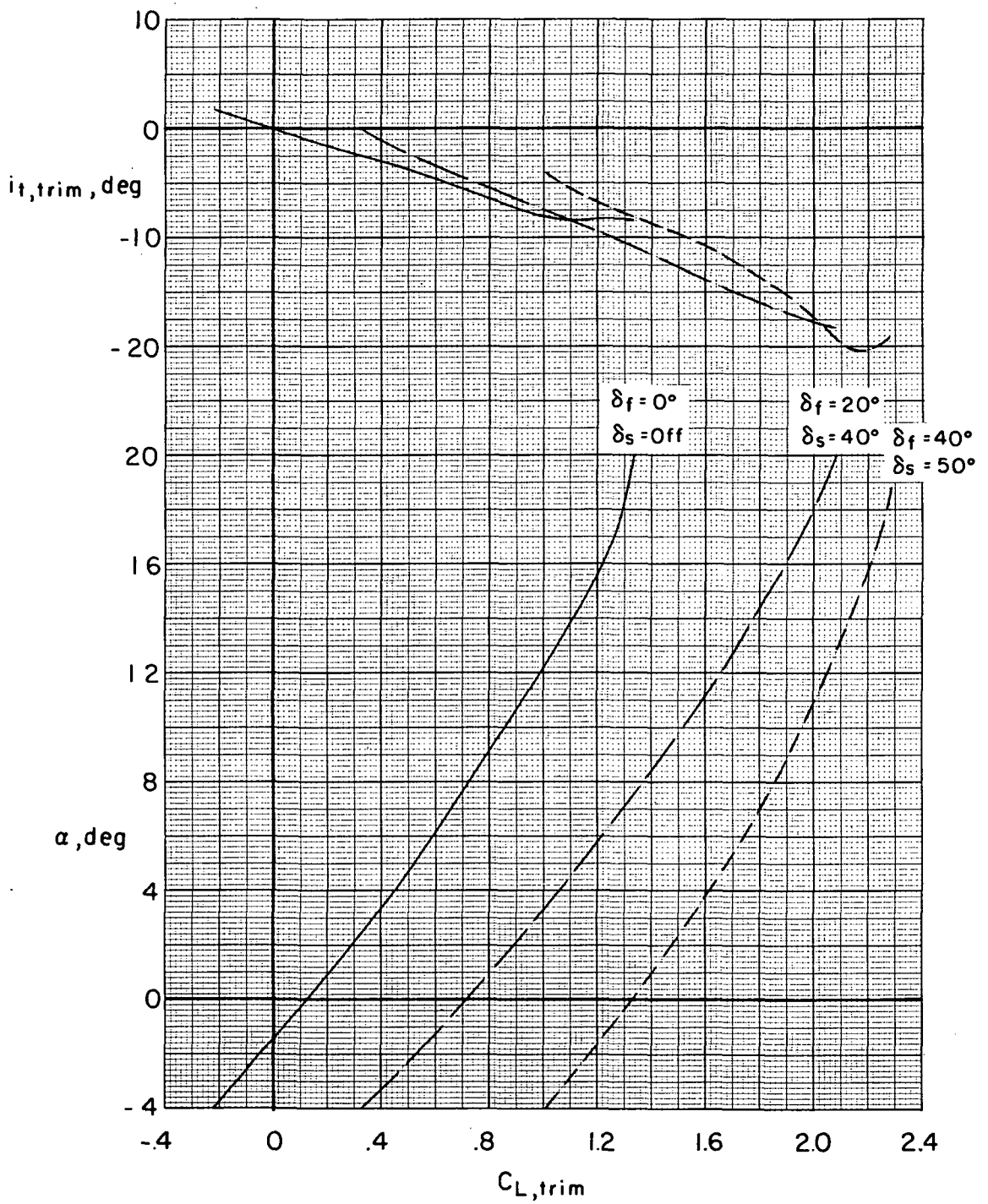


Figure 19.- Effect of adding horizontal and vertical tails on static lateral stability derivatives of low-wing model in landing configuration. $\delta_f = 40^\circ$; $\delta_s = 50^\circ$.



(a) Low-wing configuration.

Figure 20.- Effect of deflection of high-lift system on variation of angle of attack and stabilizer setting for trim and trim-lift coefficient for complete model.



(b) High-wing configuration.

Figure 20.- Concluded.

— Trimmed
 - - - Tail off

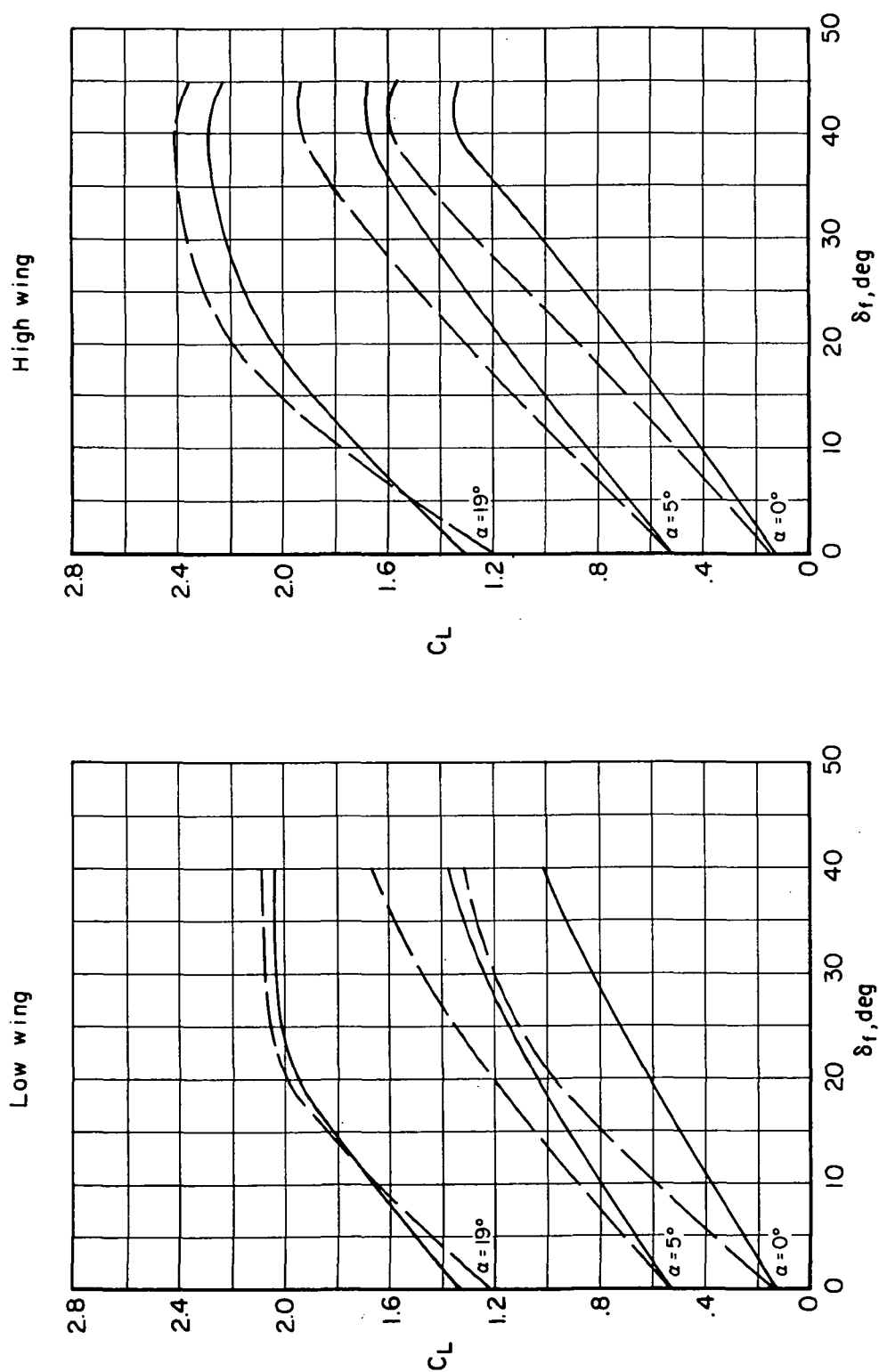


Figure 21.- Summary of effects of deflection of high-lift system on lift performance of low- and high-wing configurations.

δ_f, deg δ_s, deg

— 0 Off
 --- 20 40
 - - - 40 50

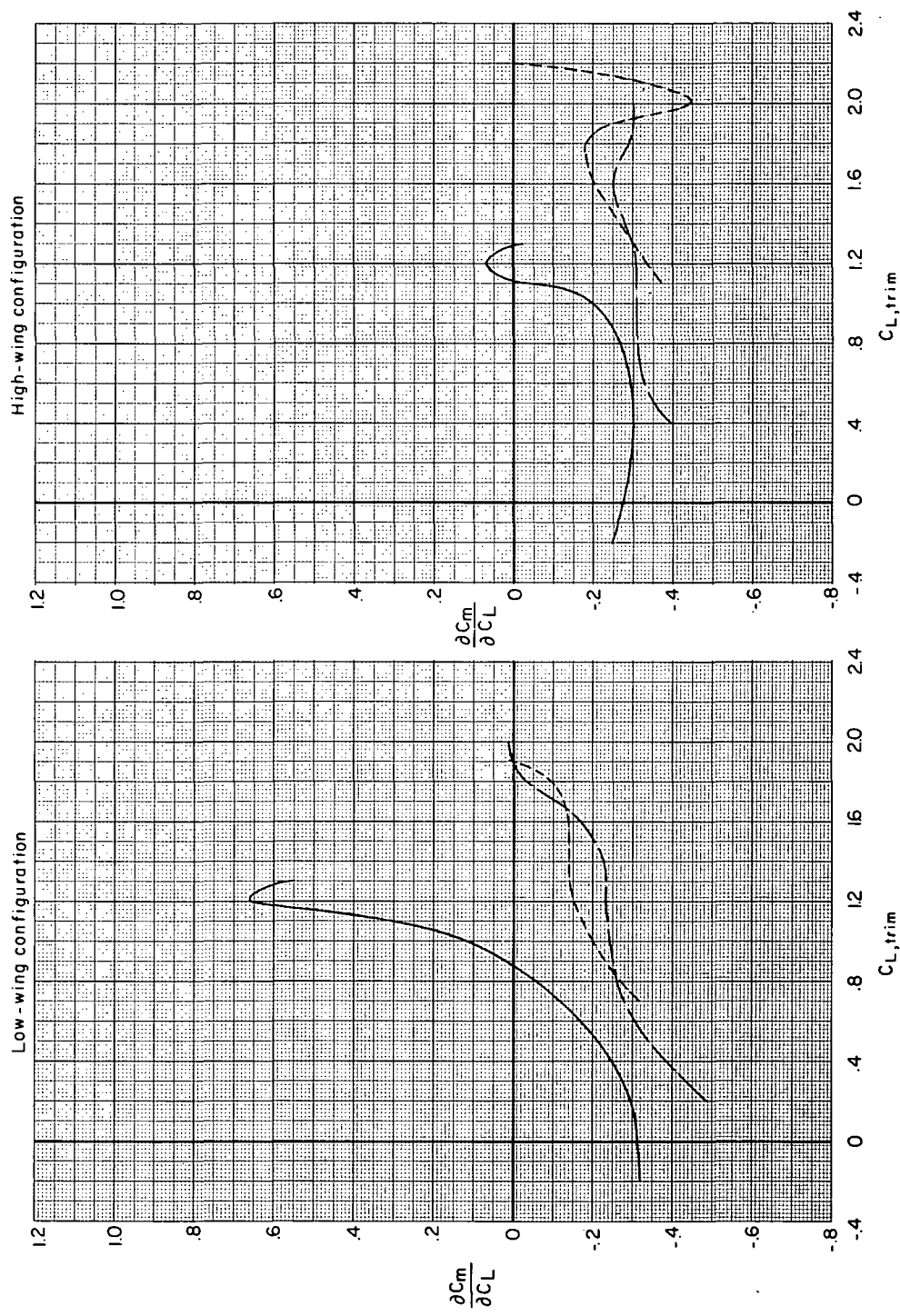
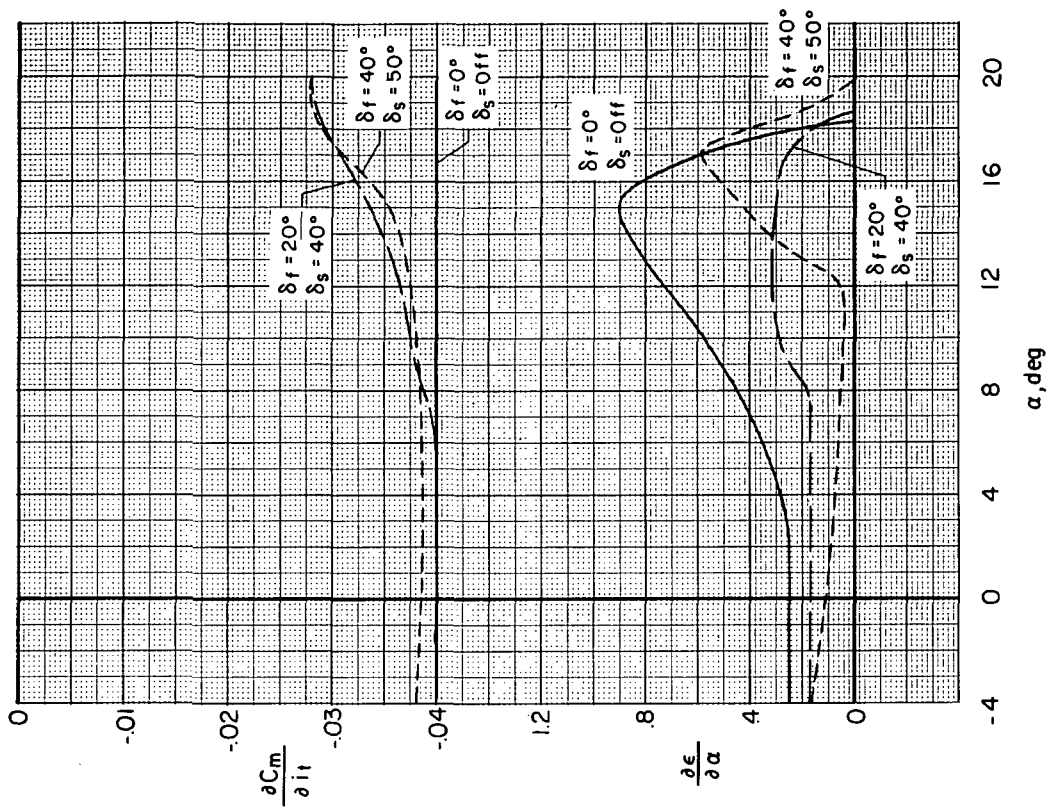
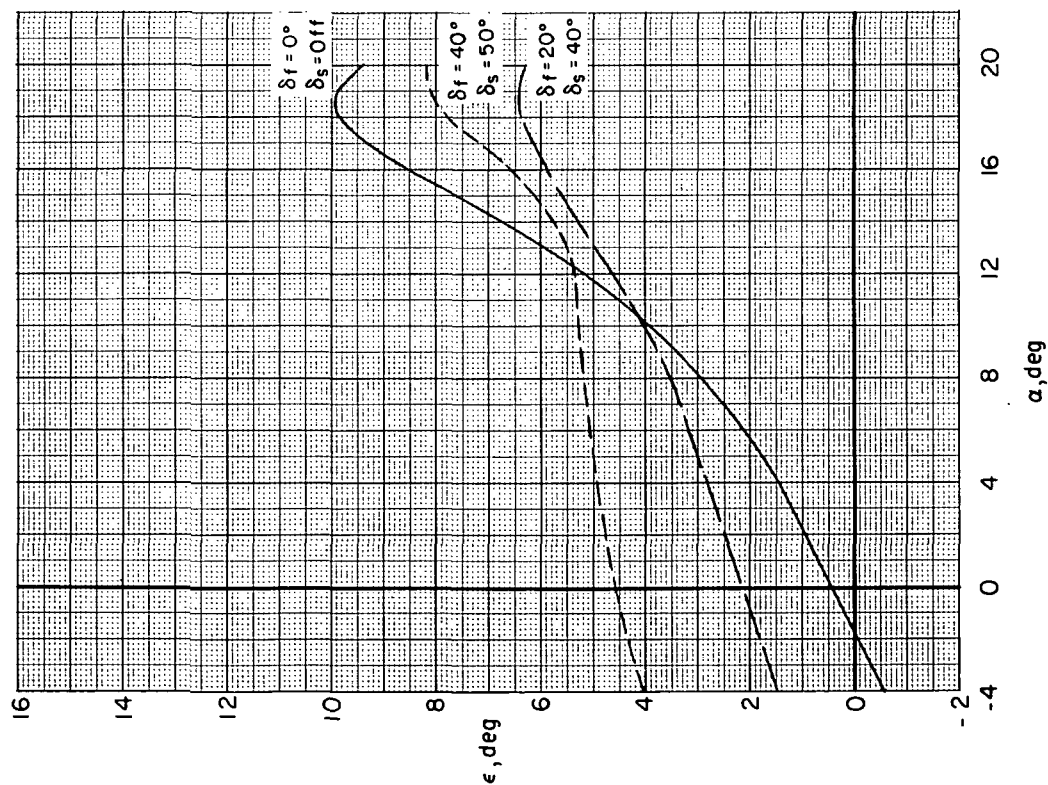
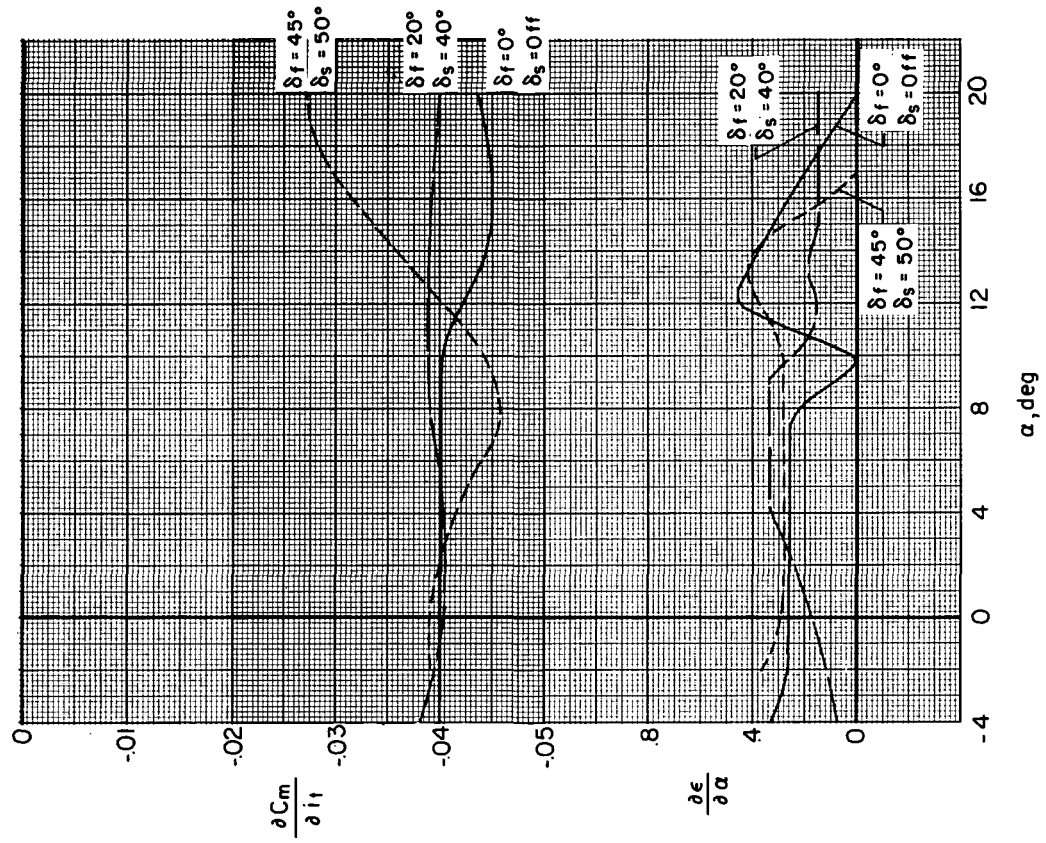
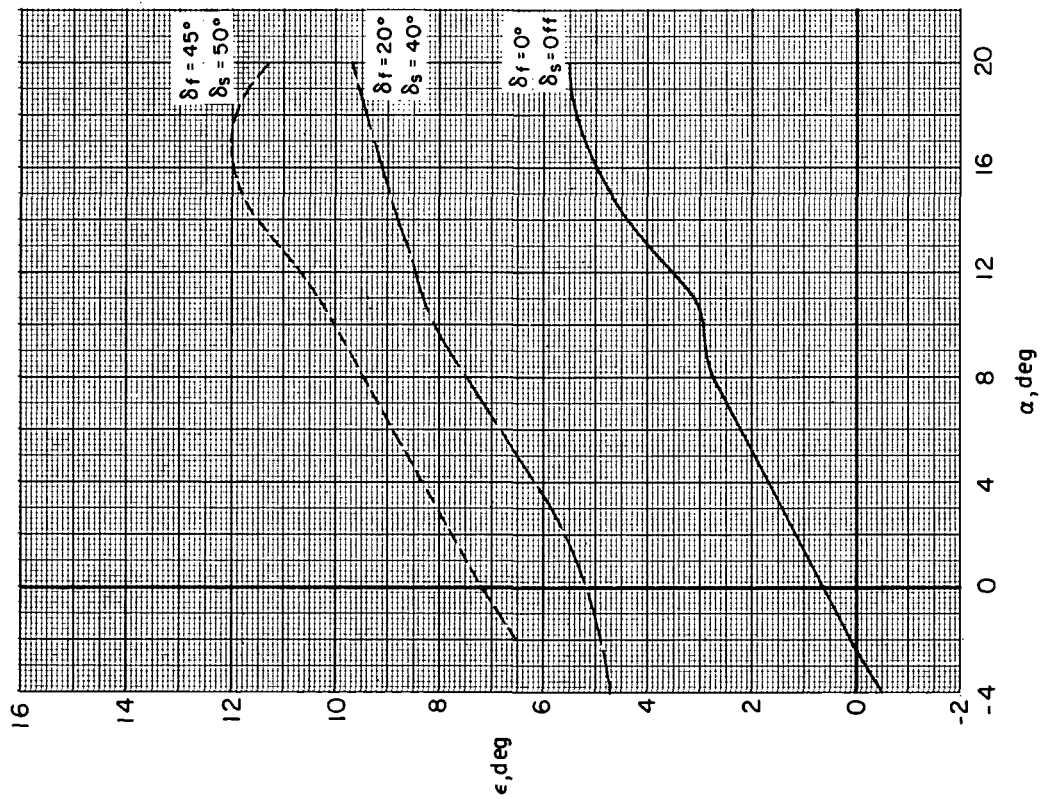


Figure 22.- Trimmed static longitudinal stability margin.



(a) Low-wing configuration.

Figure 23.- Effects of deflection of high-lift system on effective downwash angle, downwash gradient, and stabilizer effectiveness.



(b) High-wing configuration.

Figure 23.- Concluded.

~~CONFIDENTIAL~~

"The aeronautical and space activities of the United States shall be conducted so as to contribute . . . to the expansion of human knowledge of phenomena in the atmosphere and space. The Administration shall provide for the widest practicable and appropriate dissemination of information concerning its activities and the results thereof."

— NATIONAL AERONAUTICS AND SPACE ACT OF 1958

NASA SCIENTIFIC AND TECHNICAL PUBLICATIONS

TECHNICAL REPORTS: Scientific and technical information considered important, complete, and a lasting contribution to existing knowledge.

TECHNICAL NOTES: Information less broad in scope but nevertheless of importance as a contribution to existing knowledge.

TECHNICAL MEMORANDUMS: Information receiving limited distribution because of preliminary data, security classification, or other reasons.

CONTRACTOR REPORTS: Scientific and technical information generated under a NASA contract or grant and considered an important contribution to existing knowledge.

TECHNICAL TRANSLATIONS: Information published in a foreign language considered to merit NASA distribution in English.

SPECIAL PUBLICATIONS: Information derived from or of value to NASA activities. Publications include conference proceedings, monographs, data compilations, handbooks, sourcebooks, and special bibliographies.

TECHNOLOGY UTILIZATION PUBLICATIONS: Information on technology used by NASA that may be of particular interest in commercial and other non-aerospace applications. Publications include Tech Briefs, Technology Utilization Reports and Notes, and Technology Surveys.

Details on the availability of these publications may be obtained from:

**SCIENTIFIC AND TECHNICAL INFORMATION OFFICE
NATIONAL AERONAUTICS AND SPACE ADMINISTRATION
Washington, D.C. 20546**

~~CONFIDENTIAL~~